



**University of  
Zurich** <sup>UZH</sup>

Department of Geography

# Rock-ice avalanches with exceptionally long runout distances

Analysis and numerical modelling of worldwide events

GEO 511 Master's Thesis

## **Author**

Miriam Christen

12-720-421

## **Supervised by**

PD Dr. Christian Huggel ([christian.huggel@geo.uzh.ch](mailto:christian.huggel@geo.uzh.ch))

Dr. Brian McArdell, WSL ([brian.mcardell@wsl.ch](mailto:brian.mcardell@wsl.ch))

Prof. Dr. F.A. Florian Amann, RWTH Aachen ([amann@lih.rwth-aachen.de](mailto:amann@lih.rwth-aachen.de))

## **Faculty representative**

Prof. Dr. Andreas Vieli

22<sup>nd</sup> of August 2018

Department of Geography, University of Zurich



## Abstract

A recent massive landslide in the Swiss Val Bondasca drew the attention to a rare but destructive and poorly understood natural phenomenon: rock avalanches that travel over glacier surfaces and transform into debris flows. This study presents a worldwide inventory of 64 long-runout landslides with rock-, snow-, ice- and water interaction, larger than one million m<sup>3</sup> from the last 50 years and presents numerical simulations of three rock avalanche-debris flows from the inventory. For each event, specific parameters about flow properties, environmental conditions and physical mechanisms were analysed to expand the knowledge of process chains of complex landslides and to improve the understanding of still poorly understood events. Evaluating possible water sources to help explain the very long runout distances of the events in the inventory showed that it is seldom possible to define one single probable water source per event, because of the remoteness of the affected area or because of interrelated climatic processes. Moreover, findings of laboratory studies investigating the influence of ice particles on the flow behaviour of the flowing mass could not be confirmed by the analysis of the inventory events.

The numerical simulations were made with a standard RAMMS debris flow runout model, both with and without entrainment of sediment, and a special version considering entrainment and melting of ice and snow. The simulation results proved that it is possible to reconstruct large and complex landslides with high-developed numerical models, though the necessary knowledge about the physics of landslides increases with the complexity of the numerical model. Summarized, the comparability of complex and massive landslides is only possible on an intraregional level, because of limiting environmental influencing factors. However, it is possible to reconstruct well-documented events with two-dimensional numerical models with geomechanical input parameters used to model other events and which led to satisfactory simulation results. This thesis shows how landslides can transform from an initially dry rock avalanche into a destructive and powerful debris flow through the input of water and emphasizes how climate change impacts the stability of high mountain rock walls and glaciated regimes.



# Contents

1	Introduction.....	1
1.1	Research questions .....	2
1.2	Structure of the thesis.....	2
2	Scientific background .....	3
2.1	Erosion and entrainment of saturated material .....	3
2.2	Glacier trajectory and snow entrainment .....	3
2.3	Climate impact on rock slope stability .....	4
2.4	Triggering mechanisms.....	4
2.5	Numerical modelling of landslides.....	5
2.6	Terms and definitions.....	5
3	Data and methods .....	7
3.1	Inventory of events .....	7
3.1.1	Parameter description.....	13
3.1.1.1	<i>Flow parameters</i> .....	13
3.1.1.2	<i>Environmental conditions</i> .....	14
3.1.1.3	<i>Physical parameters</i> .....	15
3.2	Process understanding through numerical simulation .....	16
3.2.1	RAMMS .....	16
3.2.1.1	<i>Standard version</i> .....	18
3.2.1.2	<i>Entrainment version</i> .....	18
3.2.1.3	<i>Extended version</i> .....	19
3.2.2	Modelled events.....	20
3.2.2.1	<i>Mount Meager rock slide-debris flow, British Columbia, 2010</i> .....	22
3.2.2.2	<i>Howson II rock slide, British Columbia, 1999</i> .....	24
3.2.2.3	<i>Harold Price rock avalanche-debris flow, British Columbia, 2002</i> .....	25
4	Results.....	26
4.1	Parameter investigation .....	26
4.1.1	Flow parameters .....	26
4.1.2	Environmental conditions .....	31
4.1.3	Physical parameters .....	31
4.2	Simulation results.....	33
4.2.1	Mount Meager rock slide-debris flow, 2010.....	34
4.2.2	Howson II rock slide, 1999 .....	35
4.2.3	Harold Price rock avalanche-debris flow, 2002 .....	37
5	Discussion.....	41
5.1	Inventory evaluation .....	41
5.1.1	Event location .....	41
5.1.2	Documentation quality.....	41

5.1.3	Flow transformation .....	41
5.1.3.1	<i>Influence of transition over a glacier surface</i> .....	41
5.1.3.2	<i>Influence of different water sources on flow mechanism</i> .....	42
5.1.4	Comparability of events.....	43
5.2	RAMMS results.....	44
5.2.1	Reconstruction of events.....	44
5.2.2	Evaluation of RAMMS versions .....	45
5.2.3	Comparability to actual events.....	47
5.3	Embedment in the context of Bondo .....	48
6	Conclusion.....	49
7	Literature.....	52
7.1	Online Sources .....	57
8	Appendix.....	58
8.1	Complete inventory of events .....	58
8.2	RAMMS logfiles.....	70
8.2.1	Mount Meager .....	70
8.2.2	Howson II .....	73
8.2.3	Harold Price .....	76
	Acknowledgements.....	79
	Personal Declaration .....	81

## List of Figures

Figure 1 Debris flow deposit in Bondasca Valley and the village of Bondo, 30.08.2017.....	1
Figure 2 Fahrböschung angle / Angle of reach .....	14
Figure 3 RAMMS project workflow .....	16
Figure 4 Entrainment ratio of events .....	20
Figure 5 Entrainment ratio vs. Angle of reach.....	21
Figure 6 Location of British Columbia and modelled events .....	21
Figure 7 Slope Angle [°] of the Mount Meager environment (RAMMS interface) .....	22
Figure 8 Elevation [m.a.s.l.] of the Mount Meager environment (RAMMS interface) .....	23
Figure 9 Extent of the Mount Meager rock slide-debris flow .....	23
Figure 10 Approximate release area and extent of the Howson rock slide .....	24
Figure 11 Slope angle [°] of the Howson II environment (RAMMS interface) .....	24
Figure 12 Elevation [m.a.s.l.] of the Howson II environment (RAMMS interface) .....	24
Figure 13 Approximate release area and extent of the Harold Price rock avalanche-debris flow .....	25
Figure 14 Slope angle [°] of the Harold Price environment (RAMMS interface) .....	25
Figure 15 Elevation [m.a.s.l.] of the Harold Price environment (RAMMS interface) .....	25
Figure 16 World map with inventory events.....	26
Figure 17 Average flow speed distribution of events .....	27
Figure 18 Number of events with and without Flow transformation .....	27
Figure 19 Initial volume vs Angle of reach .....	28
Figure 20 Deposited volume vs Angle of reach.....	28
Figure 21 H/L ratio for each event.....	29
Figure 23 Influence of Glacier trajectory on Entrainment ratio.....	30
Figure 22 Influence of Path over glacier surface on Angle of reach and Entrainment ratio.....	30
Figure 24 Initial vs Deposited volume .....	31
Figure 25 Meltwater production vs Deposited volume.....	32
Figure 26 Mount Meager simulation results .....	38
Figure 27 Howson II simulation result .....	39
Figure 28 Harold Price simulation result .....	40
Figure 29 Influence of Path over glacier surface on Area of deposition .....	42
Figure 30 Influence of Glacier trajectory on Angle of reach.....	42
Figure 31 Extended simulation result of the Harold Price event.....	47

## List of Tables

Table 1 Characterized empirical parameters .....	7
Table 2 Inventory of events .....	8
Table 3 Rock densities used to calculate energies in the inventory .....	15
Table 4 Parameters for erosion rates.....	19
Table 5 Sensitivity analysis of erosion parameters for the Mount Meager event .....	33
Table 6 Parameters used in simulations with the extended version .....	34
Table 7 Simulation results Mount Meager landslide .....	34
Table 8 Simulation results Howson II landslide .....	36
Table 9 Simulation results Harold Price landslide .....	37
Table 10 Measurable, calculable and estimated input parameters of RAMMS.....	45
Table 11 Complete inventory of events.....	58

## Abbreviations

ALOS	Advanced Land Observing Satellite
ASTER GDEM	Advanced Spaceborne Thermal Emission and Reflection Radiometer Global Digital Elevation Map
DAN-W	Dynamic ANalysis
DEM	Digital Elevation Model
DFEM	Debris flow Finite Element Model
ESEC	Exotic Seismic Events Query
HB model	Herschel-Bulkley model
IRIS	Incorporated Research Institutions for Seismology
RAMMS	Rapid Mass MovementS
RKE	Random Kinetic Energy
SAR	Synthetic Aperture Radar
SRTM	Shuttle Radar Topography Mission



# 1 Introduction

Massive landslides happen in high mountain regions all over the world but are usually rarely documented since they occur in remote areas, and most of the time they are not noticed immediately (Huggel, 2009). The impact power of large landslides like rock avalanches is immense and, although the initially failing material is dry, the flow behaviour can change to a fluid like flow through fluidisation, which happens when the pore pressure and particle pressure in the moving mass are equal. Such fluidised flows can reach longer runout distances as expected and cause severe damage on forests, infrastructure and rivers but also threaten human life in high mountain or touristic areas (Carey et al., 2012; Clague and Evans, 2000; Evans and Delaney, 2014; Haeberli et al., 2004). A somewhat unusual landslide type in glaciated high mountain areas are rock avalanches that travel over glacier surfaces (Bottino et al., 2002). Such landslides can reach extremely high velocities, entrain high volumes of saturated sediment, snow and ice and reach vast horizontal distances to a relatively low vertical drop (Evans and Clague, 1988; Evans and Delaney, 2014; Jiskoot, 2011). In cases of such large landslides, scientists speak about *flow transformation*. Flow transformation reflects the interaction between the solid and the fluid component of the flow. The solid part consists of fragmented rocks, surficial sediment and glacial ice with different volumetric compositions changing during the discharge. The liquid part is determined by the melting of entrained snow or ice, the water content of entrained material and the incorporation of water from glacial lakes or rivers (Evans and Delaney, 2014). The exact mechanism of flow transformation of landslides is not yet fully understood and especially the source of water necessary for a flow transformation and long runout distance is highly debated. Different studies are trying to find water sources in glacial environments large enough to elongate the runout distance of rock avalanches (Evans and Delaney, 2014). The two most probable water sources are erosion and entrainment of saturated sediment, and entrainment and melting of snow and ice. Scientists are convinced that both effects are essential in causing flow transformation (Hungr and Evans, 2004). A recent massive rock avalanche that triggered a subsequent debris flow in the Swiss Bondasca Valley caused scientists of this research area to refocus on the process chain of large landslides and to investigate the importance of water availability for flow transformations further.

On the 23<sup>rd</sup> of August 2017, rock masses of around 3.15 million m<sup>3</sup> collapsed on the Northern slope of Piz Cengalo in the Swiss Alps (46° 17' 41.63" N, 9° 36' 07.22" E) and hit the lower laying glacier Vadrec del Cengal, mobilising another 0.6 million m<sup>3</sup>. The rock-ice mass travelled into the Bondasca Valley and deposited around three kilometres below the release area (Amann et al., 2017). Shortly after the rock-ice avalanche, a debris flow initiated in the upper part of the deposition area (Baer et al., 2017). The debris flow reached the village Bondo at the bottom of the valley where around 500'000 m<sup>3</sup> of debris was deposited (www.gr.ch). Unfortunately, this landslide killed eight hikers in the upper part of the Bondasca Valley but did not cause severe damage in the village Bondo. Two days later, another debris flow initiated in the deposited material and hit the village Bondo harder than the first one and destroyed houses, roads and farms (Figure 1). Fortunately, the village Bondo was evacuated after the first debris flow and no people were harmed (Baer et al., 2017). Experts call this event a chain of unexpected processes which is very rare in Swiss and worldwide landslide history (www.gr.ch). The exact sequence of events was not fully understood for a long time. Also, there are open questions about the exact initiation zone of the debris flow and the role of the glacier ice in the flow mechanism. A possibility to enhance the understanding of the different processes which interacted at this event is to have a look at other, similar landslides that happened all around the world and to analyse the role of glacier ice and saturated sediment for flow transformations.



*Figure 1 Debris flow deposit in Bondasca Valley and the village of Bondo, 30.08.2017  
Images: VBS Swisstopo*

## 1.1 Research questions

The ongoing research on the exact chain of events in the Bondasca Valley as well as ongoing debates over the source of water for flow transformations of rock-ice avalanches leads to the urge to understand flow mechanisms and process chains of massive landslides further, generating the primary objectives and research questions of this thesis:

- I Create a worldwide inventory of large landslide events with long runout distances from the last 50 years, characterised by empirical parameters.
  - Where do such events happen usually?
  - How well are the events documented?
  
- II Gain process understanding through the analysis of the empirical parameters.
  - How does transition over glaciers influence the flow behaviour?
  - How do different water sources influence flow transformation mechanisms?
  
- III Gain process understanding through numerical modelling of events of the inventory.
  - Is it possible to reconstruct such complex events with state of the art two-dimensional numerical models?
  - Which model is best suited to reconstruct large landslides?
  - Which information is needed to model an event?
  
- IV Synthesizing of the findings and embedment of a recent event in the Swiss Alps.
  - How well can such complex events be compared?
  - Is it possible to gain process understanding of a recent event in the Swiss Alps with knowledge about other similar events?

## 1.2 Structure of the thesis

As a start, this thesis gives a first introduction into topics related to large landslide motion and development in chapter 2 Scientific background. This chapter also introduces numerical simulation models used for the reconstruction of such events and a list of terms and definitions used in science about this topic.

Chapter 3 Data and methods presents an inventory of events composed of large landslides from all over the world, completed with different parameters (flow parameters, environmental conditions and physical parameters). Chapter 3 also describes a two-dimensional numerical model used in this study to simulate selected landslides from the inventory. According to an analysis of the parameters in the inventory, three events were selected to reconstruct with the presented numerical model.

Chapter 4 Results includes an analysis of the parameters collected in the inventory of events and presents the simulation results of the three selected events.

In the first section of chapter 5 Discussion, the whole inventory is evaluated based on the parameter analysis in the results section. This section discusses the research questions of the first two objectives (5.1). The second part of this chapter analysis the simulation results of the numerical modelling and discusses the research questions of the third objective (5.2). The last section synthesises the findings of the inventory evaluation and the numerical modelling and discusses the third objective of this thesis (5.3).

As a close, chapter 6 Conclusion summarises the most important results and findings of this thesis, presents the limitations of the used methods and gives an outlook.

In chapter 8 Appendix, the complete inventory with all analysed parameters can be found, as well as the input and output logfiles of the numerical simulations.

## 2 Scientific background

### 2.1 Erosion and entrainment of saturated material

There are several current studies about the entrainment of saturated material into rock avalanches and subsequent enlargement of the runout distance (Calhoun and Clague, 2018; Crosta et al., 2009; De Blasio, 2014; Hungr and Evans, 2004; Schneider et al., 2011b). As first scientists, Buss and Heim mentioned the interaction of saturated sediment and rock avalanche material while investigating the Bergsturz in Elm, Switzerland in 1881 (Buss and Heim, 1881 in Hungr and Evans, 2004). Later proponents were Sassa, Abele, and Voight and Sousa (Abele, 1997; Sassa, 1985; Voight and Sousa, 1994). Abele (1997) describes the interaction between saturated sediment and rock avalanche runout as following: As soon as the mass of a rock avalanche travels over saturated sediment (gravel or also finer sediments), the pressure on the sediment is so immense and happens so fast, that the water in it cannot escape unpressurized and starts to support the weight of the rock mass partly. The water is so acting as a lubricant and enlarges the runout distance. This process is called lubrication and is only valid if the sediment can be compressed sufficiently and if the water cannot escape elsewhere (Abele, 1997). Hungr and Evans, who are proponents of Abeles theory, called this effect *undrained loading* (Hungr and Evans, 2004). Abele (1997) found that the bottom part of the rock mass travelling on the saturated material may saturate as well and mobilise and entrain further material from the ground in its flow. This mechanism enables the rock mass to spread while getting thinner, leading to a high spreading ratio, especially in wider valleys. In more narrow valleys, the spreading ratio is lower because the mass cannot spread laterally, but an elongated runout distance can be observed instead. Furthermore, Abele detected sediment displacement at the frontal part of a rock mass moving over it, whereas, in the centre part of the mass, a coherent mass of rock avalanche material travels on the mobilised ground sediment (Abele, 1997). Hungr and Evans even speak of a debris flow-like movement of the mass in the final stage (Hungr and Evans, 2004). Abele concluded that the existence of sediment does not necessarily favour long runout distances, after all, enough water for saturation needs to be present. Hungr and Evans (2004) suggest geology, sediment composition and valley shape differences as critical influencing factors for the flow transformation into a debris flow. However, saturated valley material can enlarge runout distances of initially dry rock avalanches drastically and unexpectedly and thus must be concerned when investigating areas threatened by landslides.

### 2.2 Glacier trajectory and snow entrainment

Glacier ice and snow surfaces can have significant influences on the runout behaviour of giant rock avalanches passing onto them. Evans and Clague (1988) investigated several landslides travelling over glacier surfaces and concluded, that rock avalanches may interact with glaciers or glacial environment in two ways: (1) Travel over a glacier and (2) Incorporate ice and snow.

(1) Travel over a glacier: Glacier ice may have a substantial effect on a rock mass sliding over it because of its low frictional resistance. Scientists tested this effect by sliding different materials over ice. They saw that basal friction coefficients decrease drastically with increasing velocity. The same effect works on rock masses sliding over glacier ice, where lubrication leads to a decrease of basal friction, an increase of velocity and an elongation of the runout distance (Persson, 2000; Tusima, 2010 in De Blasio, 2014). Further, frictional heating of the rock mass sliding over the glacier surface may generate meltwater or steam pressure, reducing frictional resistance even more.

(2) Incorporation of ice and snow: Many landslides in glacierized terrain contain significant amounts of snow or ice through different processes:

- The initially detaching mass already contains snow or ice either in the form of permafrost, pore-ice or glacier ice
  - Kolka/Karmadon rock-ice avalanche 1978 (Haeberli et al., 2004; Huggel et al., 2005)
  - Harold Price rock slide-debris flow 2002 (Geertsema et al., 2006; Schwab et al., 2003)
  - Mount Steller rock-ice avalanche 2005 (Huggel et al., 2008b)
- The impact of a rock avalanche on the glacier destroys part or all of it, and the rock mass entrains glacier ice in its flow
  - Brenva Glacier rock slide 1997 (Barla et al., 2000; Bottino et al., 2002)

- Snow and ice get entrained into the moving mass during the passage of the landslide over a glacier or snow-laden surface
  - Lamplugh Glacier rock avalanche 2016 (Bessette-Kirton, 2017; Bessette-Kirton et al., 2018)

Melting of entrained snow or ice through frictional heating may cause liquefaction of a part of or the whole moving mass, which leads to a flow transformation into a debris flow and enlarges the runout distance. Petrakov and colleagues (2008) could find this effect too, they saw that through the entrainment of liquid water or meltwater production inside the flow, flow strength decreases and thus increases the runout distance and decreases the angle of reach necessary for the mass to flow. Other scientists tested this effect in rotating drums filled with gravel and ice in different concentrations (Schneider et al., 2011b). They found out that the ice content and the friction coefficient of the gravel-ice mixture are linearly related, which means that a more substantial ice content leads to smaller internal friction.

### 2.3 Climate impact on rock slope stability

Temperature and precipitation rates profoundly influence the stability of rock walls. It is known that degradation of permafrost and retreat of glaciers through long-time gradual temperature changes can negatively affect the stability of rock walls and soils and thus enhance failure (Huggel, 2009; Scheuner et al., 2009; Stoffel and Huggel, 2012). On the other hand, the effect of short-time extreme temperature changes on delicate high mountain systems is still highly unknown (Huggel et al., 2010) and may cause very fast changes which cannot be foreseen. In the last decades an increase in slope failures in steep rock walls has been observed in the European Alps (Allen and Huggel, 2013) and future climate conditions will further change the thermal state of permafrost and the water cycle in high mountain regions worldwide (Schneider et al., 2010). Thus an increased destabilisation of mountain walls and an accumulation of massive landslides like rock avalanches can be expected (Bottino et al., 2002; Gruber et al., 2004; Huggel et al., 2008a; Schneider et al., 2010). Additionally, downwasting glaciers because of future climate warming will cause the formation of new periglacial lakes. These lakes cause the problem of glacier lake outburst floods, so called GLOFs, which may initiate through rock fall, rock avalanches or lake-dam breaking and hence threaten underlying villages. On steep slopes, temperature rise will cause destabilization of hanging glaciers and thus cause ice falls and ice avalanches (Stoffel and Huggel, 2012). Combined, an increase in massive rock avalanches and ice availability means an increase in landslides consisting of rock and ice or snow, and thus an increase in complex mass flow processes including flow transformation and longer runout distances as expected.

The growing presence of people in high mountain environments due to tourism and mountaineering activities further enhances the vulnerability and value in cases of hazards (Bottino et al., 2002; Stoffel and Huggel, 2012) and supports the urge to improve the understanding of large landslides.

### 2.4 Triggering mechanisms

In cold environments, rock avalanches are frequently triggered by earthquakes, especially in regions with high seismic activity (Alean, 1984; Hancox et al., 2005; Jibson et al., 2006; Petrakov et al., 2008; Yamasaki et al., 2014). However, other factors like heavy rain events or periods with unusually high temperature changes, causing high meltwater rates and freeze-thawing cycles in fractured rocks, can also trigger rock avalanches (Huggel et al., 2010). In rare cases, one single triggering event can be determined (Carey et al., 2015; Feng, 2011; Geertsema et al., 2006; Haerberli et al., 2004; Huggel et al., 2010; Iribarren Anaconda and Bodin, 2010), but typically, this is not possible since mostly a combination of different factors act together and influence the stability of rock walls (Delaney and Evans, 2008; Geertsema, 2012; Gordon et al., 1978; Huggel et al., 2007; Jiskoot, 2011; Schwab et al., 2003) or an event that favours failure happens a few days before the actual event and scientists are not sure about the actual trigger (Hancox et al., 2005; Hancox and Thomson, 2013).

## 2.5 Numerical modelling of landslides

Realistic modelling of large landslides like rock avalanches and debris flows is gaining importance because of an increase in hazard occurrence in mountain regions (Scheuner et al., 2009). Such models can support the assessment of hazard intensity and extent, and further are the basis for the drawing up and modification of hazard maps.

There are different two-dimensional numerical models used to reconstruct debris flows like DAN (Dynamic Analysis), DFEM (Debris flow Finite Element Model), FLO-2D, HB (Herschel-Bulkley) model, Bingham, Coulomb, turbulent model and RAMMS (Rapid Mass MovementS) to only mention a few. In some of the mentioned numerical models, an erosion and entrainment algorithm is implemented to improve the modelling of the flow behaviour of mass flows. Due to material entrainment, the volume of mass flows grows and the flow behaviour changes due to this volume increase but also due to entrainment of water. Frank and colleagues (2015) compared simulation results of the numerical model RAMMS with and without an erosion and entrainment algorithm. They found that including the algorithm can substantially improve the reconstruction of the flow path and flow patterns and thus improve the accuracy of the model results. Different studies showed that more complex models have a higher information output than simpler models. On the other hand, the use of complex models needs more experience of modelling and more specialised knowledge (Scheuner et al., 2009). A detailed comparison of different simulation models for debris flows can be found in Rickenmann et al., 2006. In this master thesis, the numerical model RAMMS is used to model rock-ice avalanches and subsequent debris flows.

Numerical modelling improves process understanding of complex landslide events and helps in evaluating appropriate protection measures. Some recent studies and the most important findings are mentioned here:

- Schneider and colleagues compared simulation results of numerical models with RAMMS with seismic recordings of two ice-rock avalanches (Schneider et al., 2010). They concluded, that this comparison can verify the dynamic consistency of model results over the entire process of the modelled event and thus help to calibrate friction parameters used in the numerical model.
- Sosio and colleagues (2008) modelled the Thurwieser rock avalanche with the numerical model DAN and calibrated friction parameters. They elucidate the importance to change friction parameters of glacier surfaces overridden by the landslide to improve simulation results of the flow path.
- Knowledge gained from reconstructing well-analysed landslides with numerical simulation models can help to understand and model poorly analysed landslide events. Bottino and colleagues (2002) modelled the 1997 Brenva Glacier rock avalanche with a two-dimensional numerical model and used geomechanical input parameters of another landslide which could be reconstructed with this model quite accurately. They concluded that the maximum runout distances could be modelled quite precisely for both landslides, which ensures the possibility to reconstruct landslides in two-dimensional numerical models with geomechanical parameters of other, well-documented events.

## 2.6 Terms and definitions

The definition of landslides is based on a landslide classification of Varnes (1978, 1954) and is used worldwide. Hungr and colleagues (2014) modified the classification based on new understanding of landslide mechanisms and involved materials. The following terms are those used in literature about the events in the inventory.

### **Rockfall**

*“Detachment, fall, rolling, and bouncing of rock fragments. [...] there is little dynamic interaction between the most mobile moving fragments [...].” Hungr et al., 2014; p. 171*

A rockfall differs from a rock avalanche as the rock fall is a movement of individual fragments and a rock avalanche is a flow-like movement of a mass of fragments. Some authors proposed a maximum volume to distinguish between a rock fall and a rock avalanche of  $10'000 \text{ m}^3$ , but since fixed boundaries are difficult to set, this criterion is not used in Hungr et al. (2014).

### **Rock slide**

Hungr and colleagues subdivide rock slides into five subclasses depending on the surface the rock mass slides on which can be seen in Hungr et al., 2014, pp. 173–175. In literature about landslides listed in the inventory of events, the term rock slide is often used without any clarification about the surface of the ground the mass is sliding on and describes a sliding of a mass of rock on a surface.

### **Debris slide**

*“Sliding of a mass of granular material on a shallow, planar surface parallel with the ground. Usually, the sliding mass is a veneer of colluvium, weathered soil, or pyroclastic deposits sliding over a stronger substrate. Many debris slides become flow-like after moving a short distance and transform into extremely rapid debris avalanches.” Hungr et al., 2014; p.177*

Such debris slides occur where a weak substrate overlies bedrock or a stronger substrate. The weak substrate starts to slide if the interface to the hard underground is smooth and thus weaker than the soil itself or, e.g. after a fire, destroying all vegetation and root enforcement. Usually, a debris slide is an initial component of a debris avalanche or debris flow (see below) since liquefaction accelerates the material into a fluid mass.

### **Rock/ice avalanche**

*“Extremely rapid, massive, flow-like motion of fragmented rock from a large rock slide or rock fall.” Hungr et al., 2014; p. 180*

The disintegration of large rock slides or rockfalls leads to such extraordinarily rapid and massive rock avalanches. An explanation for the rapid movement from Hungr and Evans (2004) is the entrainment of saturated material from the flow path, which gets liquefied under the pressure of the rock mass. However, there are continued discussions about this theme. Initial or entrained glacier ice can remarkably enhance the mobility of rock avalanches.

### **Debris flow**

*“Very rapid to extremely rapid surging flow of saturated debris in a steep channel. Strong entrainment of material and water from the flow path.” Hungr et al., 2014; p.183*

Debris flows occur periodically in mountainous regions all over the world and are phenomena specific to given paths and deposition area. Different triggers like landslides, debris avalanches and rock falls or spontaneous instability of the steep stream bed can initiate a debris flow. Once the debris starts to flow, bed material becomes entrained, and as the flow surges down, it erodes further a lot of debris and liquid water. The entrainment ratio of debris flows is so high that most of the volume comes from entrainment. A debris flow can consist of one or several surges and already flows on slopes steeper than 10-20° in confined channels. When the channel exits in flatter area the boulders at the front of the debris flow get deposited rapidly, and the finer material flows further downslope usually in a flow that is comparable to a **Debris flood** (*“Very rapid flow of water, heavily charged with debris, in a steep channel.” Hungr et al., 2014; p.185*).

The extremely rapid movement coupled with high discharge and high entrainment rate make debris flows to one of the most dangerous and destroying natural hazard in mountainous regions.

### **Debris avalanche**

*“Very rapid to extremely rapid shallow flow of partially or fully saturated debris on a steep slope, without confinement in an established channel. Occurs at all scales.” Hungr et al., 2014; p.186*

The difference of debris avalanches and debris flow is that the debris avalanche is a unique event and does not happen periodically as a debris flow and that it can happen anywhere on a steep slope, whereas debris flows happen in channels. Debris avalanches get initiated by debris slides.

### 3 Data and methods

To improve process understanding and flow mechanisms of the rock avalanche and subsequent debris flow in the Bondasca Valley, a global inventory of similar massive landslides happening at comparable conditions was compiled and triggering factors, climatic conditions, flow movement and flow transformation were investigated.

#### 3.1 Inventory of events

The inventory is based on an analysis of large rock-ice avalanches from Schneider and colleagues (2011a). They selected large rock-ice avalanches from the 20<sup>th</sup> and 21<sup>st</sup> century showing interaction with snow and ice, with rapid, avalanche-like flow dynamics and larger than 1 million m<sup>3</sup>. This list was enlarged with events of landslides which were not mentioned in Schneider's study, as well as with events which happened between 2011 and 2017. The inventory does not aim for completeness but provides insights into large landslide events from different parts of the world.

As already Schneider and colleagues concluded, events with small volumes, earlier dates and more remote location are less well described (Schneider et al., 2011a). Thus, only events happening after 1965 were chosen for this inventory here. Schneider and colleagues derived selected empirical parameters for each of the events in their study, which were also extended with other carefully chosen parameters (Table 1). These parameters were chosen to represent the landslide motion at its best and to enable the possibility to compare the events. The parameters are divided into three groups: flow parameters, environmental conditions and physical parameters. The inventory considers large landslides with deposited volumes larger than 1 million m<sup>3</sup> and ice contents smaller than 100 %. Schneider and colleagues also considered pure ice avalanches, but because comparability to the rock avalanche and debris flow in the Bondasca Valley should be maintained, these events were not added to the inventory.

Massive landslides happening between 2011 and 2017 were compiled from different studies, but mostly from the *Exotic Seismic Events Query* (ESEC) provided by the *Incorporated Research Institutions for Seismology* (IRIS). IRIS provides aggregated event data from different independently-operated catalogues, e.g. *the Catalogue of the United States Geological Survey, the Bulletin of the International Seismological Centre and others* (<http://ds.iris.edu/ds/>; <http://ds.iris.edu/spud/ecec>). The events found in ESEC were all detected in seismic measurements. Seismic measurements are especially useful in remote areas, where landslides are mostly not immediately noticed. Rock avalanches show distinctive seismic signals and can be distinguished from earthquake signals (Feng, 2011; Huggel et al., 2007). This method is not explained further in here because it goes beyond the scope of this thesis.

Table 2 shows a shortened version of the inventory with a selection of the analysed parameters; the complete inventory with all parameters can be found in the appendix (8.1, pp.58).

*Table 1 Characterized empirical parameters Distinguished into three groups:  
Flow parameters, Environmental conditions and Physical parameters*

<i>Flow parameters</i>		<i>Environmental conditions</i>	<i>Physical parameters</i>
Fall height [m]	Angle of reach [°]	Triggering Factor	Rock Type
Initial rockfall volume [m]	Area of deposition [km <sup>2</sup> ]	Water source	Density [kg/m <sup>3</sup> ]
Path over glacier surface [m]	Volume of deposition [m <sup>3</sup> ]		Energy balance calculated [J]
Duration [s]	Ratio initial vs deposited volume		Energy balance in literature [J]
Number of surges [n]	Flow transformation [0, NO; 1, YES; X, no information]		Meltwater production [m <sup>3</sup> ]
Flow speed [m/s]			
Water content [%] or [m <sup>3</sup> ]			
Vertical distance [m]			
Horizontal distance [m]			

Table 2 Inventory of events  
shortened parameterisation, modelled events in orange

Place Name of event	Year	$V_i$ [m <sup>3</sup> ]	$p_g$ [m]	$v_f$ [m/s]	Water source	Water content	H [m]	L [m]	$\alpha$ [°]	$A_d$ [km <sup>2</sup> ]	$V_d$ [m <sup>3</sup> ]	ER	FT	Reference
<b>Alps, Italy</b>														
Brenva Gl.	1997	2.0E+06	5'400		S, G	>4.5E+06 m <sup>3</sup>	2'325	5'849	21.7	2.5	6.5E+06	3.3	X	[1], [2], [3]
Thurwieser	2004	2.0E+06	550	30-40	No source	10 %	1'296	2'697	25.7	0.4	2.9E+06	1.5	0	[4], [5], [3]
<b>Greenland</b>														
Nuugaatsiaq	2017							1'900	0.0		4.3E+07		X	[10]
<b>Alaska, USA</b>														
Iliamna Red Gl.	1978	6.5E+06	7'000		G	60 %	1'782	7'691	13.0		1.7E+07	2.6	0	[3], [6]
Iliamna Red Gl.	1980	1.1E+07	7'300		S, G	60 %	1'679	7'806	12.1		2.8E+07	2.6	0	[3], [6]
Iliamna Red Gl.	1994		9'500	22-46	G	60 %	1'796	9'993	10.2	11.0	1.7E+07		0	[3], [6], [7], [8]
Iliamna Red Gl.	1997		7'100	22-51	G	~50-60 %	1'706	7'694	12.5	9.0	1.5E+07		0	[3], [6], [7], [8]
Iliamna Red Gl.	2000		8'400	60-75	G	60 %	1'832	8'890	11.6		1.5E+07		0	[3], [6]
Iliamna Red Gl.	2003	6.0E+06	8'000	37-46	S, G	60-80 %	1'769	8'556	11.7	4.0	1.6E+07	2.7	0	[3], [6], [7]
Iliamna Red Gl.	2008				G		1'708	7'447	12.9		1.1E+07		0	[6]
Iliamna Red Gl.	2016				G		1'700	8'200	11.7	8.6	1.6E+07		0	[6], [10]
Iliamna Lateral Gl.	2004	2.5E+06		29-65	S, G, Ini		1'740	5'160	18.6		5.0E+06	2.0	0	[6], [7]
Iliamna Umbrella Gl.	2004	1.0E+06	5'550	35-70	G	50 %	1'765	6'036	16.3		4.0E+06	4.0	0	[3], [6], [7]
Iliamna	2013				G		1'400	4'900	15.9	5.6	3.0E+06		0	[10]
Hitchcock Hills, Marvine	1983	1.0E+06	2'050		Firn	70 %	860	3'144	15.3	0.6	3.0E+06	3.0	0	[3], [9]
McGinnis Peak North	2002	1.8E+07	10'500	40-54	S, G, Ini	2.0E+06 m <sup>3</sup>	1'718	10'960	8.9	10.2	2.0E+07	1.1	0	[3], [11]
McGinnis Peak South	2002	1.1E+07	10'700		Possibly SD		1'904	11'463	9.4	5.7	1.1E+07	1.0	0	[3], [11]
Black Rapids East	2002	1.2E+07	3'600		G		997	4'605	12.2	4.6	1.4E+07	1.2	X	[3], [11]
Black Rapids Middle	2002	1.0E+07	3'200		G		827	4'478	10.5	4.6	1.4E+07	1.4	X	[3], [11]



Place Name of event	Year	$V_i$ [m <sup>3</sup> ]	$p_g$ [m]	$v_f$ [m/s]	Water source	Water content	$H$ [m]	$L$ [m]	$\alpha$ [°]	$A_d$ [km <sup>2</sup> ]	$V_d$ [m <sup>3</sup> ]	ER	FT	Reference
Black Rapids West	2002	6.0E+06	2'200		G		724	3'307	12.3	3.2	9.7E+06	1.6	X	[3], [11]
West Fork Gl. North	2002			30-32	Possibly G		737	3'296	12.6	1.4	4.1E+06		X	[11]
West Fork Gl. South	2002			30-32	G		1'005	4'249	13.3	1.5	4.4E+06		X	[11]
Mount Steller	2005	1.5E+07	4'000	≥100	S, G, Ini	3.6E+05 m <sup>3</sup>	2'430	9'000	15.1	4.0	5.0E+07	3.3	X	[3], [12]
Mount Steller North 1	2008	5.5E+05			Ini		822	1'767	24.9		1.5E+06	2.7	0	[13]
Mount Steller North 2	2008				G		476	2'200	12.2	0.5	1.5E+06		X	[13]
Mount Miller	2008		3'650		Ini		910	4'507	11.4	~5.5	2.2E+07		X	[3], [13]
Lituya Mountain	2012		6'500		G		2'400	9'300	14.5	7.9	1.3E+07		X	[3], [10], [14]
Redoubt Gl.	2015						1'372	3'700	20.3	0.8	1.1E+06		X	[10]
Lamplugh Gl.	2016	5.2E+07	6'700		S, I		1'500	10'500	8.1	22.2	7.0E+07	1.4	X	[15], [16]
Mount La Perouse	2014						1'779	7'374	13.6	5.5	1.4E+07		X	[10]
<b>British Columbia, Canada</b>														
Devastation Gl., Mount Meager	1975		2'500	30			1'170	6'568	10.1		1.2E+07		1	[3], [17], [18]
North Creek	1986		1'000				745	2'683	15.5		2.0E+06		X	[3], [19]
Kshwan Gl.	1992/ 93		1'400		G		675	2'205	17.0	0.68	3.1E+06		X	[3], [20]
Mount Munday	1997	3.2E+06	> 4500	11	G		850	4'650	10.4	2.6	5.0E+06	1.6	high frag- ment.	[3], [20], [21], [22]
Howson II	1999	9.0E+05	150	18-30	G		1'296	2'700	25.6		2.5E+06	2.8	sub-seq. debris fl.	[19], [23]
Tsar Mountain	2000	1.6E+06	1'700	22-45	S, G, SD	40 %	615	2'230	15.4		3.0E+06	1.9	X	[3], [24]
Zymoetz River	2002	1.1E+06		15-25	SD, Ini		1'245	3'500	19.6		1.5E+06	1.4	1	[23], [25], [26]
Mount Steele, Yukon	2007	3.0E+06	4'050	35-65	S, G	95 %	2'160	5'800	20.4	5.3	4.0E+06	1.3	high fluidity	[3], [10], [27]

<i>Place Name of event</i>	<i>Year</i>	<i>V<sub>i</sub> [m<sup>3</sup>]</i>	<i>p<sub>g</sub> [m]</i>	<i>v<sub>f</sub> [m/s]</i>	<i>Water source</i>	<i>Water content</i>	<i>H [m]</i>	<i>L [m]</i>	<i>α [°]</i>	<i>A<sub>d</sub> [km<sup>2</sup>]</i>	<i>V<sub>d</sub> [m<sup>3</sup>]</i>	<i>ER</i>	<i>FT</i>	<i>Reference</i>
Mount Steele, Yukon	2015						2'200	3'700	30.7		2.0E+07		X	[10]
Mount Meager, Capricorn Gl.	2010	4.9E+07	< 500	64	G, SD	< 1 %	2'183	12'700	9.8	9.7	4.9E+07	1.0	1	[3], [10], [28], [29], [30], [31]
Harold Price	2002	7.0E+05	0	28-35	Ini (rock glacier)		720	4'000	10.2		2.0E+06	2.9	1	[19], [23]
<b>Colorado, USA</b>														
West Salt Creek main	2014			20-26	SD		636	4'590	7.9	2.3	5.4E+07		1	[32]
<b>Utah, USA</b>														
Bingham Canyon	2013	5.2E+07		36			850	2'950	16.1		5.3E+07	1.0	0	[10], [33], [34], [35]
<b>Cascade Volcanoes, Washington, USA</b>														
Mount Adams	1997						1'561	3'995	21.3		5.0E+06		X	[36]
Mount Adams	1997						1'683	4'472	20.6		4.0E+06		X	[36]
Mount Adams	2008						1'300	3'500	20.4	0.9	1.7E+06		X	[10]
<b>Cordillera Blanca, Peru</b>														
Nevados Huascarán	1970	7.5E+06	2'400	76	S, G	35 %	3'966	16'880	13.2	22.0	5.8E+07	7.7	1	[3], [4], [18], [37]
<b>Chile</b>														
Estero Parraguirre	1987	6.0E+06		19			3'400	17'981	10.7		1.5E+07	2.5	1	[18], [38]
Tinguiririca	2007				SD, S, Ini		1'426	8'287	9.8		1.4E+07		X	[39]
<b>South Georgia, Antarctica</b>														
Lyell Gl.	1975		84km <sup>2</sup>	60	SD, G	90 %	1'572	5'171	16.9		2.7E+06			sub-se- quent debris flow [40], [41]

<i>Place Name of event</i>	<i>Year</i>	<i>V<sub>i</sub> [m<sup>3</sup>]</i>	<i>p<sub>g</sub> [m]</i>	<i>v<sub>f</sub> [m/s]</i>	<i>Water source</i>	<i>Water content</i>	<i>H [m]</i>	<i>L [m]</i>	<i>α [°]</i>	<i>A<sub>d</sub> [km<sup>2</sup>]</i>	<i>V<sub>d</sub> [m<sup>3</sup>]</i>	<i>ER</i>	<i>FT</i>	<i>Reference</i>
<b>Southern Alps, New Zealand</b>														
Beelzebub Gl.	1984						402	1'012	21.7	0.2	2.0E+06		X	[42]
Aoraki/Mount Cook	1991	1.2E+07	6'660	55-58	S, G	> 30E+06 m <sup>3</sup>	2'720	7'008	21.2	7.0	6.0E+07	5.0	X	[3], [13], [43]
Mount Fletcher 1	1992	7.8E+06	2'290				1'364	3'806	19.7	1.8	1.0E+07	1.3	X	[3]
Mount Fletcher 2	1992	5.0E+06	2'360				1'440	3'800		1.8		0.0	X	[3]
Mount Adams	1999	1.3E+07					1'850	2'800	33.5	1.6	1.5E+07	1.2	X	[42], [44]
Hillary (South) Ridge/ Aoraki, Mount Cook	2014	9.0E+05		51	S, G, SD		1'600	3'900	22.3	1.4	3.0E+06	3.3		[45]
Mount Haast/ Aoraki, Mount Cook	2013	1.0E+06		44.44	S, G		290			0.8	2.0E+06	2.0	0	[46]
<b>Westland, New Zealand</b>														
Wanganui River Mt Evans	2013	3.8E+06		> 35	G			5'000	0.0		4.5E+06	1.2	X	[47]
<b>Pamir, Tajikistan</b>														
Vanch valley	2002						1'549	9'138	9.6		8.0E+06		X	[48]
<b>Cashmir, Pakistan</b>														
Bualtar I	1986		3'000	62	G		1'490	4'808	17.2	4.5	2.0E+07		X	[49], [50]
<b>Taiwan</b>														
Shiaolin	2009			20.4- 33.7	W		830	2'830	16.3		2.5E+07		X	[51], [52]
<b>Japan</b>														
Tatsunokuchi	2011	5.0E+04		14	S							0.0	X	[53]
<b>Nepal</b>														
Pokhara valley	2012	1.3E+07		13.3	G			23'500	0.0		2.2E+07	1.8	1	[54]

Place Name of event	Year	$V_i$ [m <sup>3</sup> ]	$p_g$ [m]	$v_f$ [m/s]	Water source	Water content	$H$ [m]	$L$ [m]	$\alpha$ [°]	$A_d$ [km <sup>2</sup> ]	$V_d$ [m <sup>3</sup> ]	ER	FT	Reference
<b>Caucasus, Russia</b>														
Kolka/Karmadon	2002	2.3E+07	3'100	70-90	S, G, W, SD, Firn	9.0E+07 m <sup>3</sup>	2'047	19'379	6.0		1.3E+08	5.7	1	[3], [4], [18], [55], [56], [57], [58], [59], [60]

$V_i$ , initial volume;  $p_g$ , path onto glacier surface;  $v_f$ , flow speed; water source (W, Water; S, Snow; G, Glacier ice; SD, Saturated debris; Ini, Ice and snow in initial failure mass);  $H$ , vertical distance;  $V$ , horizontal distance;  $\alpha$ , angle of reach;  $A_d$ , area of deposition;  $V_d$ , deposited volume; ER, entrainment ratio (Initial vs deposited volume); FT, flow transformation (0, NO; 1, YES; X, no information).

[1] (Bottino et al., 2002), [2] (Barla et al., 2000), [3] (Deline et al., 2015), [4] (Sosio et al., 2008), [5] (Pirulli, 2009), [6] (Huggel et al., 2007), [7] (Caplan-Auerbach et al., 2007), [8] (Waythomas et al., 2000), [9] (Alean, 1984), [10] IRIS, [11] (Jibson et al., 2006), [12] (Huggel et al., 2008b), [13] (Huggel et al., 2010), [14] (Geertsema, 2012), [15] (Bessette-Kirton, 2017), [16] (Bessette-Kirton et al., 2018), [17] (Clague and Souther, 1982), [18] (Petrakov et al., 2008), [19] (Geertsema et al., 2006), [20] (Evans and Clague, 1999), [21] (Delaney and Evans, 2008), [22] (Delaney and Evans, 2014), [23] (Schwab et al., 2003), [24] (Jiskoot, 2011), [25] (McDougall et al., 2006), [26] (Boulton et al., 2006), [27] (Lipovsky et al., 2008), [28] (Allstadt, 2013), [29] (Guthrie et al., 2012), [30] (Roberti et al., 2017), [31] (Roberti et al., 2018), [32] (Coe et al., 2016), [33] (Pankow et al., 2014), [34] (Moore et al., 2017), [35] (Hibert et al., 2014), [36] (Schneider et al., 2011a), [37] (Evans et al., 2009a), [38] (Hauser, 2002), [39] (Iribarren Anaconda and Bodin, 2010), [40] (Deline, 2009), [41] (Gordon et al., 1978), [42] (Korup, 2005), [43] (Schneider et al., 2010), [44] (Hancox et al., 2005), [45] (Cox et al., 2015), [46] (Hancox and Thomson, 2013), [47] (Carey et al., 2015), [48] (Schneider, 2006), [49] (Hewitt, 1988), [50] (Hewitt, 2009), [51] (Feng, 2011), [52] (Tsou et al., 2011), [53] (Yamasaki et al., 2014), [54] (Hanisch et al., 2013), [55] (Haeberli et al., 2003), [56] (Haeberli et al., 2004), [57] (Kotlyakov et al., 2004), [58] (Huggel et al., 2005), [59] (Evans et al., 2009b), [60] (Huggel, 2009)

### 3.1.1 Parameter description

#### 3.1.1.1 Flow parameters

##### ***Fall height [m]***

The height from the release area to the impact point on the ground. This height can give information about the energy available at the impact point, e.g. to calculate how much glacier ice can be eroded or melt up.

##### ***Initial rockfall volume [m]***

The initial rockfall volume is the volume which started to move at the release area. Mostly this volume is calculated as the difference in two DEMs taken before and after the event since it cannot be determined from the deposited material because of disintegration and entrainment effects. Dependent on the spatial resolution of the DEMs, the calculation of the initial volume may vary in ranges of a few thousand m<sup>3</sup>.

##### ***Path over glacier surface [m]***

As mentioned above in chapter 2.2, the path of a rock avalanche onto a glacier surface can have distinctive impacts on the runout behaviour and is thus of utmost importance for the analysis of flow mechanisms and runout length. At the moment, there is no global glacier inventory which is always up to date about current debris cover changes and volume changes of glaciers through impacts of rock avalanches. Therefore, it is difficult to determine the path of a landslide over a glacier surface, especially in remote areas, where no glacier inventory exists at all (Lipovsky et al., 2008).

##### ***Duration [s]***

The duration of a landslide gives information about the flow speed of the mass movement. In most cases, the duration is determined with seismic recordings (Schneider et al., 2010), in rare cases, eyewitnesses can give details about approximate durations of a landslide.

##### ***Number of surges [n]***

Sometimes, a rock avalanche or debris flow does not happen at constant pace but shows surges of higher speed and higher discharge. This is especially important in regions where retention basins or dams could be filled up and break under high pressure, or in populated areas. In remote areas, where landslides are not noticed immediately it is quite impossible to determine the number of surges of the event, except when depositions of several subsequent events like rockfalls and debris flows are superimposed. As the duration of a landslide, the number of surges can only be witnessed by eye or determined with seismic records of the event.

##### ***Flow speed [m/s]***

Flow speed is rarely measured directly when a rock avalanche or a debris flow happens. Most of the time, seismic signals give the timespan of the mass movement, and with distance measurements of the runout length, flow speed can be calculated. In other, rather rare cases, where eyewitnesses were able to film the event, flow speed can be estimated from the time span of the film or with observations of moving objects, like large boulders or trees.

##### ***Water content [%] or [m<sup>3</sup>]***

The water content is measured in the deposited material, shortly after the event. In remote areas, landslides are mostly noticed only a few days to weeks after the event happened, thus, water content information are rare. This parameter gives information about the fluidity of the mass and may also give information about entrained and melted snow or ice, or saturated sediments.

##### ***Vertical distance (H) [m]***

The vertical distance defines the vertical drop from the highest to the lowest point of the whole mass movement, from the start point of the landslide down to the maximum extent of the deposition area.

##### ***Horizontal distance (L) [m]***

The horizontal distance or runout length is the horizontal travel distance of an event from the start point to the maximum extent of the deposition area.

##### ***Angle of reach [°]***

Albert Heim was the first scientist who mentioned the term *fahrböschung*, in English *angle of reach*, *travel angle*, or *shadow angle* (Heim, 1932). He defined it as the angle of the connecting line between the uppermost

point of the release area and the lowest point of the deposition area (Figure 2: De Graaf and Bowman, 2016). Thus, the angle of reach is calculated from the vertical (H) and the horizontal distance (L) of the landslide. This angle defines the efficiency of the conversion of gravitational energy into kinetic energy (De Blasio, 2014). The lower the angle, the larger the initial volume or the more fluid and mobile the mass flowed.

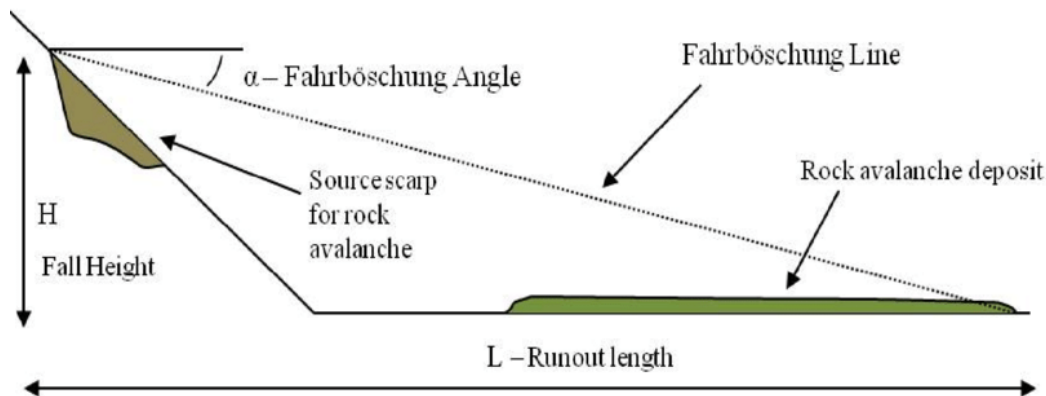


Figure 2 Fahrböschung angle / Angle of reach  
Figure: DeGraaf and Bowman, 2016

### **Area of deposition [km<sup>2</sup>]**

The area of deposition as well as the shape of deposited material gives information about flow properties of the mass and may also reflect the fluidity of the mass. This parameter can also give information about the roughness of the surface, where the mass slid on and stopped.

### **Volume of deposition [m<sup>3</sup>]**

The volume of deposition is generally calculated with DEMs taken before and after the event. In most cases, DEM resolution is slightly coarse (5-30 m) and the depth of deposition is estimated which makes correct calculations of the deposited volume more difficult (Bessette-Kirton et al., 2018). Furthermore, unnoticed pre-event glacier changes, as well as post-event volume changes through melting of snow and ice in the deposited material may influence the calculation of the deposited volume (Deline et al., 2015; Jiskoot, 2011; Lipovsky et al., 2008). The deposited volumes of rock avalanches and debris flows are usually larger than the initial volumes because of disintegration, which describes the volume increase through a decrease in pore pressure, or because of material entrainment.

### **Ratio initial vs deposited volume**

The ratio of initial vs deposited volume or entrainment ratio (ER) indicates how the volume increased from the initial rock avalanche until the deposition fan. Hungr and Evans (2004) expect a volume increase of 250% for large landslides, as they tested in a study about the volume increase of rock avalanches through disintegration and entrainment of material.

### **Flow transformation [0, NO; 1, YES; X, no information]**

Flow transformation describes the change of a landslide type into another. In this study, focusing on rock avalanches and debris flows, flow transformation describes the change of an initially relatively dry mass of rock (and ice) into a more liquid and fluid mass, characteristic in long runout distances. In experiments with rotational drums filled with gravel and ice, scientists found that an initial ice content of more than 40% by volume leads to liquefaction and thus to flow transformation (Schneider et al., 2011b). In nature, rock avalanches entrain much snow, ice and saturated material and can thus reach this high amount of water, in solid or liquid form, although, the initial mass was relatively dry.

#### **3.1.1.2 Environmental conditions**

##### **Triggering factor**

There are different possible triggering factors for rock avalanches like earthquakes, changing thermal conditions, changing precipitation rates, glacier retreat leading to a debuitressing effect, meltwater in cracks leading to increased pore water pressure and others (chapter 2.4). Usually, there is no single triggering

factor for large landslides, apart from earthquakes, since the mentioned mechanisms are all connected to climatic change and are thus interrelated. Scientists are still researching the relation between earthquakes and landslides because there are several intense earthquakes like the Denali Fault earthquake of 2002, which caused fewer landslides as expected, which were distributed only in a narrow band along the fault rupture (Jibson et al., 2006). Scientists suggest that the central mass has to be conditioned by, e.g. disaggregation of rocks or glacier ice, or formation of rupture planes for possibly many years before a final trigger can start the landslide (Petrakov et al., 2008).

### **Water source**

Flow transformation from, e.g. a dry rock avalanche into a debris flow necessitates a water source for the liquefaction of the mass. There are different sources of water in glacial environments like glacial ice, snow or saturated sediments which can get entrained into the mass flow and serve as a water source for flow transformation. In case of entrained snow or ice, the material must first be melted through internal friction before liquid water is available for a liquefaction. If the source of water is saturated sediment, liquid water is available from the beginning of the entrainment and flow transformation can occur immediately (Delcamp et al., 2016; Roberti et al., 2017).

#### *3.1.1.3 Physical parameters*

### **Rock type**

The rock type defines the stability of a rock wall as well as the disintegration behaviour of a collapsing rock mass. In two of the documented events, the landslide started as glacier collapse with only a few rock particles in it. For those events, the density of ice (920 kg/m<sup>3</sup>) was taken to calculate the energy.

### **Density [g/cm<sup>3</sup>]**

The density of the different rock types is needed to calculate the energy which is produced through the downward movement of the avalanche. Table 3 shows the densities needed for the calculation in the catalogue.

*Table 3 Rock densities used to calculate energies in the inventory*

<i>Rock type</i>	<i>Density</i>	<i>Source</i>
<i>Andesitee, Gneiss, Granite, Granodiorite, Greywacke, Schist, Volcanic, Volcaniclastic</i>	2'700 kg/m <sup>3</sup>	www.thoughtco.com; www.britannica.com/science; www.edumine.com; (Hatherton and Leopard, 1964)
<i>Basalt, Dolomitee, Gabbro</i>	3'000 kg/m <sup>3</sup>	www.thoughtco.com
<i>Porphyric Copper (Copper ore)</i>	2'000 kg/m <sup>3</sup>	www.edumine.com
<i>Limestone, Silt, Sandstone, Marble, Sedimentary</i>	2'500 kg/m <sup>3</sup>	www.thoughtco.com
<i>Ice</i>	920 kg/m <sup>3</sup>	(Shumskiy, 1960)

### **Energy balance calculated [J]**

The energy balance is calculated with the formula  $E = V * \rho * g * h$ , where  $V$  is the initial rock volume, in case this information is available, and the deposited volume otherwise,  $\rho$  is the density of the rock,  $g$  is gravitational acceleration (9.81 ms<sup>-2</sup>) and  $h$  is the fall height of the rock avalanche, in case this information is available, and the vertical distance ( $H$ ) otherwise. The energy balance can be used to define how much entrained snow or ice can be melt at maximum and thus helps to define if flow transformation is possible or not.

### **Energy balance in literature [J]**

In some cases, scientists calculated the energy of a landslide in their investigation of the event. If this is the case, a comparison with the calculated energy balance shows how accurate the calculation is.

### **Meltwater production [m<sup>3</sup>]**

Meltwater production was calculated with the calculated energy balance, the specific heat energy to melt ice (334 kJ/kg, <https://www.britannica.com/science/latent-heat>) and converted into m<sup>3</sup> by dividing with the

density of ice. With this calculation it is assumed that the complete energy available is used for meltwater production, thus the calculated value is the maximum possible amount of produced meltwater.

### 3.2 Process understanding through numerical simulation

There are around 64 landslides worldwide comparable to the event in Bondo (Table 2), but a lot of the searched parameters are not available for the events. To improve the understanding of the process chain in Bondo and to define numerical models which are best suited for future hazard assessment, differently high-developed versions of the numerical model RAMMS (Rapid Mass MovementS) are used. The model RAMMS was chosen because it is widely used in practice and scientific projects (Frank et al., 2015; Hussin et al., 2012 in Scheuner et al., 2011). The aim here is to test the capability of the different versions of the software to reconstruct well-documented events and to see how accurate the simulation results are, compared to observations of the real events.

#### 3.2.1 RAMMS

RAMMS is a software developed by the WSL Institute for Snow and Avalanche Research (slf) and the Swiss Federal Institute for Forest, Snow and Landscape Research (WSL) and is used to numerically model two-dimensional rapid mass movements in three-dimensional terrain like avalanches, debris flows and rock falls. In this study, a standard and an erosion version of the debris flow module as well as an extended version of the avalanche module are used, hence only those modules are described here. The numerical model was developed and calibrated with real scale data from a test site in the Vallée de la Sionne, Switzerland for the avalanche module and in Illgraben and Spreitgraben, Switzerland for the debris flow module and with data from well-documented historical avalanches and debris flows in Switzerland (Christen et al., 2012). The software needs different input data (Figure 3). One is the terrain data in the form of a digital elevation model (DEM). The spatial resolution of the DEM is of utmost importance. Studies showed that DEMs with coarse resolutions of 25 m or worse might miss essential terrain features, while a too fine spatial resolution of 1 m or better yields immensely long calculation time and even lead to incorrect calculation results (Bühler et al., 2011). The best spatial resolution is dependent on the process to be modelled and on the mass.

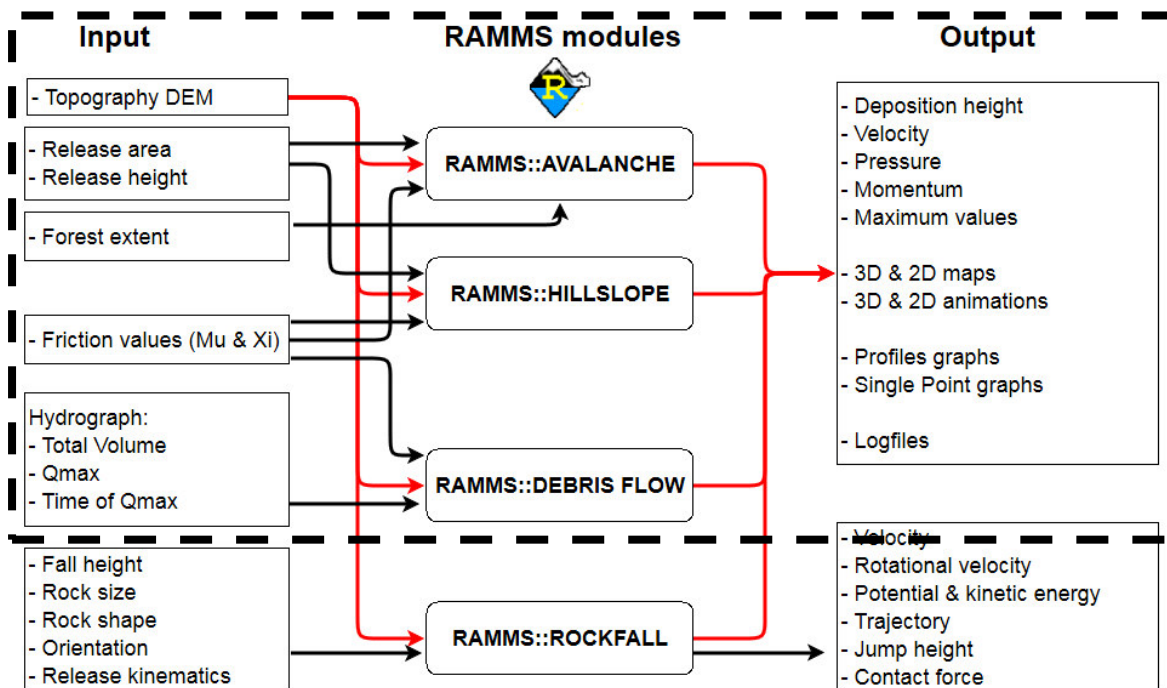


Figure 3 RAMMS project workflow  
Christen et al., 2012

Another input parameter is the release area which can be drawn directly in RAMMS or imported from GIS software. One or several release areas can be drawn, and release height can be set in the RAMMS interface



separately for each release area. The forest extent can also be drawn directly in RAMMS or imported from GIS software and is especially useful for the modelling of avalanches and smaller debris flows since flow mechanisms of those hazards are profoundly influenced by forested area. Because this study models huge landslides like rock avalanches transforming into debris flows with high impact power, whose flow mechanisms are not relevantly influenced by forest, the simulations do not consider forest extent.

The physical basis of RAMMS model for the avalanches, debris flow, and hillslope models is the shallow water equations for granular flows, which are solved in two dimensions (Bartelt et al., 2013). The shallow water equations for granular flows are gravity driven standard equations used to calculate flow mechanisms of snow, debris and mud.

The rheology to describe the flow behaviour of avalanche and debris flow simulations in RAMMS is the Voellmy-Salm (VS-) model (Salm, 1993). This model is implemented because it is used in the SWISS Guidelines for avalanche runout calculations (Christen et al., 2010) and has proven to be numerically accurate and straightforward (Gruber and Bartelt, 2007; Sartoris and Bartelt, 2000). Also, other numerical models like e.g. DAN-3D have implemented the VS-model (Hungri and McDougall, 2009; Rickenmann et al., 2006). The RAMMS model solves for the unknowns of flow depth and velocity, in the horizontal x- and y- directions (Christen et al., 2010). The VS-friction model includes two parameters, the dry-Coulomb friction parameter  $\mu$  which is independent of the velocity and proportional to the normal stress at the bottom of the flow, and the velocity dependent “turbulent” or “viscous” friction parameter  $\xi$  which is a function of the velocity squared (Salm, 1993). The parameter  $\mu$  dominates when the mass is moving slowly and thus defines deceleration behaviour, and  $\xi$  dominates when the mass is moving faster (Bartelt et al., 2013). These two parameters can be set constant for the whole area of interest or regions can be defined, where the parameters vary because of vegetation, surface roughness differences or topographic changes (Christen et al., 2012). In simulations,  $\mu$  is usually set to the tangent of the slope angle in the deposition zone (used for calibration in RAMMS) (Bartelt et al., 2013). Calculation stops at a pre-defined threshold value of the maximum momentum [%]. For this, the momenta of all grid cells are summed and compared with the maximum momentum sum. If the momenta of all grid cells are less than the set threshold value, the debris flow is regarded as stopped and calculation is stopped (RAMMS::DEBRISFLOW interface). A more detailed explanation of the VS-model can be found in Salm, 1993 and Salm et al., 1990.

The velocity of the simulated moving mass is defined as the depth-averaged mean speed of the moving mass parallel to the slope. Because dense snow avalanches as well as debris flows are not homogeneously fluid and show clumps of denser material, wood or rock, there may be velocity fluctuations parallel to the slope but also non-parallel to it. Those fluctuations interact with the depth-averaged flow field, and this interaction is defined by the *Random Kinetic Energy (RKE)* extension of the VS-model in RAMMS (Preuth et al., 2010). This RKE extension is implemented as following: The total avalanche velocity in each coordinate direction x, y and z is composed of two parts, one is the steady-on-average velocity  $U_x$ ,  $U_y$  and  $U_z$  and one is the fluctuation velocity  $u_x$ ,  $u_y$  and  $u_z$ , while assuming the mean velocity in z-direction is  $U_z = 0$ . Both parts, the steady-on-average, as well as the fluctuation velocity are time dependent, but the first one is time dependent on a much longer timescale. Thus the kinetic energy of the flow can also be split into two parts, one associated with the slope parallel, steady-on-average movement of the flow and one with the fluctuating movement (Christen et al., 2010). By integrating the kinetic energy part of the fluctuation movement over the whole flow depth, the depth-averaged random kinetic energy is calculated. The depth-averaged production of energy determines RKE through shear work and its decay (Christen et al., 2010). While the transformation of potential energy into kinetic energy parallel to the slope is reversible, the RKE production is irreversible, because energy must be conserved which means that the rate of change of total energy inside the moving mass has to be equal to the rate of work done by external forces (Anderson, 1996; Davidson, 2004 in Buser and Bartelt, 2009). The rate of change of internal energies is composed of the heat rise and the net random kinetic energy, and external forces are the rate of change of translational kinetic energy, the change of potential energy of the avalanche and the frictional work rate. More detailed description about the RKE model can be found in (Buser and Bartelt, 2009).

The release of the mass can either be set to a single or multiple block release, where the whole mass is assumed to collapse at once, or set to a hydrograph. For a hydrograph, release information about the total volume, maximum discharge and time must be set. The events modelled in this study initiate as rock avalanches, where the whole mass collapses at once (block release). Because of this and because information

on velocity estimates and maximum discharge were either missing or broadly estimated, the events were modelled with a block release.

Output data of the model are two-dimensional maps and animations which can also be draped over topography. The results are not three-dimensional, because shallow water equations for granular flows do not give any vertical velocity information, which would result in different flow speeds at the top and the bottom of any given cell. Flow information is given on flow height, velocity, and pressure, for which also the maximum values can be displayed, and the results can be displayed over time. In the whole simulation area, profiles and point graphs can be generated and displayed. This feature is beneficial to determine runout distances, runup heights at valley sides and to compare the results at exactly the same position. Logfiles give information about the input data and every dump step calculation of the flow, when the results are written to the file used for visualisation, including the total mass at the end of the calculation time (Bartelt et al., 2013).

The DEMs used in this thesis are ALOS PALSAR elevation models. ALOS (Advanced Land Observation Satellite) was launched in 2006 by the Japan Aerospace and Exploration Agency (JAXA) and was active until 2011. The sensor PALSAR on the ALOS was an active microwave sensor which operated day and night independent of weather conditions ([https://lta.cr.usgs.gov/ALOS\\_Palsar](https://lta.cr.usgs.gov/ALOS_Palsar)). The DEM has a spatial resolution of 12.5 m and is thus better used for simulations as a 25 m ASTER GDEM or a 75 m SRTM DEM.

### 3.2.1.1 Standard version

The standard version of RAMMS::DEBRISFLOW models the event with input data of the topography (DEM), *release area*, *release volume* and *friction parameters*  $\mu$  and  $\xi$ . The flow calculation does not include erosion and entrainment of material.

### 3.2.1.2 Entrainment version

Different studies showed that the inclusion of erosion and entrainment of sediment material in debris flow modelling could increase the accuracy of runout predictions including runout distance, location, flow and depositional pattern (Frank et al., 2015; Scheuner et al., 2009), thus an entrainment algorithm was included in RAMMS::DEBRISFLOW. The entrainment algorithm is described in a study by Frank and colleagues (2015) where they describe the importance of entrainment in debris flow modelling. This chapter is mainly based on their study and further cited with other studies if necessary.

The entrainment algorithm is implemented in the standard version of RAMMS::DEBRISFLOW. This algorithm predicts the rate and depth of erosion as a function of basal shear stress with parameters derived from measurements at the test site in Illgraben, where the basal shear stress is determined by the product of the bulk mass density of the flow, the flow height, the acceleration due to gravity, and the inclination of the slope. Additional to the input parameters of the standard version, some more information about the erodible material must be given: *shapefile* of the area of erodible material, material properties like *erosion density*, *erosion rate*, *potential erosion depth*, *critical shear stress* and *maximum erosion depth*. The meaning of the additional parameters is given in the user manual of RAMMS::DEBRISFLOW (Bartelt et al., 2013) and summarised in Table 4.

In the RAMMS interface, default values for the erosion parameters are given. Those values were tested at the Illgraben and Spreitgraben test sites in Switzerland, which are two of the most studied debris flow sites in Switzerland. Both places show high debris flow activity and were therefore chosen to install several measurement installations to measure flow depth, front velocity and basal and lateral stresses.

Although the entrainment algorithm predicts channel bed erosion, the DEM is not modified during the simulation. Additionally, the collapse of lateral moraines and subsequent sediment input cannot be modelled in RAMMS. However, it is possible to subtract the predicted erosion depth after the simulation in the user interface which permits to model multi-event scenarios.

In their study, Frank and colleagues compared the front arrival time of hydrographs in standard and entrainment modelling and found that they are very similar. They concluded that calibrated  $\mu$  and  $\xi$  values

from standard modelling could also be used in the entrainment model for the same study site. Therefore,  $\mu$  and  $\xi$  values were calibrated in this study only for the standard version of all three modelled events (3.2.2) and used then also for simulations with the entrainment version.

Table 4 Parameters for erosion rates (summary of RAMMS::DEBRISFLOW user manual (Bartelt et al., 2013))

<i>Erosion density [kg/m<sup>3</sup>]</i>	The erosion density describes the density of the entrained material.
<i>Erosion rate [m/s]</i>	The erosion rate is the rate at which debris flows entrain material from the sediment bed. This erosion rate is active from the time when the critical shear stress is exceeded until the actual erosion depth reaches the maximum erosion depth (Frank et al., 2015). Increased erosion rate will cause sediment to be entrained at a faster rate, potentially resulting in relatively large debris flow snouts.
<i>Potential erosion depth [per kPa]</i>	The potential erosion depth is a function of the maximum shear stress calculated in each grid cell and determines the maximum possible depth of erosion in the z-direction (vertically).
<i>Critical shear stress [kPa]</i>	The critical shear stress is the value at which erosion can start occurring. It might be reasonable to expect that a channel bed consisting of interlocked boulders would have larger critical shear stress, while a channel bed of saturated sandy gravel would have a lower value.
<i>Maximum erosion depth [m]</i>	The maximum erosion depth defines the maximum thickness of the layer of erodible sediment.

### 3.2.1.3 Extended version

The extended version was initially developed for snow and powder avalanches and was then extended for debris flows. Compared to the entrainment version, the extended model takes rock, ice, water and air into consideration. Temperature changes through friction inside the moving mass can cause meltwater production and thus a flow transformation. Here, all dissipative energy generated through shearing, granular collision and entrainment is used to raise the temperature of the moving mass. As soon as the temperature goes over 0°, the dissipative energy is used to melt ice and thus produce meltwater. Temperature remains at 0°C then until nothing is left to be melt (Bartelt et al., 2018, in review).

The model needs the same input parameters as the standard version and some additional information about the released and the entrained material. Additional information about the release part is the *initial temperature* [°C] which also defines the amount of meltwater production, and the *volumetric water content* [mm/m<sup>2</sup>]. The areas where material can be eroded can be drawn in GIS software as for the entrainment version. Here, information is needed about the *thickness* [m], *density* [kg/m<sup>3</sup>], *temperature* [°], *volumetric water content* [%] and *erodibility* of the material. The erodibility defines, how much of the material can be eroded and hence corresponds to the maximum erosion depth of the entrainment version. For the entrainment rate, which is the amount of material which was initially at rest and now moving with the mass at the same speed, *yield stress* can be used, if a shear factor is known as in the entrainment version (Bartelt et al., 2018, in review). The *erosion law* can be set to *velocity driven*, then the velocity of the moving mass defines, if and how much material gets eroded. Further, the *activation energy* [kJ/m<sup>3</sup>] and a *dry-wet-transition value* [mm] can be defined. The *activation energy* defines how fast the volume of the moving mass expands and hence decreases the flow density (Bartelt et al., 2018, in review). The *dry-wet-transition value* is a measure of the water film on particles and thus defines the lubrication of the mass.

This version of the model RAMMS needs a lot of specific parameters which can only be known when measured in the field. For the events which will be modelled here, values measured at the event in Bondo are used, if not better known from literature, since those values have proven to represent the event most realistic and accurate (Personal communication with Perry Bartelt, slf).

### 3.2.2 Modelled events

To choose the events to be modelled, a selection process was needed to define the events, which are most comparable to the event in Bondo. As a first criterion, the ratio of initial versus deposited volume (entrainment ratio) had to be higher than two (Figure 4). For more than half of the events in the inventory, no information was given about the initial volume since scientists were merely interested in the deposited mass.

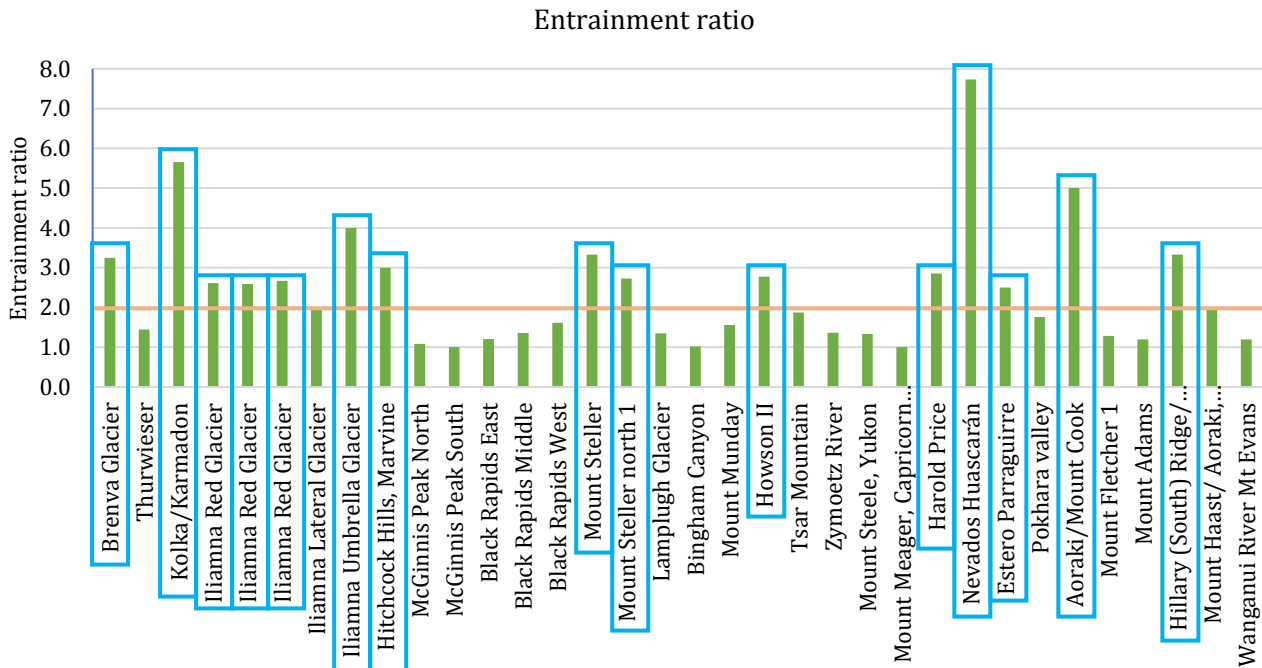


Figure 4 Entrainment ratio of events  
Orange line marking the set threshold of ER = 2 for the modelled events  
Blue squares show events with ER  $\geq$  2

Events meeting this criterion are Brenva Glacier, Kolka/Karmadon, Iliamna Red Glacier (1978, 1980, 2003), Iliamna Umbrella Glacier, Hitchcock Hills Marvine, Mount Steller, Mount Steller North 1, Howson II, Harold Price, Nevados Huascarán, Estero Parraguirre, Aoraki Mount Cook and Hillary South Ridge.

The Mc Ginnis South Peak event and the Mount Meager event show both ratios of initial versus deposited volume of one. In the case of the Mc Ginnis South Peak landslide, this is because scientists talk about the involved material and do not distinguish between initial and deposited one (Jibson et al., 2006). In the case of the Mount Meager event, the initial and the deposited volume are both only assumed by scientists in the absence of highly resolved DEMs (Allstadt, 2013; Guthrie et al., 2012; Roberti et al., 2018, 2017). Although the ratio is 1.1 for the Mount Meager event, this event was also considered for modelling, since scientists are sure about the entrainment of a significant amount of sediments and ice.

As a second criterion, the events should have entrained saturated sediment, snow or ice. This criterion was not explicitly mentioned in most studies, and for this, the entrainment ratio was compared to the angle of reach. Here, events with low angles of reach (lower than 15°), meaning events with fluid-like motion, and entrainment ratios larger than two, represent events which must have entrained a significant amount of snow, ice or saturated sediment (Figure 5 blue square). Events meeting this criterion are Kolka/Karmadon, Iliamna Red Glacier (1978, 1980, 2003), Harold Price, Nevados Huascarán and Estero Parraguirre.

A third criterion was a mentioned flow transformation. Since the event in Bondo started as a dry rock avalanche and resulted in a debris flow, even though there was no flow transformation but more remobilisation of deposited material, this criterion is fundamental to gain process understanding of events showing similar flow mechanisms.

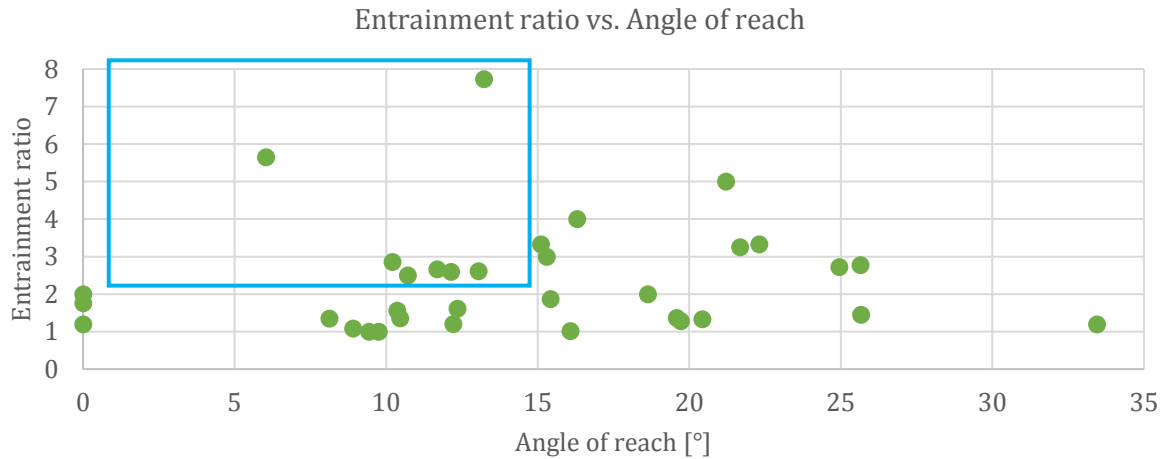


Figure 5 Entrainment ratio vs. Angle of reach  
 Blue square indicates events with Angles of reach lower than 15° and Entrainment ratios larger than two

Events with entrainment ratios greater than two and mentioned flow transformation are Kolka/Karmadon, Harold Price, Nevados Huascarán and Estero Parraguirre. Events where a flow transformation is not explicitly mentioned, but which showed flow-like behaviour are Brenva Glacier, Mount Steller, Howson II, Aoraki Mount Cook and Hillary South Ridge. From these ten events, those were dismissed, which showed high snow cover (2-4 m of snow), because these events are not comparable to the event in Bondo. Such events with high snow cover are Kolka/Karmadon, Nevados Huascarán and Estero Parraguirre. The only event meeting all three criteria is Harold Price rock avalanche-debris flow. From the other events left, Brenva Glacier, Mount Steller, Aoraki Mount Cook and Hillary South Ridge were dismissed because they are not well documented, show high temperature changes before the event or show high ice content in the initial detaching mass. The Howson II rockslide event was modelled as well although it shows a high angle of reach. Here, the environmental conditions of a thinning glacier and thus a debutting and destabilising effect on adjacent mountain walls as well as the path travelled onto a glacier surface of 150 m can be compared well to the event in Bondo. As a third event to be modelled, the Mount Meager rock slide-debris flow was chosen. This event shows distinguishing features of a flow transformation into a debris flow, although not explicitly mentioned. This event was already modelled with the numerical model DAN-W (one-dimensional) and is very well documented (Guthrie et al., 2012).

So, the three modelled events are Mount Meager 2010, Howson II 1999 and Harold Price 2002. These three events took all place in the Coast Mountains of British Columbia, USA. In British Columbia, the majority of giant rock avalanches happened at slopes above glaciers, where the retreat of glaciers in the last century caused debutting and expansion of cracks of adjacent slopes (Geertsema et al., 2006). The Coast Mountains show very high annual rainfall (more than 2500 mm) and heavy snowfall in winter. The landscape is dominated by dense coniferous trees ([www.britannica.com/place/Coast-Mountains](http://www.britannica.com/place/Coast-Mountains)).



Figure 6 Location of British Columbia and modelled events (black stars)  
 (<https://geology.com/canada/british-columbia.shtml>)

### 3.2.2.1 Mount Meager rock slide-debris flow, British Columbia, 2010

The description of the Mount Meager event is based on information from a paper of Guthrie and colleagues (2012), one of Allstadt (2013) and two papers of Roberti and colleagues (2018, 2017).

Mount Meager lies in the Coast Mountains of British Columbia ( $50^{\circ} 37.38' N$ ,  $123^{\circ} 30.06' W$ ). On the 6<sup>th</sup> of August 2010, an immense landslide started as the collapse of the southern flank and the secondary peak of Mount Meager. The failure occurred in four stages happening with 20 seconds to two minutes delay. The collapsed material of 48-50 million  $m^3$  travelled over the Capricorn Glacier for around 500 m and flowed then 7 km onto the saturated flank of Capricorn Creek where it entrained a significant volume of material and transformed into a very rapid channelized debris avalanche. At the Capricorn Creek – Meager Creek confluence, the mass ran around 270 m up the opposing wall and then divided into two minor flows, one flowing around 3.4 km up Meager Creek and one flowing 4.7 km downstream into the Lillooet River Valley. In the Lillooet River Valley, the mass spread out on the valley floor and stopped around 2 km below the confluence of Meager Creek and Lillooet River (Figure 9). Deposited material was found on the whole flow path, but most of the debris was deposited in the Lillooet River Valley and at the mouth of Capricorn Creek. The deposited volume was estimated around  $53 \pm 3.8$  million  $m^3$ , the average velocity was 45 m/s. The landslide travelled a vertical distance (H) of 2'183 m and a horizontal distance (L) of 12'700 m yielding an angle of reach of  $9.8^{\circ}$ . The damage of this massive landslide was high, although it happened in remote area. The costs of the destruction of roads, bridges and around 110'000  $m^3$  of wood, the damming and subsequent threat of an outburst flood of Meager Creek, causing the evacuation of around 1'500 inhabitants, were estimated around 10 million Canadian Dollars.

This landslide is one of the largest to have occurred all over the world since 1945. The collapse was probably triggered by elevated pore water pressures after a late summer heatwave which enhanced glacier melt and permafrost thaw. After the event, Roberti et al. observed a great quantity of water issuing from the scarp. The location of the seepage zone as well as estimations of possible water storage of fractured volcanic rocks of 30 % (Delcamp et al., 2016), led to estimations of around 6 million  $m^3$  of water which was released with the initially collapsing rock mass.

This landslide can be compared very well to the event in Bondo. Although the volume of the Mount Meager landslide is more than 15 times higher, the movement of the rock avalanche and the debris flow are very similar to the ones in Bondo. Figure 7 shows the steep terrain and the narrow valley Capricorn Creek, which channelized the flow path of the Mount Meager landslide. Though the low slope angle at the mouth of Capricorn Creek, the landslide streamed a considerably long distance into the Lillooet River Valley. Figure 8 shows the steep terrain in the initiation zone of the landslide and indicates the very high vertical distance of the landslide.

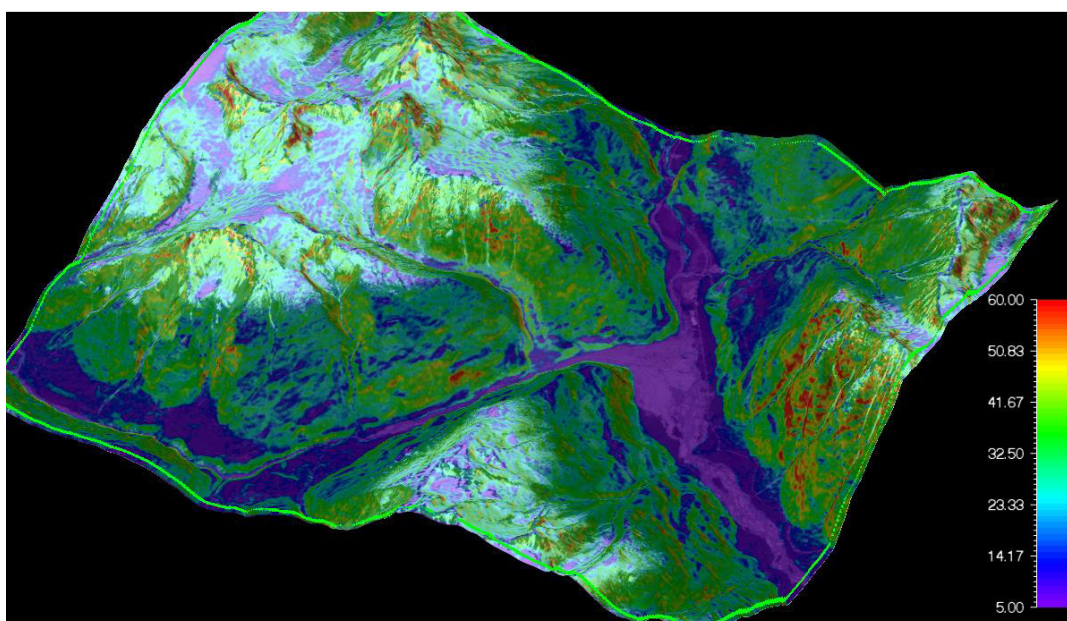


Figure 7 Slope Angle [ $^{\circ}$ ] of the Mount Meager environment (RAMMS interface)  
Dashed, red line indicates the release area of the landslide

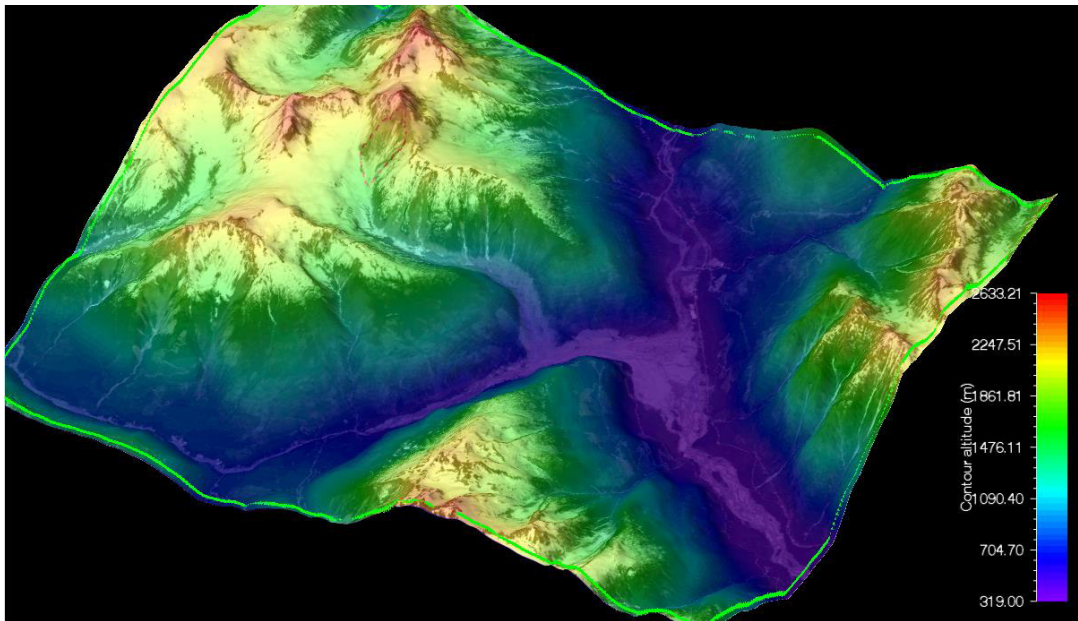


Figure 8 Elevation [m.a.s.l.] of the Mount Meager environment (RAMMS interface)  
Dashed, red line indicates the release area of the landslide

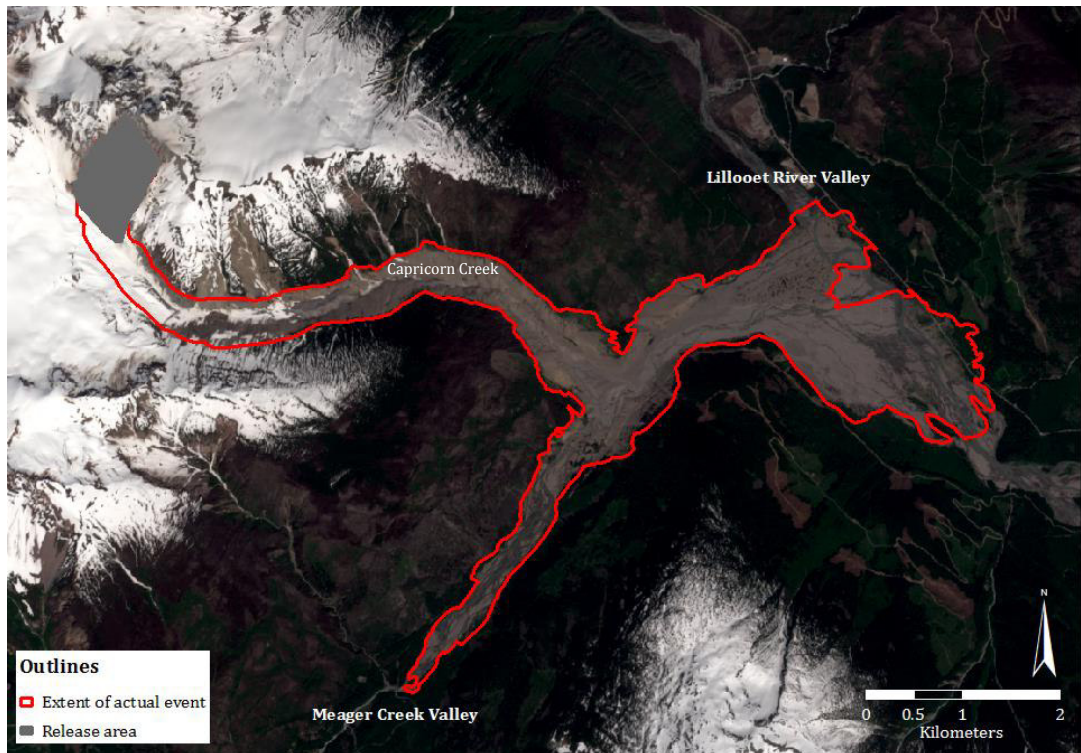


Figure 9 Extent of the Mount Meager rock slide-debris flow  
Shapefiles of release area and event extent received from Gioachino Roberti  
Orthophoto: Sentinel-2A, 25.06.2017

3.2.2.2 Howson II rock slide, British Columbia, 1999

The description of the Howson II event is based on information of the two papers of Schwab and colleagues (2003) and Geertsema and colleagues (2006).

Howson is located west of Smithers British Columbia (53° 31' N; 127° 46' W). On the 11<sup>th</sup> of September 1999, a rock avalanche originated at 1'923 m.a.s.l. on a north-western slope as a topple of around 0.9 million m<sup>3</sup> of rock. The rock avalanche slid 150 m over glacial ice on a width of 300 m before it fell into Limonite Creek valley and travelled through forested area until it deposited at flatter slopes (5-10°) (Figure 10). In the forested area, the slide path covered an area of 1200 m length and up to 400 m width. Trees were uprooted and snapped, which leads to velocity estimates of 18-30 m/s necessary for this effect (Cruden and Lu, 1992 in Schwab et al., 2003). The deposited material showed a surprisingly low content of trees, although the

travel distance through the forest was very far. The rock slide flowed channelized between lateral moraines (Figure 11). The total volume of deposition was around 2.5 million m<sup>3</sup>, leading to a high entrainment ratio of 2.8. The vertical distance (H) was 1'296 m, and the horizontal distance (L) was 2'700 m, yielding an angle of reach of 25.64°. A contributing factor for the release of the mass is the thinning of Howson glacier, leading to a debuttressing and thus destabilising effect. Precipitation rates above average causing excessive joint water pressures and freezing night temperatures leading to frost wedging may possibly have been the triggering factor. The damage of the rock avalanche was quite high. The immense energy of the avalanche and the resulting air blast destroyed part of the forest and a natural gas pipeline and dammed the Limonite Creek creating a lake which was filled the days after the event. Figure 11 and Figure 12 show the steep release zone and the rather low slope angle of the flow path. At the end of the lateral moraines, the slope angle increases slightly, which allowed high velocities of the landslide and possibly caused the tree uprooting.

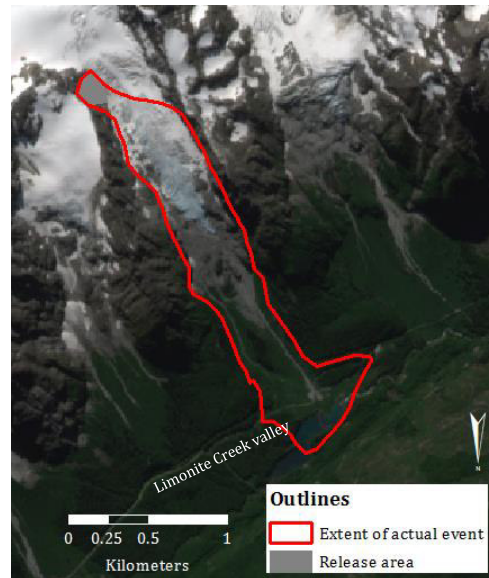


Figure 10 Approximate release area and extent of the Howson rock slide  
Orthophoto: Sentinel-2A, 03.08.2017

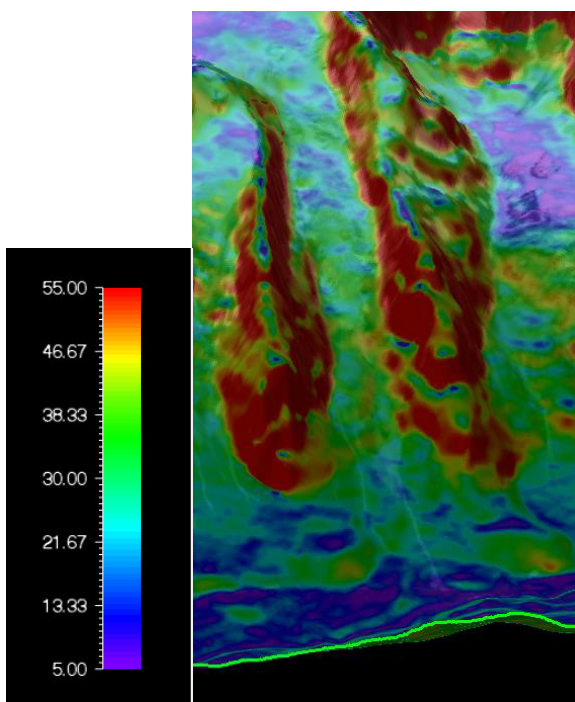


Figure 11 Slope angle [°] of the Howson II environment (RAMMS interface)  
Dashed, red line indicates the release area of the landslide

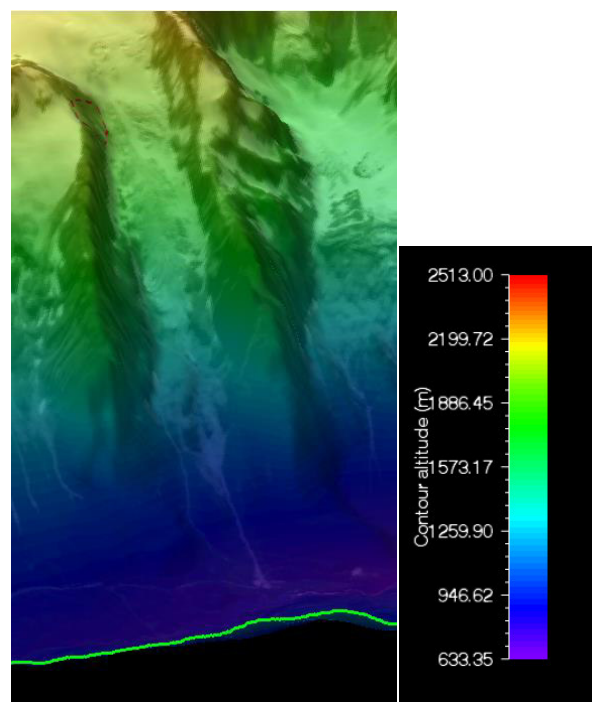


Figure 12 Elevation [m.a.s.l.] of the Howson II environment (RAMMS interface)  
Dashed, red line indicates the release area of the landslide



3.2.2.3 Harold Price rock avalanche-debris flow, British Columbia, 2002

The description of the Harold Price event is based information of the two papers of Schwab and colleagues (2003) and Geertsema and colleagues (2006).

Harold Price is located northeast of Smithers British Columbia (55° 04' N; 126° 57' W). The avalanche originated at the lip of a south-west facing cirque covered by a rock glacier at an elevation of 1'723 m.a.s.l. and happened sometime between the 22<sup>nd</sup> and 24<sup>th</sup> of June 2002. The failed material of around 0.7 million m<sup>3</sup> collapsed in an initiation zone around 175 m wide and 30 m deep. The collapsed material of weathered volcanic bedrock and rock glacier material fell 300 m onto the open valley, spread to a width of about 360 m and moved for around 1.3 km until it transformed into a debris flow. About 2.2 km below the initiation zone, the debris flow entered a small stream channel and flowed further downstream for around 1.8 km to Harold Price Creek. Reaching Harold Price Creek, the debris flow re-routed the stream and transported logs and forest debris 3.5 km further downstream (Figure 13). Most of the transported material were trees and forest debris, and only a small part of the rock and debris from the initial landslide reached the Harold Price Creek. The vertical distance (H) was 720 m, and the horizontal distance (L) was 4000 m, which yields an angle of reach of 10.2°. The total displaced volume was estimated to be around two million m<sup>3</sup> leading to a rather high entrainment ratio of 2.9. Calculated flow velocities from runup and superelevation, where the rock avalanche reached the base of the mountain, were 28-35 m/s. In the channelized zone, the debris flow showed slower velocities than 7 m/s. Figure 14 and Figure 15 show the steep slope angle in and below the initiation zone. The rest of the flow path shows rather low slope angles and a regular terrain.

On the day of the event, there was much snow (150 to 200% of normal for June) and the Harold Price river had high discharge. The water from the river could have supported the fluidity of the debris flow and enlarged the runout distance. A triggering factor for the event could have been degrading permafrost in the rock glacier. Furthermore, mild temperatures in winter and cool summer temperatures could have increased freeze-thaw cycles within the active layer of mountain permafrost and therefore destabilised mountain flanks.



Figure 13 Approximate release area and extent of the Harold Price rock avalanche-debris flow  
Orthophoto: Sentinel-2A, 02.10.2017

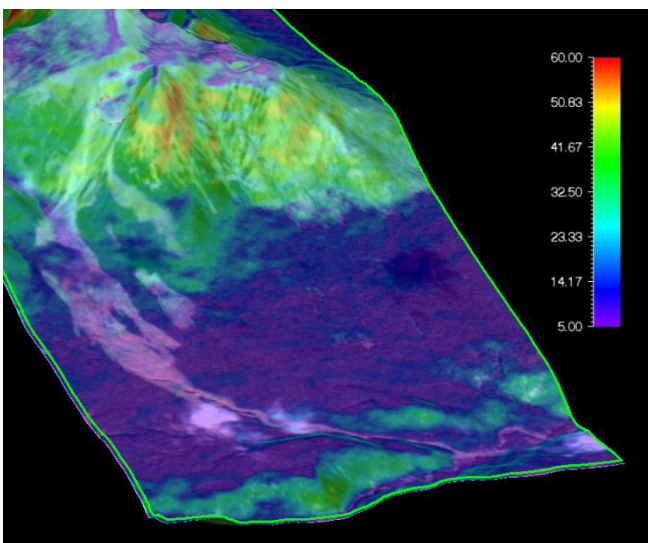


Figure 14 Slope angle [°] of the Harold Price environment (RAMMS interface)  
Dashed, red line indicates the release area of the landslide

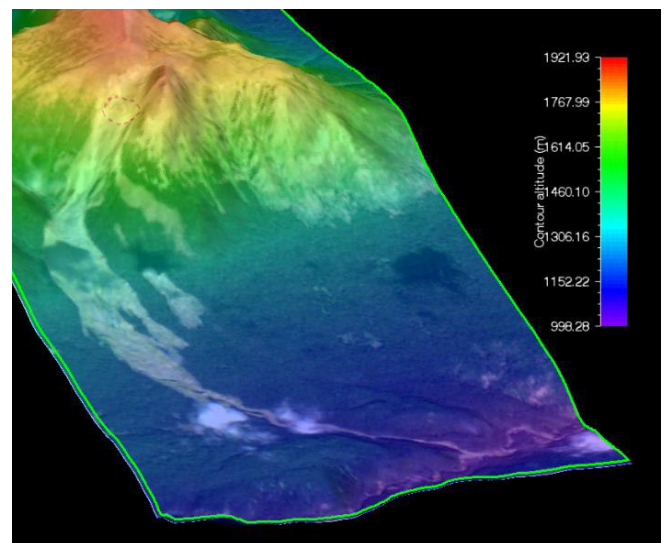


Figure 15 Elevation [m.a.s.l.] of the Harold Price environment (RAMMS interface)  
Dashed, red line indicates the release area of the landslide

## 4 Results

### 4.1 Parameter investigation

The parameters collected in the inventory were investigated quantitatively to decide if it is possible to compare the events. As an overview, Figure 16 shows a map with the events from the inventory marked in blue.



Figure 16 World map with inventory events  
Blue marks indicating the place of the events

The naming of an event differs from literature to literature. In some cases, the naming follows the landslide classification (chapter 2.6), in other cases, the naming is based on an analysis of the deposited material from scientists investigating the event. Especially for events containing rock and ice the two terms rock-ice avalanche and ice-rock avalanche are used interchangeably.

#### 4.1.1 Flow parameters

Fall height [m]	Flow speed [m/s]	Area of deposition [km <sup>2</sup> ]
Initial rockfall volume [m <sup>3</sup> ]	Water content [%] or [m <sup>3</sup> ]	Volume of deposition [m <sup>3</sup> ]
Path over glacier surface [m]	Vertical distance [m]	Ratio initial vs deposited volume
Duration [s]	Horizontal distance [m]	Flow transformation [0; 1; X]
Number of surges [n]	Angle of reach [°]	

In most cases, there is no information given about the *initial fall height*. Usually, rockfalls or rock avalanches do not fall in free fall but initiate in a sliding motion. Thus, the fall height is mostly not given in literature, because the impact point cannot be determined precisely.

Unfortunately, the *duration* of massive landslides is seldom analysed. In the few cases, where the duration is given, it is calculated from seismic measurements from which the landslide could be detected. It would be interesting to compare the duration of a landslide with its initial volume and its path over a glacier surface to detect if the path over a glacier surface increases flow speed and thus decreases the duration of a landslide. For this inventory, there is not enough information given about the duration of the landslides to detect a correlation between these parameters.

Seismic measurements can also give information about the *number of surges* of a landslide. In seldom cases, where eyewitnesses see the event happening, they can also give information about the number of surges.

Nevertheless, eyewitnesses' information is subjective and may not represent the actual event. Table 11 shows that this information is only given for a very few events.

Information about *flow speed* is given for around half of the events in the inventory. The distribution of the average speed shows that there are only a few events which flowed faster than 70 m/s and that the majority of the events in this inventory flowed with 29 to 37 m/s (Figure 17).

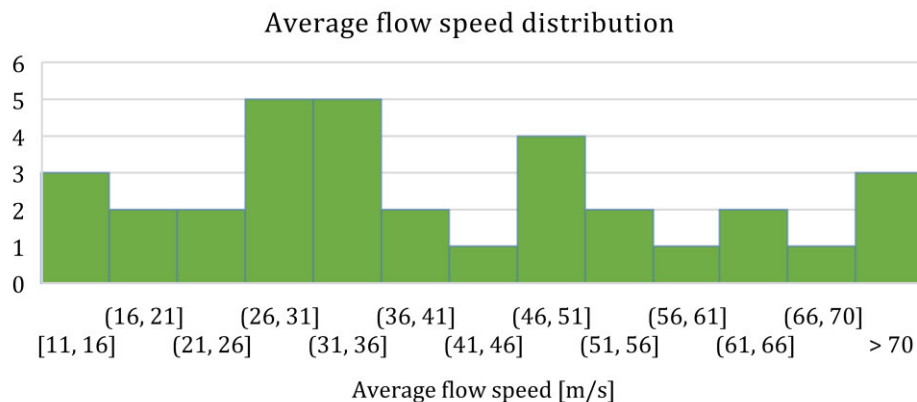


Figure 17 Average flow speed distribution of events

Deline and colleagues (2015) investigated rock avalanches which travelled over glacier surfaces and analysed different parameters of these events including ice and snow content. In the inventory presented here, information about *water content* is mostly taken from their study. The information is given either in *m<sup>3</sup> ice and snow volume of the deposit*, or *% of the total rock and ice deposited volume*. For other events, which were not investigated by Deline et al., scientists estimated water content depending on the flow behaviour of the debris flow or on the volume increase of the event. It would be fascinating to take measurements of the liquid water content of the deposited volume of an event. This information could help in analysing meltwater production and give information about energy production and dissipation during the flow. Unfortunately, measurements of liquid water content in deposited materials of landslides are unusually taken just after the event happened and hence do not represent the meltwater production or entrainment of liquid water during the event.

For around half of the events in the inventory, it is mentioned, if there was a *flow transformation* or not (Figure 18). For the other half of the events, there is no information given about a flow transformation process. There are nine events in the inventory, which did show a flow transformation Kolka/Karmadon, West Salt Creek main, Devastation Glacier, Zymoetz River, Mount Meager (Capricorn Glacier), Harold Price, Nevados Huascaràn, Estero Paraguirre and Pokhara Valley.

The *initial volume* is not given for most of the analysed events. In cases, where the initial volume is given in literature, the volume was calculated from DEMs taken before and after the event. This method is an excellent attempt to calculate the initial volume since it is simple, but the acquisition time of the DEMs plays an essential role for exact calculations. When the DEM has been taken a long time before the event, the topography could have been changed in the time until the event, e.g. by rockfall-, rock avalanche activity or erosion and hence does not represent the actual topography before the event. This time interruption can cause calculation errors of the detached volume. Furthermore, DEMs from steep mountainous regions might show artefacts or low spatial resolution because of shadowing effects.

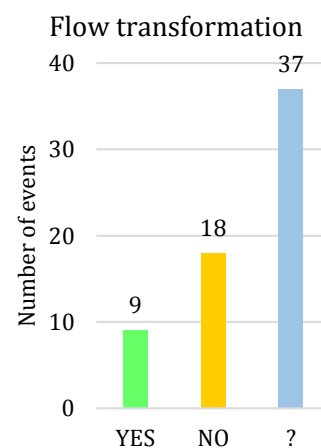
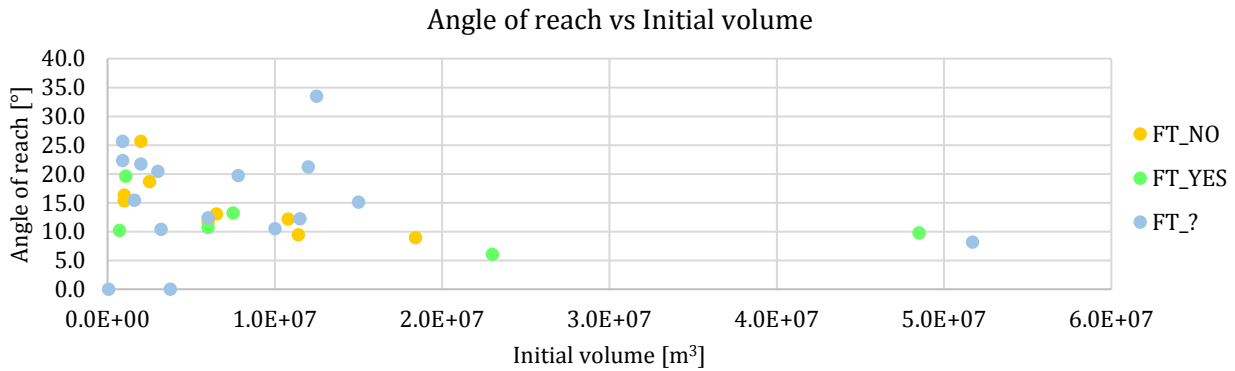
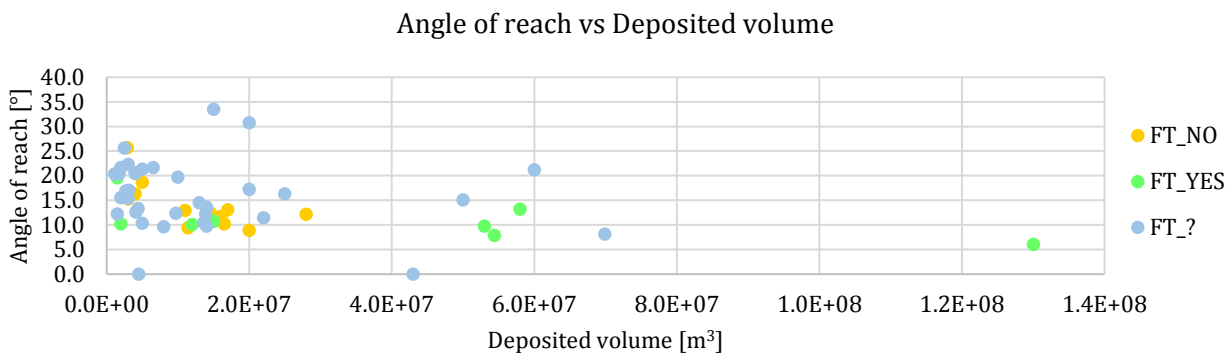


Figure 18 Number of events with and without Flow transformation



*Figure 19 Initial volume vs Angle of reach*  
*Orange: No flow transformation*  
*Green: Flow transformation*  
*Blue: No information about flow transformation*



*Figure 20 Deposited volume vs Angle of reach*  
*Orange: No flow transformation*  
*Green: Flow transformation*  
*Blue: No information about flow transformation*

Figure 19 and Figure 20 show the initial volume and the deposited volume respectively compared to the angle of reach, subdivided into events without flow transformation (orange, FT\_NO), events with flow transformation (green, FT\_YES) and events with no information about a flow transformation (blue, FT\_?). Figure 19 indicates a slight trend that events with low initial volumes show high angles of reach and events with large initial volumes show low angles of reach. This trend was expected, because events with large initial volumes, and thus large mass and high potential energy, reach longer horizontal distances with lower vertical distances as events with low initial volumes and hence low mass and low potential energy. On the other hand, the subdivision into events with and without flow transformation does not indicate the expected result. Expectations were to see events with flow transformation to indicate much lower angles of reach than events with no flow transformation. Figure 20 visualises that all events without flow transformation have total volumes lower than 30 million m<sup>3</sup> and angles of reach between 10° and 19°. Half of the events with flow transformation show similar deposited volumes and angles of reach as events without flow transformation. The other half of the events with flow transformation show deposited volumes of 50 million m<sup>3</sup> up to 130 million m<sup>3</sup>, which is 180% to 400% of the events without flow transformation. The angle of reach of such large events is slightly lower than the average angle of reach of events without flow transformation. The events, where no information is given about a flow transformation, are spread in this figure and show deposited volumes up to 70 million m<sup>3</sup> and angles of reach between 8° and 33.5°.

Information about the *horizontal* and the *vertical distance* of a landslide explains a lot about the flow mechanism. I would expect a correlation between these two parameters, as a high vertical distance generates high potential energy and thus leads to a long horizontal distance. For the events in this inventory, the ratio

of vertical and horizontal distance shows no real trend (Figure 21).  $R^2$  is relatively low for all events (0.55), and even without the three unusually huge events Kolka/Karmadon, Nevados Huascarán and Estero Parraguirre (marked in blue square in Figure 21),  $R^2$  is even lower (0.43).

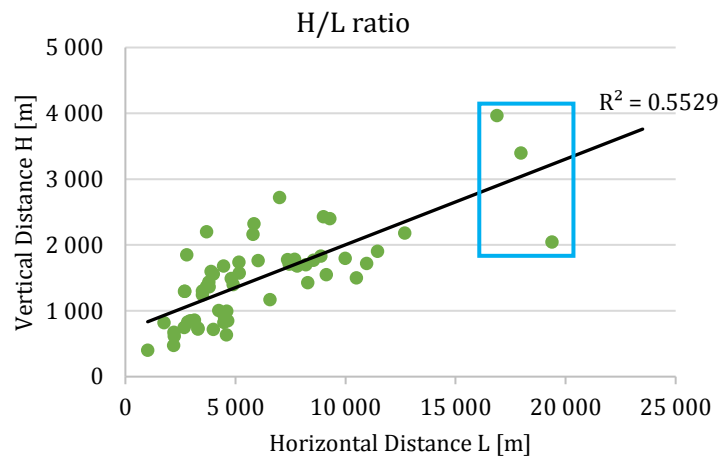


Figure 21 H/L ratio for each event  
 black: regression of all events  
 blue square indicating three unusually large events  
 (Kolka/Karmadon, Nevados Huascarán, Estero Parraguirre)

Schneider and colleagues (2011b) found that the surface roughness of the ground a landslide is sliding on has an essential impact on the runout behaviour of the moving mass. Thus, the not existing correlation can be explained by the different surface roughness, as well as by differing climatic and environmental conditions of the events. Another reason for the non-existing correlation could be different ways to determine H and L of large landslides: There are some massive landslides in the inventory that did initiate in a mountain flank or as a glacier collapse, after some smaller rock- or snow avalanches loaded material on the failing surface. This loading could have occurred days to months or years before the actual large landslide initiated. In such cases, H and L must be determined from the starting zone of the large landslide itself and not from the failure zone of the smaller rock- and snow avalanches. This is because the H/L concept is based on potential energy considerations and the potential energy of these smaller avalanches has nothing to do with the potential energy of the actual massive landslide. Also, for large rock- or rock-ice avalanches that deposited in steep terrain, from which a debris flow initiated seconds, minutes, hours or years later, H and L must be determined separately for the avalanche and the debris flow, because the material stopped in the time between these two events. If H and L are not determined separately for such subsequent events, they do not represent the potential energy of the different processes and therefore cannot be compared to events with flow transformations, where H and L are correctly determined from the starting point of the initially failing mass to the end of the deposition area of the transformed flow.

The length of the *path over a glacier surface* is mostly given for the events in the inventory. The path over a glacier surface can significantly influence the flow mechanism of landslides and thus may impact the angle of reach and the entrainment ratio. Figure 22 shows that the path over a glacier surface does not have a significant impact on the angle of reach, but the entrainment ratio increases slightly for some events with path lengths over a glacier surface longer than 8'000 m. These events are Iliamna Red Glacier 1994 and 2000, McGinnis North and South Peak 2002. For these events, glacier trajectory was 93% or more, meaning that almost the whole horizontal distance travelled by the landslide was over a glacier surface. Looking at the influence of the glacier trajectory on the entrainment ratio of all events (Figure 23), one can see that higher entrainment ratios of two and more can be expected for glacier trajectories of 60% or more. There are two events with very high entrainment ratios and comparably low glacier trajectories. These events are the Kolka/Karmadon rock-ice avalanche 2002 and the Nevados Huascarán 1970 debris flow, which both entrained immense amounts of snow and ice and showed extremely long runout distances. Thus, the low glacier trajectories did not have any influence on the long runout distance of these two events.

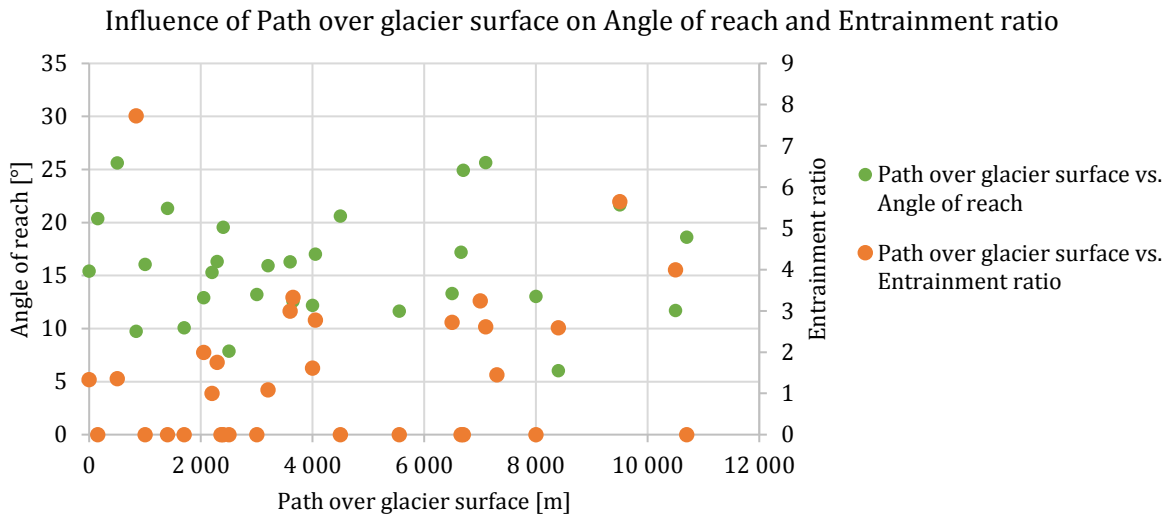


Figure 22 Influence of Path over glacier surface on Angle of reach (green) and Entrainment ratio (orange)

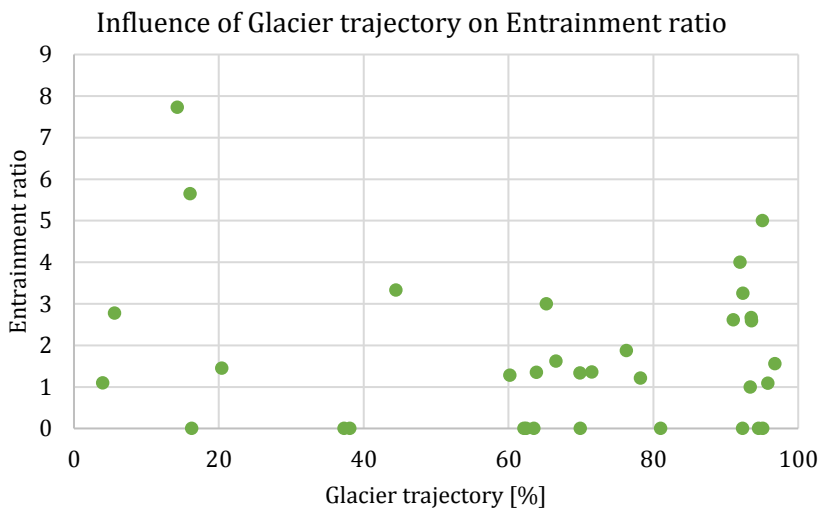
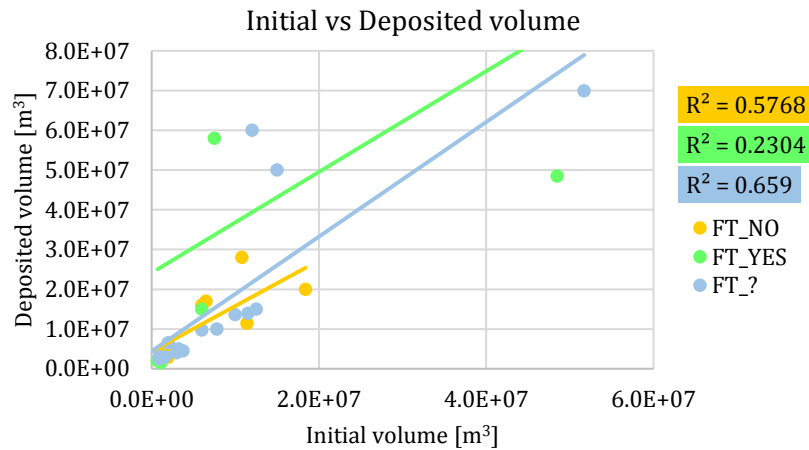


Figure 23 Influence of Glacier trajectory on Entrainment ratio

For 37 out of the 64 events in the inventory, information is given about the *area of deposition*. For events happening in remote areas, the area of deposition is mostly derived from satellite images. As mentioned before, the steep mountainous topography and cloudy weather may negatively impact the quality of satellite images and thus complicate the precise detection of the area of deposition. Furthermore, it may be difficult to define where the area affected by the landslide ends and where the area of deposition starts.

Apart from the vertical and horizontal distance, the *volume of deposition*, or total volume, is one of the most critical parameters of a landslide. Combined these three parameters give information about the impact energy of a landslide and are hence very important for the construction of protection measures. Compared to the initial volume, the volume of deposition indicates how much material has been entrained into the moving mass during the event. Figure 24 shows the correlation between the initial and the deposited volume of the events in the inventory. The figure shows a rather low  $R^2$  for the events with flow transformation ( $R^2 = 0.23$ ) and higher, but still low  $R^2$  for the events without flow transformation ( $R^2 = 0.58$ ) or without any information about it ( $R^2 = 0.66$ ).



*Figure 24 Initial vs Deposited volume*  
*Orange: No flow transformation*  
*Green: Flow transformation*  
*Blue: No information about flow transformation*

#### 4.1.2 Environmental conditions

Triggering Factor  
 Water source

In most cases, the *triggering factor* is not 100 % identifiable. In cases where an earthquake happened shortly before the event, scientists defined these as the triggering factor, although other circumstances have possibly conditioned the starting mass. Usually, different factors are interacting and finally triggering a landslide, as e.g. Exceptionally warm spring and summer temperatures which lead to glacier downwasting, permafrost thawing and meltwater production; raising pore water pressure through freeze-thaw cycles; unusually high precipitation rates in summer mobilising loosely deposited sediment.

There are all possible *water sources* represented in the inventory. In cases with high rainfall or snowfall activity before the event, saturated sediment and snow are mentioned as possible water sources. For a few events, no additional water source is mentioned next to the ice or snow already contained in the initially collapsing mass. For these events, the flow path of the landslide was analysed and possible water sources on the way of the mass flow as saturated sediment, glacier ice or water from rivers are mentioned as possible sources of water for flow transformation.

#### 4.1.3 Physical parameters

Rock type  
 Density [kg/m³]  
 Energy balance calculated [J]  
 Energy balance in literature [J]  
 Meltwater production [m³]

The physical parameters *Rock type* and thus *density* were used to calculate the energy of the landslide. The *energy calculated* is similar to the energy mentioned in literature, if there is information about this parameter, which is seldom the case.

To calculate *meltwater production* the specific melting heat of ice is needed: 334 kJ/kg. The temperature of the ice must first be heated to 0° Celsius before it can be melted. Thus, in a moving landslide, the energy is first used to heat up the entrained snow and ice up to 0° Celsius before meltwater can be produced. Next to the available energy, meltwater production is also depending on the size of the ice particles: Small ice particles will melt relatively quickly, however, large particles, if they are not crushed by the flow, will take longer to melt because the rate of heat transfer in the ice is not instantaneous. However, this process is not

## Results

considered in this thesis because it would require information on the size distribution of the ice particles, which is unavailable. Figure 25 shows the amount of possible meltwater production compared to the deposited volume. One can see clearly that events without flow transformation and small deposited volumes show low possible meltwater production and events with flow transformation and larger deposited volumes indicate higher possible meltwater production. The two events with very high possible meltwater production are the Kolka/Karmadon rock-ice avalanche 2002 and the Lamplugh Glacier rock avalanche 2016. Both these events were very large with high initial and deposited volumes leading to high energies and thus high possible meltwater production. Both, the Kolka/Karmadon and the Lamplugh Glacier avalanche entrained an immense amount of ice and snow and showed very long runout distances (Besette-Kirton, 2017; Besette-Kirton et al., 2018; Haerberli et al., 2004, 2003; Huggel et al., 2005; Kotlyakov et al., 2004). Thus, the maximum possible meltwater production calculated here appears to be useful to estimate the meltwater production of the actual events.

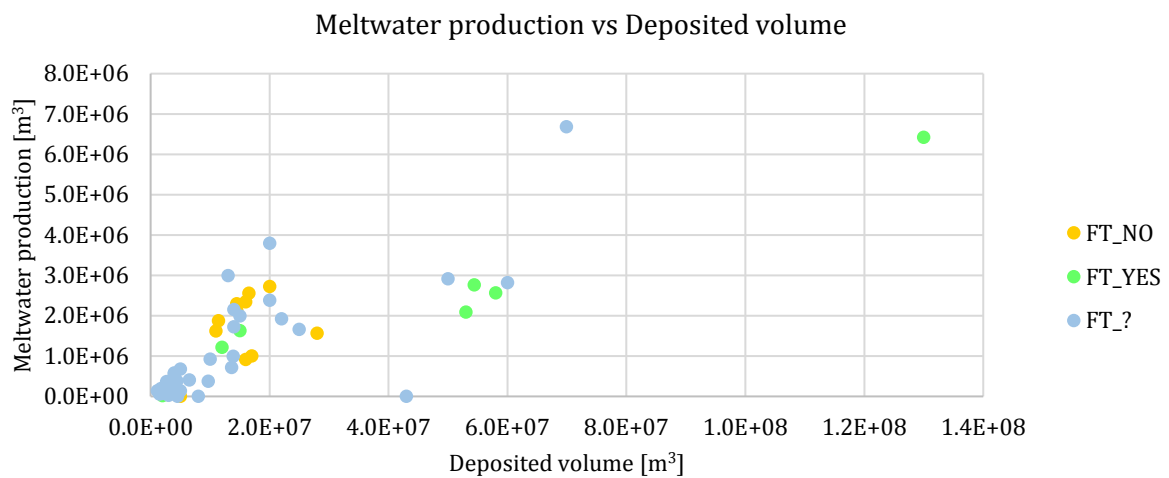


*Figure 25 Meltwater production vs Deposited volume*  
*Orange: No flow transformation*  
*Green: Flow transformation*  
*Blue: No information about flow transformation*



## 4.2 Simulation results

This section shows the simulation results of the modelling with the standard and entrainment version of RAMMS::DEBRISFLOW and the extended version of RAMMS::AVALANCHE. For each modelling, the duration of the simulation, runout distance, maximum flow height at specific points, maximum velocity, released and total volume and runup height at valley turns are displayed (Table 7, Table 8 and Table 9) and compared in the chapter Discussion to analyse the quality of the different versions. All input and output parameters can be found in the logfiles of the simulations in the appendix (chapter 8.2, pp. 70). The total volume is calculated as the sum of the initial plus the eroded volume for the entrainment and the extended version. For these two versions, it is thus not possible to determine, how much material was deposited in the affected area. For the standard version, the moving volume calculated at the last time step was taken as total volume. Here, the mass deposited in the affected area could be calculated as the difference between the initial and total volume, since this version does not include material erosion and entrainment.

Different friction parameters  $\mu$  and  $\xi$  were tested in the standard version of RAMMS for each event. Those friction values which resulted in runout distance and flow behaviour most like the actual event were chosen for the simulation with all three versions to maintain comparability.

*Table 5 Sensitivity analysis of erosion parameters for the Mount Meager event  
Orange: erosion parameters set as default in the entrainment version of RAMMS*

<i>Erosion rate</i>	<i>Duration [s]</i>	<i>Max. Height P1 [m]</i>	<i>Runout distance [m]</i>	<i>Distance Diff. [%]</i>	<i>Total Volume [m3]</i>	<i>Volume Diff. [%]</i>
0.025	279.8	116.241	9 461	-	48 575 237.00	-
0.05	279	41.4073	9 461.5	0.01	48 726 566.68	0.31
0.013	284.7	115.29	9 442	-0.20	47898569.33	-1.39
<i>Potential erosion depth</i>	<i>Duration [s]</i>	<i>Max. Height P1 [m]</i>	<i>Runout distance [m]</i>	<i>Distance Diff. [%]</i>	<i>Total Volume [m3]</i>	<i>Volume Diff. [%]</i>
0.1	279.8	116.241	9 461	-	48 575 237.00	-
0.2	280	116.241	9 499.5	0.41	48 579 624.09	0.01
0.05	279.8	116.239	9 499.5	0.41	48 564 602.34	-0.02
<i>Critical shear stress</i>	<i>Duration [s]</i>	<i>Max. Height P1 [m]</i>	<i>Runout distance [m]</i>	<i>Distance Diff. [%]</i>	<i>Total Volume [m3]</i>	<i>Volume Diff. [%]</i>
1	279.8	116.241	9 461	-	48 575 237.00	-
2	280	116.241	9 430.5	-0.32	48 571 994.86	-0.01
0.5	280	116.242	9 428.5	-0.34	48 576 746.83	0.00
<i>Max. Erosion depth</i>	<i>Duration [s]</i>	<i>Max. Height P1 [m]</i>	<i>Runout distance [m]</i>	<i>Distance Diff. [%]</i>	<i>Total Volume [m3]</i>	<i>Volume Diff. [%]</i>
2	279.8	116.241	9 461	-	48 575 237.00	-
4	288.3	116.241	9 496	0.37	50 248 546.00	3.44
1	278.7	116.244	9 432.5	-0.30	47 492 067.27	-2.23

For the entrainment version, a sensitivity analysis of the erosion parameters was necessary to evaluate the influence of each parameter on the simulation result. For a separate analysis of the parameters, the Mount Meager event was modelled with changing parameters. Each parameter was changed twice, once doubled, once halved, while keeping the other parameters at medium positions. The influence of the parameters *Erosion rate*, *Potential erosion depth*, *Critical shear stress* and *Maximum erosion depth* on the results of the duration of the simulation, maximum flow height at a specific position, runout distance and total volume was

## Results

tested. The results show that the influence of the different parameters on all results is negligible (Table 5). Thus, erosion parameters were left at default (marked in yellow in Table 5), meaning at medium positions for the simulation of all three events.

The parameters chosen to model the events with the extended version can be seen in Table 6. These parameters were calibrated and used to reconstruct the rock avalanche and debris flow in the Bondasca Valley by Perry Bartelt and colleagues from the slf. The scientists recommended using the same parameters for the simulation of the three events in this thesis because they showed similar ice- and water contents in the initial and the entrained mass and yielded reliable results in the simulation of the event in Bondo (Personal communication with Perry Bartelt, 21.03.2018).

*Table 6 Parameters used in simulations with the extended version*

Additional information about the release area			Additional information about the erosion layers		
Initial temperature	[°C]	-2		Glacier	Sediment
Volumetric water content	[mm/m <sup>2</sup> ]	2000	Thickness	[m]	2
			Density	[kg/m <sup>3</sup> ]	2700
			Temperature	[°C]	-2
			Volumetric water content	[%]	0
			Erodibility		1
Additional physical information					
Activation Energy	[kJ/m <sup>3</sup> ]	12			
Dry-wet transition value	[mm]	10			

### 4.2.1 Mount Meager rock slide-debris flow, 2010

The tested  $\xi$  values for the Mount Meager event were 500 m/s<sup>2</sup> and 1000 m/s<sup>2</sup>, which led to a difference in runout distance of less than 1%. The tested  $\mu$  values were 0.1 and 0.15, and the results of runout distance measurements showed differences around 8%. This shows that  $\mu$  has a higher influence on the runout distance as  $\xi$ . For the modelling of the Mount Meager event,  $\xi$  was set to 500 m/s<sup>2</sup> and  $\mu$  to 0.1 since those values led to most realistic simulation results.

The DEM used to simulate the Mount Meager was taken at the 2<sup>nd</sup> of April 2009, thus before the event happened.

*Table 7 Simulation results Mount Meager landslide  
Orange: Information for validation available of actual event*

			Standard	Entrainment	Extended	Actual event
Duration		[s]	278	280	540	324
Runout distance	Lillooet R. V.	[m]	9'207	9'263	12'746	
	Meager C. V.	[m]	8'735	8'761	11'020	
Max flow height	P1	[m]	114.9	116.2	26.9	
	P2	[m]	72.5	72.5	91.6	
	P3	[m]	83.9	84.8	47.3	
Max runup height		[m]	96.4	99.3	140.9	270
Max flow velocity		[m/s]	71.17	71.17	100	Average: 64
Release volume		[m <sup>3</sup> ]	46'575'072	46'575'072	46'532'464	48'500'000
Eroded volume		[m <sup>3</sup> ]	-	2'324'972	4'236'856	
Total volume		[m <sup>3</sup> ]	46'250'516	48'900'044	50'769'320	53'000'000
Entrainment ratio			0.99	1.05	1.09	1.1

The results of the standard and the entrainment simulation are very similar (Table 7). Differences in all measured parameters are less than or around 1%. The maximum runup height is 3% higher in the entrainment simulation, which can be explained by the higher volume of flowing mass through the entrainment of material. The eroded material of the entrainment simulation is 5% of the released volume,

leading to a total volume of 48'900'044 m<sup>3</sup> which corresponds to the volume estimated by Guthrie and colleagues (2012). Compared to Hungr and Evans' (2004) estimation of an entrainment ratio of 2.5 for massive landslides, this entrainment ratio is rather small. The durations of the simulations with the standard and the entrainment version were around 15% shorter than the duration of the actual event. Runup heights of the simulations were also much smaller than the runup height of the real event.

The results of the extended simulation differ more from the entrainment simulation results and correspond more to the actual event. The duration of the mass flow was nearly twice as long in the extended simulation, while the runout distance was 37% longer into the Lillooet River Valley and 25% longer into the Meager Creek Valley respectively. Compared to the actual event, the duration of the extended simulation was 66% longer. Maximum flow velocity was 100 m/s in the extended version and thus 40% higher as in the standard and the entrainment version simulations. Compared to the average velocity of the actual event (64 m/s) this value is quite realistic. The results of the extended simulation show much lower maximum flow heights at the points P1 and P3 and slightly higher maximum flow height at point P2. This represents a more fluid mass movement around point P2 in the extended simulation compared to the other versions. The visualisations of the simulations (Figure 26a-c) shows that the points P1 and P3 are not set in the centre of the flow path and thus do not represent maximum flow height in the center of the moving mass. This explains the differences of maximum flow height at these two points. The entrainment ratio of the extended simulation is 1.09, which almost corresponds to the entrainment ratio of the actual event of 1.1. Maximum runup height at the mouth of the Capricorn Creek Valley was measured by Roberti and colleagues (2017) to be 270 m. This high runup height could not be simulated with RAMMS. The highest runup height resulted with the extended simulation, 140.9 m.

Visualized simulation results show that a part of the released volume flowed on the north-eastern side of the mountain flank (Figure 26 a-c). In the actual event, no mass flowed to this part of the mountain. This could be explained by the calculation of the release part of the event. In RAMMS, the released volume is calculated as the release area times the release depth, which was adjusted, so that the calculated release volume corresponded to the estimated release volume of the actual event, meaning to 60 m. Thus, RAMMS simulates a collapse of a block with set height for the whole release area, which happens rather seldom in nature, where such a large mass of rock usually initiates in a sliding motion.

Visualized simulation results of the standard and entrainment simulation look very similar. The flow path corresponds to the one of the actual event, whereas the runout mass does not reach the extent of the actual event (Figure 26a-b). The result of the extended simulation shows a wider flow path, especially in the first valley turn below the release area. The runout mass does reach the extent of the actual event and even overflows it in the Lillooet River valley (Figure 26c).

#### 4.2.2 Howson II rock slide, 1999

Different friction parameters were tested here as well to choose those leading to the most realistic results. Tested  $\xi$  values were as well as for the Mount Meager event 500 m/s<sup>2</sup> and 1000 m/s<sup>2</sup>. Simulations with friction value  $\xi$  set to 1000 m/s<sup>2</sup> led to maximum flow velocity results of 64 m/s, whereas friction value  $\xi$  set to 500 m/s<sup>2</sup> led to a maximum flow velocity of 46 m/s. Schwab et al. (2003), who investigated this event, noticed tree uprooting through the impact of the debris flow and concluded that a minimum flow velocity of 18-30 m/s is necessary for this effect. Therefore, friction value  $\xi$  was set to 1000 m/s<sup>2</sup> for the simulation of this event, because the resulting maximum flow velocity of 64 m/s corresponds better with the suggested minimum velocity.

Tested  $\mu$  values were 0.1, 0.15, 0.2 and 0.3. The first value resulted in a very liquid flow of the mass, not corresponding to a moving mass of rock and ice but rather of a mudflow. The latter two resulted in a vertical runup when the mass stopped in the flat part of the area, which does not represent realistic results. Thus, friction values  $\mu$  was set to 0.15.

The DEM to model the Howson II event was taken at the 21<sup>st</sup> of August 2009, hence nearly ten years after the event happened.

## Results

*Table 8 Simulation results Howson II landslide  
Orange: Information for validation available of actual event*

		<i>Standard</i>	<i>Entrainment</i>	<i>Extended</i>	<i>Actual event</i>
<i>Duration</i>	<i>[s]</i>	146	185	175	
<i>Runout distance</i>	<i>[m]</i>	3'080	3'202	> 3613	
<i>Max flow height</i>	<i>P1 [m]</i>	10.2	10.3	14.2	
	<i>P2 [m]</i>	10.7	11.0	27.8	
	<i>P3 [m]</i>	19.9	25.6	14.8	
<i>Max runup height</i>	<i>[m]</i>	23.2	23.3	34.0	
<i>Max flow velocity</i>	<i>[m/s]</i>	62.76	43.63	97.38	Min. 18-30
<i>Release volume</i>	<i>[m<sup>3</sup>]</i>	904'589	904'589	911'859	900'000
<i>Eroded volume</i>	<i>[m<sup>3</sup>]</i>	-	641'187	1'421'149	
<i>Total volume</i>	<i>[m<sup>3</sup>]</i>	904'720	1'545'776	2'333'007	2'500'000
<i>Entrainment ratio</i>		1.00	1.71	2.56	2.8

For the Howson II event, simulations with the standard and the entrainment version show greater differences as for the Mount Meager event (Table 8). The duration of the event is 41 seconds (26%) longer in the entrainment simulation, whereas the runout distance, maximum flow height at points P1, P2 and P3, as well as the maximum runup height are less prominently longer respectively higher as expected for the entrainment simulation. Maximum flow velocity is surprisingly smaller in the entrainment simulation, which possibly explains the longer duration of the simulation. It is difficult to say if the maximum velocities of the simulations are realistic, because only estimations of the minimum velocity of the real event are available. The entrainment ratio of the entrainment version is too small compared to the actual event. Despite the substantial difference in total volume of the entrainment simulation compared to the standard one, the difference in runout distance and maximum flow height at measured points is relatively small. Simulation results show that points P1 and P2 are set in the substrate erosion area, which leads to lower maximum flow height than expected (Figure 27a-b). Point P3 lies in the deposition area, which resembles a small depression in the DEM or a rather flat area. Here, the simulation stopped because of too low mass movement and the mass dammed up a bit, leading to the higher maximum flow height at P3.

The duration of the simulation with the extended version is similar to the one with the entrainment version. On the other hand, the runout distance of the extended simulation is exceptionally long, and flow heights are higher at points P1 and P2 compared to the entrainment simulation. The entrainment rate of the extended simulation is 2.56. This value is very similar to the entrainment ratio of the actual event, and thus the simulated total volume corresponds as well to the deposited volume of the real event. Maximum flow height at point P3 is half as high as for the entrainment simulation, which can be explained in the visualisation of the simulation (Figure 27c): Simulations with the standard and the entrainment version stopped around point P3 and dammed up, leading to a high maximum flow height at this point. The simulation with the extended version flowed farther down and deposited on a broader area leading to no damming up at point P3.

The standard and entrainment simulation show similar flow paths and deposition areas. The flow paths are less wide than the extent of the actual event and are limited to the sediment erosion area. The deposition area of the entrainment simulation reflects very well the deposition area of the actual event (Figure 27a-b). The flow path of the extended simulation represents precisely the one of the actual event until around 250m below P2. There, the flow width widens, and the material affects a larger area as was the case at the actual event (Figure 27c). This overflow could have happened because forested area was not considered with different friction parameters in the simulations.

### 4.2.3 Harold Price rock avalanche-debris flow, 2002

For the modelling of the Harold Price event tested friction values  $\xi$  were 500 m/s<sup>2</sup> and 1000 m/s<sup>2</sup>. Both led to realistic simulation results. To maintain comparability to simulation results of the Howson II event,  $\xi$  was set to 1000 m/s<sup>2</sup>. Tested friction values  $\mu$  were 0.1 and 0.15. A value of 0.15 resulted in unrealistic patched shapes when the flow stopped. Thus,  $\mu$  was set to 0.1 for the simulation. At this event, no runup was observed. Thus, no runup was measured in the simulation results.

The DEM to model the Harold Price event was taken at the 7<sup>th</sup> of February 2011, thus eight and a half years after the event happened.

*Table 9 Simulation results Harold Price landslide  
Orange: Information for validation available of actual event*

		<i>Standard</i>	<i>Entrainment</i>	<i>Extended</i>	<i>Actual event</i>
<i>Duration</i>	[s]	261	288	330	
<i>Runout distance</i>	[m]	2'879	2'953	3'899	
<i>Max flow height</i>	<i>P1</i> [m]	5.6	5.8	8.2	
	<i>P2</i> [m]	12.0	11.9	11.9	
	<i>P3</i> [m]	7.8	8.1	5.8	
<i>Max flow velocity</i>	[m/s]	43.94	43.62	57.39	Avg 28-35
<i>Release volume</i>	[m <sup>3</sup> ]	730'414	730'414	781'737	700'000
<i>Eroded volume</i>	[m <sup>3</sup> ]	-	131'504	181'772	
<i>Total volume</i>	[m <sup>3</sup> ]	710'842	861'917	963'509	
<i>Entrainment ratio</i>		0.97	1.18	1.23	2.9

The results of the standard and the entrainment simulations are very similar. Runout distance of the entrainment simulation is 2.5 % longer than the runout distance of the standard simulation. Also maximum flow heights at measured points P1, P2 and P3 differ in less than 1%. The entrainment ratio of the entrainment simulation is 1.18 and thus much smaller than the entrainment ratio of the actual event. Maximum flow velocities of the standard and the extended simulations are rather small compared to the calculated average flow speed of 28-35 m/s of the actual event.

Results of the extended simulation show increased duration and runout distance, as well as an increased amount of eroded volume and faster maximum flow velocity, corresponding more to the average flow velocity of the actual event. For this event, no glacier erosion area was set, because there was no glacier ice to be eroded. Thus, the erosion capacity of the entrainment and the extended simulation can be compared very well. The entrainment ratio of the extended simulation is slightly higher than the one of the entrainment simulation, showing that the erosion capacity is higher in the extended version of RAMMS. Still, the entrainment ratio of the extended version is quite low compared to the eroded and entrained volume of the actual event.

The visualisations of the simulation results show very similar results for the standard and the entrainment simulation (Figure 28a-b), as already seen in the result table. The simulation of the extended version resulted in a much longer runout distance and a wider flow path compared to the standard and the entrainment simulation (Figure 28c). The widths of the flow path of the simulations are much larger than the one of the actual event. The high forest density in the affected area, which was not considered in the simulations with RAMMS, could explain this. Forested area has a higher surface roughness and thus different  $\mu$  and  $\xi$  friction values. Considering areas with different  $\mu$  and  $\xi$  parameters would probably lead to more realistic simulation results of this event.

Results

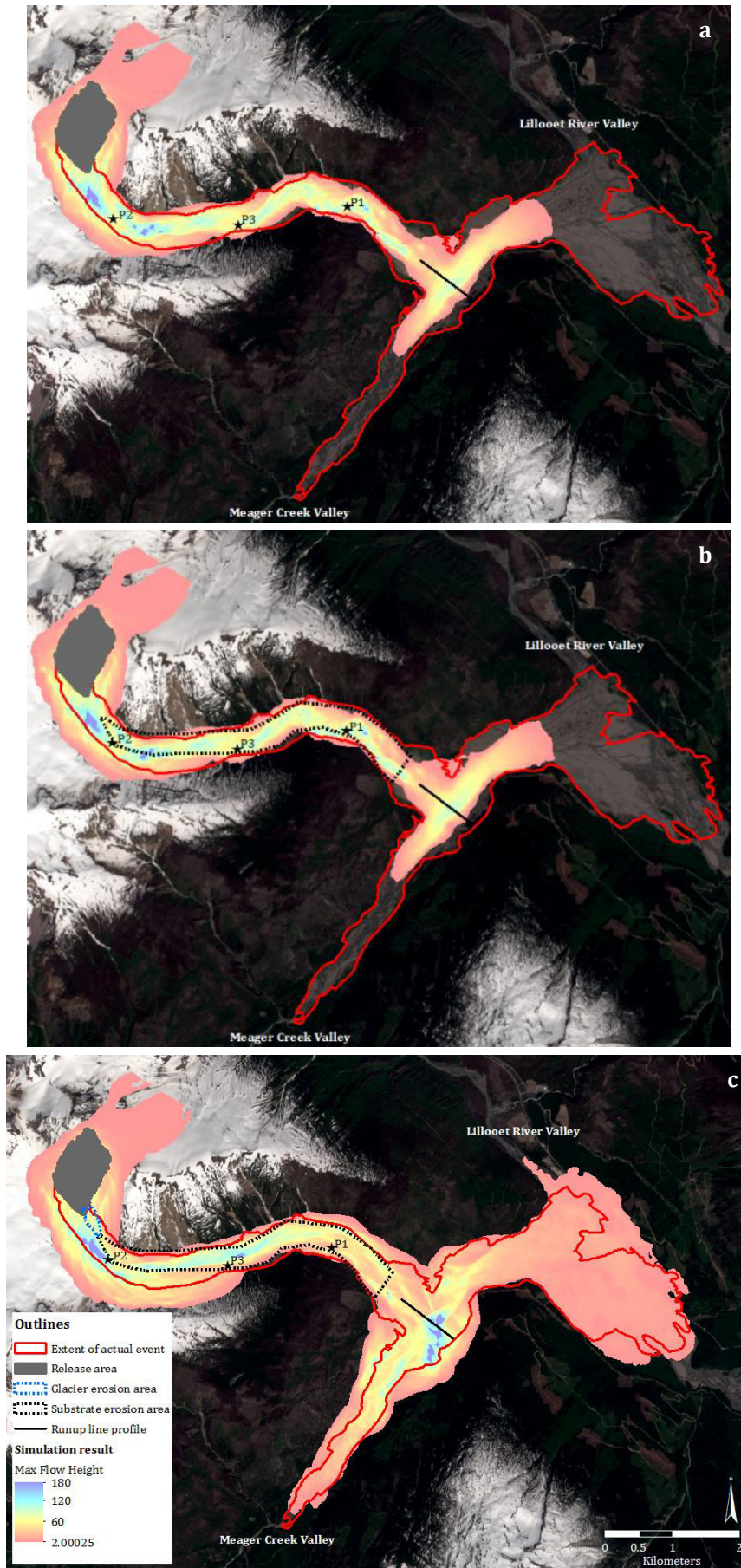


Figure 26 Mount Meager simulation results  
 a: Standard simulation, b: Erosion simulation, c: Extended simulation

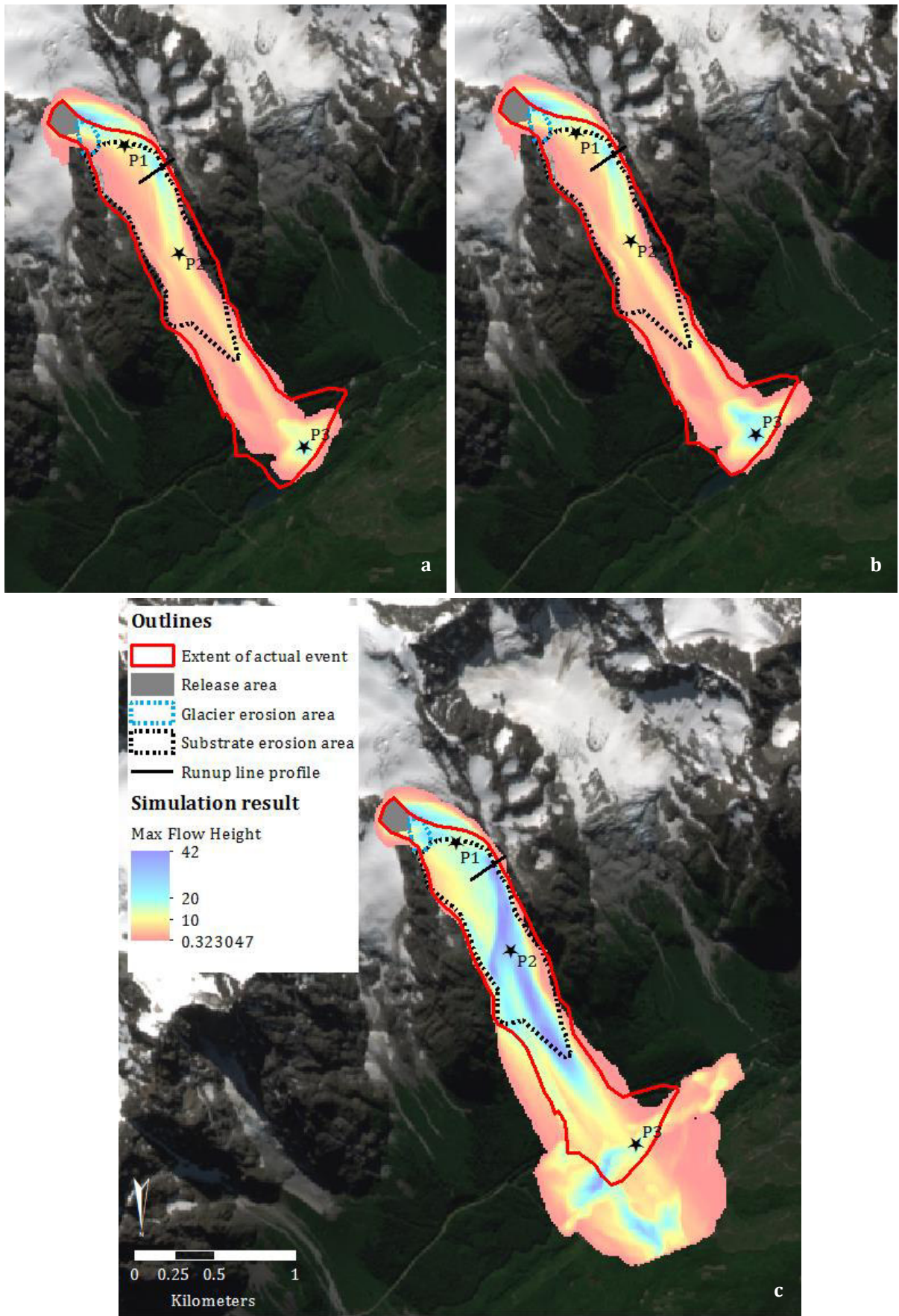


Figure 27 Howson II simulation result  
 a: Standard simulation, b: Erosion simulation, c: Extended simulation

Results

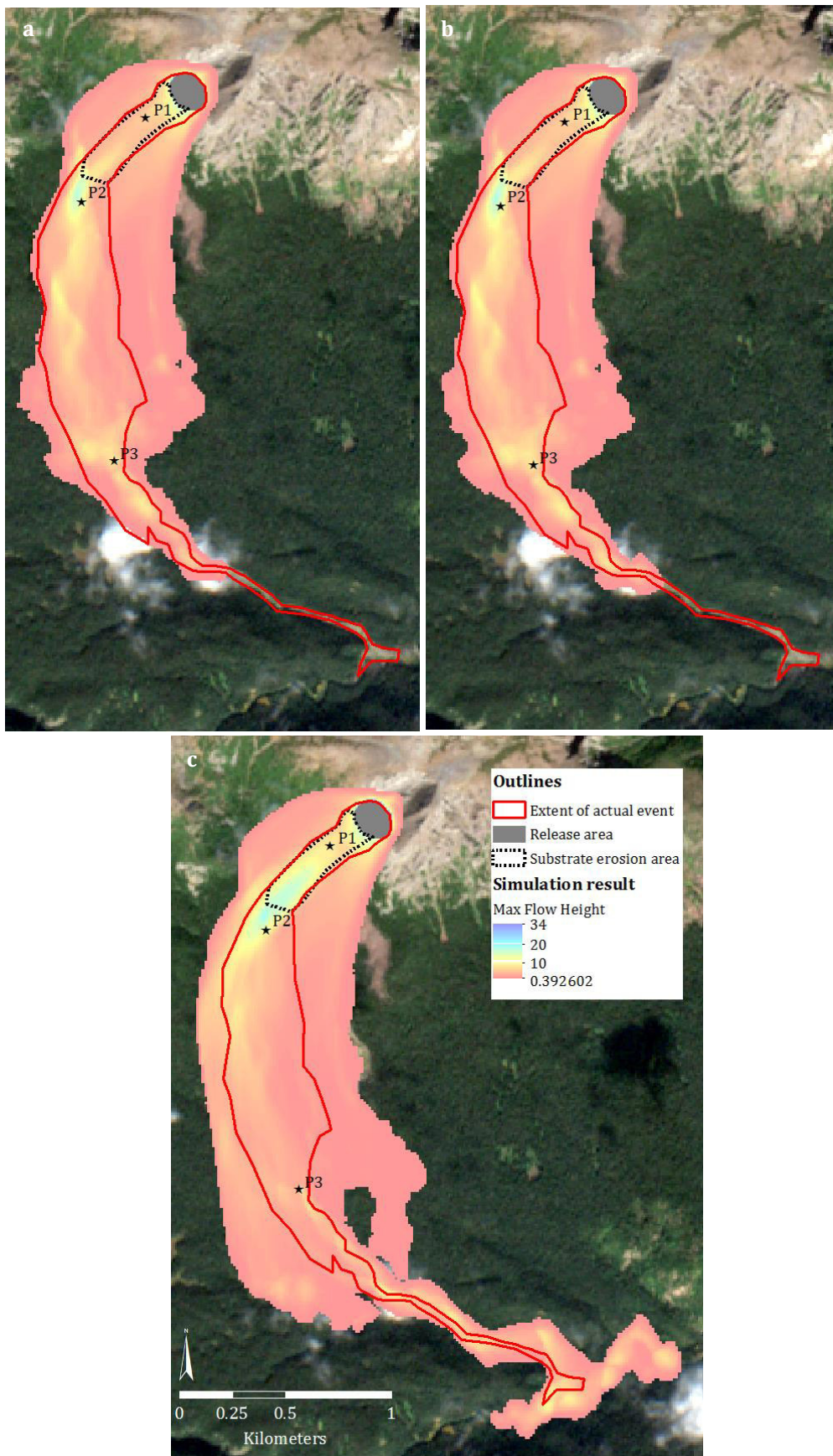


Figure 28 Harold Price simulation result  
a: Standard simulation, b: Erosion simulation, c: Extended simulation



## 5 Discussion

### 5.1 Inventory evaluation

#### 5.1.1 Event location

The inventory shows that massive landslides can happen in glaciated high mountain regions all over the world. The map of the events indicates that many events are happening in Alaska, USA and British Columbia, Canada. These regions combine favouring factors for large landslides like high snow load, steep slopes, fractured, partly volcanic, rock and earthquake activity. Nevertheless, this does not mean, that there are only a few landslides happening in other parts of the world. The marked points illustrate those regions, where the devices for the documentation of such events are available, and where it is possible to access the location of the event by helicopter, or where remote sensing data is available. Especially in very high alpine regions like the Himalaya, it is often not possible to access the area of the event by helicopter because of the high altitude. The steepness of high alpine regions further limits the acquisition of high-resolution remote sensing data and thus constrains the possibility to analyse events in these regions without access.

Schneider and colleagues found a similar distribution in their study and came to the same conclusion, that a lack of data availability may be the reason for the clustering of such events in north-western America and Europe (Schneider et al., 2011a).

#### 5.1.2 Documentation quality

The documentation quality of the events in the inventory shows high variety. In cases, where the event happened in populated regions, caused severe damage to infrastructure or was of unusually high magnitude, the quality of documentation is very good and several scientists investigated the event (e.g. Nevados Huascarán ice-rock avalanche 1970, Iliamna Red Glacier ice-rock avalanche 1994 and 1997, Mount Munday rock avalanche 1997, Howson II rockslide 1999, Tsar Mountain rockslide 2000, Zymoetz River rock avalanche 2002, Kolka/Karmadon 2002, Iliamna Umbrella Glacier ice-rock avalanche 2004, Thurwieser rock avalanche 2004, Mount Meager rockslide 2010, Bingham Canyon landslide 2013 and Mount Steele rock avalanche 2015). Other events were either detected in seismic measurements, not detected and analysed immediately or happened in too remote regions to take measurements or analyse them further (e.g. Beelzebub Glacier rockslide 1984, North Creek landslide 1986, Mount Fletcher rock avalanches 1992, Mount Adams rock-ice avalanches 1997 and 2008, McGinnis Peak South rock avalanche 2002, Vanch Valley landslide 2002, Black Rapids East, Middle and West rock avalanches 2002, West Fork Glacier North and South rock avalanches 2002, Mount Steller North landslide 2008, Pokhara valley rock avalanche/debris flow 2012, Iliamna ice avalanche 2013, Mount La Perouse rock-ice avalanche 2014, Redoubt Glacier rock-ice avalanche 2015 and Mount Steele rock avalanche 2015). These events show rather poor documentation quality and are less suitable for an event comparison.

Although there exists a landslide classification, the terms used for documenting events do not always follow the guidelines of the classification. This may represent the difficulty to find one proper expression for the event. Especially, landslides that transform during the flow are challenging to denote.

#### 5.1.3 Flow transformation

##### 5.1.3.1 *Influence of transition over a glacier surface*

Scientists mention that transition of a landslide over a glacier surface may cause flow transformation because of entrainment of subglacial water and glacier ice (Petrakov et al., 2008; Schneider et al., 2011b). The analysis of the events in the inventory shows that the transition of landslides over a glacier surface does not influence the angle of reach nor the entrainment ratio of the events (Figure 22). If there were an influence of the travel path of a landslide over a glacier surface on the runout behaviour, the angle of reach would decrease with increasing path length over the glacier surface. Furthermore, the entrainment ratio would increase with increasing path length over the glacier because of ice entrainment into the moving mass.

Most studies about the events in the inventory mention that the transition of landslides over a glacier surface does enhance flow speed and spreading of debris because of the low friction surface of glaciers or because of the lubricating effect of glacier ice. Figure 29 shows the influence of the path over a glacier surface

on the area of deposition of the events in the inventory. Most of the events are clustered in the lower third of the y-axis and spread evenly on the x-axis. It seems like the events with no flow transformation (orange) have smaller areas of deposition, even when the path over a glacier surface is long. On the other hand, the two events with flow transformation (green) show large areas of deposition with relatively short paths over a glacier surface. Unfortunately, no information about the area of deposition or the path over a glacier surface is given for the other events with flow transformation. So, it is not possible to conclude that the path over a glacier surface has a different impact on the spreading of debris in the deposition area of events with flow transformation than of those without flow transformation.

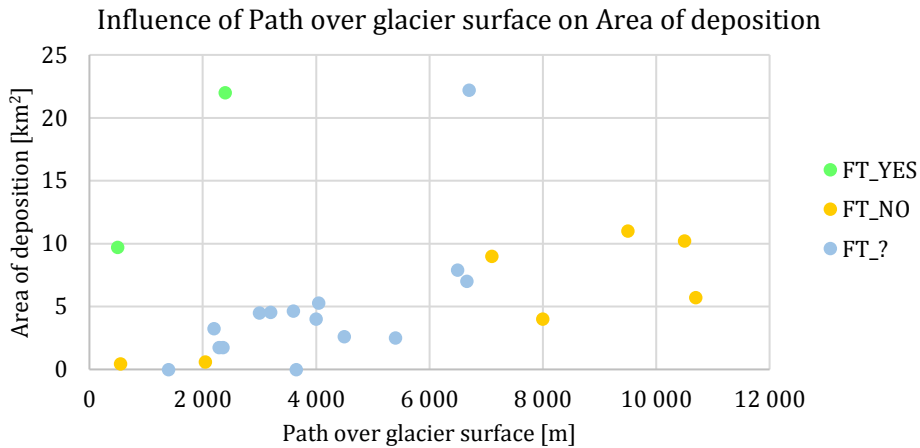


Figure 29 Influence of Path over glacier surface on Area of deposition  
 Orange: No flow transformation  
 Green: Flow transformation  
 Blue: No information about flow transformation

Schneider and colleagues (2011a) compared the glacier trajectory of the events in their list to the apparent coefficient of friction and found moderate correlation coefficients for glacier trajectories. Comparing the glacier trajectory to the angle of reach of the inventory presented here leads to no correlation between these two parameters (Figure 30).

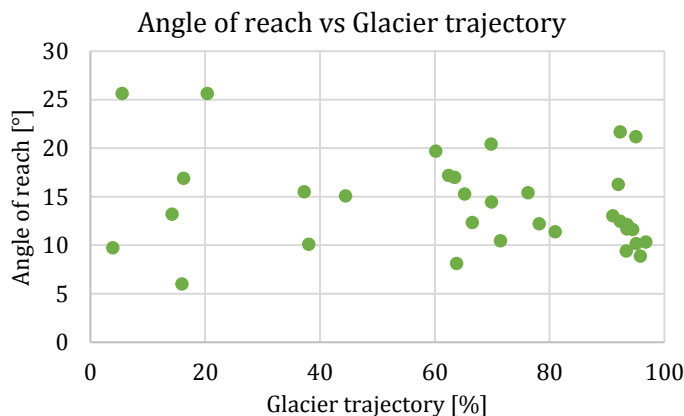


Figure 30 Influence of Glacier trajectory on Angle of reach

### 5.1.3.2 Influence of different water sources on flow mechanism

Liquid water entrained into moving landslide mass may have the most direct impact on the flow behaviour. Through the entrainment of saturated sediment or water from impacted lakes or rivers (Schneider et al., 2011a), the mass may liquify and thus cause an immediate flow transformation. In the inventory, there are several events, where saturated sediment is mentioned to be a possible source of water. However, scientists are seldom sure about the water content of entrained sediment and can thus only estimate the approximate

amount of liquid water available in it from precipitation data a few days to weeks before the event. Regarding the snow cover in winter in glaciated high mountain areas, entrainment of saturated sediment is an essential factor in spring and summer, when the snow melts and supplies meltwater to saturate loosely deposited sediment.

Possible entrainment of snow into rock avalanches travelling over glaciers or snow-covered areas is mentioned in several studies of the landslides in the inventory. However, no studies are focusing on meltwater production of entrained snow. Thus, meltwater production through snow entrainment into rock(-ice) avalanches and subsequent flow transformation is still an uncharted topic. Since possible sources of water for flow transformation are only guessed in most studies about the investigated events, the influence of snow entrainment cannot be defined explicitly.

Maximum meltwater production calculated for the events in the inventory showed that events with flow transformation show slightly larger maximum meltwater production than events without flow transformation. Furthermore, maximum meltwater production calculated for two very large events with considerably large snow and ice entrainment and long runout distances (Kolka/Karmadon and Lamplugh Glacier avalanches) show realistic amounts of possible meltwater production in comparison with the actual events. However, the calculated meltwater production is highly simplified and does not explicitly include heat production through friction at the bottom of a mass flow nor does it include meltwater production at the bottom of a landslide travelling over a glacier surface.

Another important process which is even less analysed as the process of meltwater production inside a mass flow is the vaporisation of glacier ice through the impact of a rock avalanche falling onto a glacier surface. In rare cases, rock avalanches initiate at steep flanks and fall in free fall onto a glacier surface. The impact of such an event is immense and can cause immediate vaporisation of glacier ice. It is possible that this process could explain the presence of the white fountains exploding out of the rock dust of a rock avalanche, which could be seen in a video taken of the Piz Cengalo rock avalanche in August 2017. The energy needed to vaporise ice is 2'230 kJ/kg (<https://www.britannica.com/science/latent-heat>) and thus nearly seven times as high as the energy needed for melting. Obviously, it is difficult to model ice vaporization through the impact of a rock mass because of the high energy needed for vaporisation. It is also possible that very large temperatures at the base of the flow, due to local friction, could also directly vaporize ice. However, research is not available to indicate the conditions under which this process may become important.

Finally, the findings of Schneider and colleagues (2011b), where they analysed flow behaviour, and meltwater production of gravel-ice mixtures in rotating drums cannot be supported by analysing the parameters of the events in this study. A possible explanation for this is that they put ice particles into the drums that had similar diameters as the gravel mixture (11 to 16 mm in diameter) (Schneider et al., 2011b). In nature, rock avalanches contain large boulders and gravel with much larger grain sizes. Furthermore, the ice particles displaced by the impact of a rock avalanche on a glacier are also larger. This leads to the fact that in rock-ice avalanches only the outermost part of large ice boulders can be thawed and even melted due to frictional heating, leading to a much smaller availability of meltwater than tested by Schneider and colleagues. Hence, their findings cannot be compared to such massive landslides as investigated in this study. Nevertheless, they made a huge step in analysing and understanding the effects of entrained ice in a mass flow.

#### 5.1.4 Comparability of events

There are some parameters available for almost all events in the inventory, which are measurable and thus allow a comparison of the events to see trends, e.g. *vertical and horizontal distance, deposited volume, path over glacier surface and initial volume*. Other parameters are not measurable and are thus subjectively estimated by scientists (*triggering factor, number of surges, water source, estimated water content of the initial failure mass and the deposited volume*). Those parameters make it difficult to compare different events because there is no strict way of proceeding by analysing a landslide and every scientist has another approach and different interests focusing on while investigating an event. There are also other involved factors in large landslides, which are not investigated in this inventory but may have a significant impact on the flow behaviour like *topography* and *surface roughness*. These two factors fundamentally affect flow velocity as well as the flow path, stopping mechanisms and spreading of deposited mass (Frank et al., 2017). On the

other hand, large landslide can also substantially modify the surface: Landslides travelling over glacier surface can erode debris cover, fill up crevasses and even out serac zones, leaving smoother surfaces reducing surface roughness (Schneider et al., 2011a). Therefore, it would be interesting to measure surface roughness before and after an event in a controlled area to gain knowledge about the change of surface roughness through a landslide.

Additional to the parameters which can be analysed after an event, there are climatic factors which have to be investigated a few days to weeks before the event and which vary a lot all over the world like *precipitation as rain and snow* and *temperature*. Precipitation may also vary significantly in small scale, especially in steep mountainous areas. These conditioning climatic factors challenge the comparison of massive landslides from different parts of the world. Other factors further challenging interregional comparison of landslides are *exposition, geology* and *topography*. These factors vary also spatially and may even change over time through erosion processes. Those influencing factors make it necessary to first group the events according to their climatic region, geology or exposition before analysis and comparison. For example, the events in British Columbia can be grouped into events happening in the Coast Mountains, St. Elias Mountains and the Rocky Mountains which are all regions with specific climatic conditions. Afterwards, the events in these groups can be compared, excluding the climatic factor. As another example, events can be grouped by the rock type of the initiation zone and then, compared to each other. Like this, the parameter of rock density and stability gets excluded. However, this method reduces the comparison of large landslides to one region or one climate zone and events cannot be compared interregional or intercontinental.

## 5.2 RAMMS results

### 5.2.1 Reconstruction of events

To reconstruct a landslide event with RAMMS, a DEM of the region where the event happened is imperative. The quality of this DEM has the most critical impact on the simulation result. DEMs with low spatial resolution generate fast calculation times but miss small topographic changes which can significantly impact simulation results. On the other hand, DEMs with high spatial resolution increase calculation time but also represent small topographic changes and can thus lead to more realistic simulation results (Scheuner et al., 2009). However, too good spatial resolution can lead to excessively long calculation time and even cause unrealistic simulation results. Thus, the spatial resolution of the DEM must be adequately chosen adjusted to the extent of the event and the purpose of the simulation results (Stolz and Huggel, 2008). This could also be seen in the results of the simulations with RAMMS. The spatial resolution of the DEMs of all three modelled events was 12.5 m, but the extent of the affected area was much larger for the Mount Meager event as for the Howson II and the Harold Price event. The RAMMS results show that the simulation of the Mount Meager event looks smoother than the one of the other two events. Furthermore, the simulation of the Harold Price event shows some artefacts in the area where the simulation stopped which can be explained by the relatively coarse spatial resolution compared to the small area of extent. First simulations of the events, not presented in this study, were done with ASTER GDEMs with a spatial resolution of 25 m. Simulation results of the Mount Meager event with this DEM led to realistic results and even showed much shorter calculation time, but it was not possible to model the other two events because the spatial resolution was too coarse and led to artefacts and non-natural stopping mechanisms in steep areas. This shows that a spatial resolution of a DEM of 25 m would be appropriate to model an event with an extent like the Mount Meager rock slide-debris flow. However, events with smaller extents like the Howson II and the Harold Price event require a better spatial resolution of 12.5 m to be modelled realistically.

Apart from the resolution of the used DEM, the acquisition date has also a significant influence on the simulation result, especially in cases, where landslides specifically change the topography (Schneider et al., 2010). The DEM to model the Mount Meager landslide was taken around one year before the event happened and can thus be compared to the topography at the time of the real event and should lead to realistic and comparable simulation results. The two DEMs of the Howson II and the Harold Price event were taken several years after the events happened. Next to the change in topography from the two events themselves, other landslides, glacier melting, and erosion could have changed the topography considerably and may thus lead to simulation results differing from the actual event.

The results of the simulations show that it is in some degree possible to reconstruct events like rock slides, rock avalanches and debris flows with a numerical model like RAMMS. The model is limited by the complexity of events with subsequent processes and cannot model flow transformation accurately. Furthermore, RAMMS models an instantaneous failure starting a rock (-ice) avalanche or debris flow. Thus, a progressive failure cannot be modelled, as already Frank and colleagues concluded (Frank et al., 2017).

In the following section, the usefulness of the different versions of RAMMS to model such complex events is discussed.

### 5.2.2 Evaluation of RAMMS versions

To simulate landslides with numerical models, some proper analysis of the event is necessary. This analysis includes exact evaluation of the release area and released mass, evaluation of the travel path and the affected area, examination of the deposition area and deposited material (depth, density, composition, water- and ice content) and estimation of possible environmental influencing factors like temperature and precipitation changes, weather changes, earthquakes etc. After analysing all these points, the event can be reconstructed with numerical simulation models like RAMMS. RAMMS needs different input parameters which sometimes can be measured or calculated through the analysis of mentioned points, but sometimes need to be assessed from experiences of other, similar events. Table 10 shows the needed parameters for the simulation with the different versions of RAMMS used in this study and shows which parameters are measurable and which must be estimated from experience.

Table 10 Measurable, calculable and estimated input parameters of RAMMS

RAMMS version	Parameter	Measurable/ calculable	Estimation
<i>All</i>	Release area	X	
	Release depth	X	
	Density	X	
	$\mu$ $\xi$		X X
<i>Entrainment</i>	Erosion shapefile	(X)	X
	Erosion density	(X)	X
	Erosion rate		X
	Potential erosion depth		X
	Critical shear stress		X
	Maximum erosion depth	(X)	X
<i>Extended</i>	Initial temperature	X	
	Vol. Water content (release material)		X
	Temperature of eroded material	(X)	X
	Vol. water content of eroded material	(X)	X
	Erodibility		X
	Activation Energy		X
	Dry-Wet Transition value		X

Friction values  $\mu$  and  $\xi$  are parameters which cannot be measured or calculated from an event analysis, but these two parameters were tested in different studies about landslides and can thus be looked up in literature, or for RAMMS, there is a table with common  $\mu$  and  $\xi$  parameters included in the software. Nevertheless, the parameters must be calibrated for a simulated case study and may be adjusted to generate realistic results. For simulations with the entrainment version, some of the needed parameters about the eroded material, like erosion shapefile, erosion density and maximum erosion depth would be measurable before the event but must be estimated once the event happened. In controlled regions, where debris flows are investigated (e.g. Illgraben or Spreitgraben, Switzerland), sensors are built into the ground measuring shear stress, temperature and other parameters. There it is possible to observe these parameters before, during and after an event and use these observations to investigate events in non-controlled areas. Input

parameters used in the extended version are nearly all not measurable or calculable and must be estimated. The initial temperature can be measured at the mountain flank where the mass collapsed, although this temperature may differ from the one in the collapsed material. Information about the volumetric water content can be assessed from the ice content of the mountain flank where the landslide initiated. The temperature and the volumetric water content of the eroded material can only be measured before the event happens, as it is for the entrainment version. After the event, these parameters can only be estimated from experience of other events. Hence, the better an event should be modelled with RAMMS, the more information is needed about this specific event, and the more knowledge is required, to estimate the parameters which cannot be measured or calculated.

The simulation results demonstrate that the standard version of RAMMS::DEBRISFLOW cannot be used to reconstruct complex events initiating as a rock avalanche and transforming into a debris flow. This version does not include material erosion and entrainment, and thus no change of the flowing volume and mass composition can be modelled.

Simulations with the entrainment version showed small volumes of eroded and entrained material compared to the actual event. Frank and colleagues (2015) saw in their study of debris flow modelling with the entrainment version of RAMMS that  $\xi$ -values higher than  $500 \text{ m/s}^2$  led to almost no erosion. Thus, as an improvement of further simulations,  $\mu$  and  $\xi$  calibration should be done separately for the standard and the entrainment version, even though comparability cannot be maintained then. As the developers of the entrainment algorithm found, the simulation results show a more realistic reconstruction of flow patterns compared to the standard version (Frank et al., 2015). Furthermore, they found that the entrainment version shows less lateral spreading of the flowing mass, compared to the standard version. Simulation results of this study show that especially smaller landslides like the Howson II or the Harold Price event can be modelled realistic with the entrainment version. On the other hand, results of the Mount Meager simulation showed short runout distances and low runup heights, which cannot be compared to the actual event. A decrease in lateral spreading of the simulated flow path could not be detected in the entrainment simulations of this study compared to the standard simulations. The entrainment version is limited because it does not include meltwater production through entrainment of snow and ice, nor does it consider process changes like liquefaction through the entrainment of liquid water.

The extended version of RAMMS::AVALANCHE is entirely suitable for the modelling of massive and complex landslides with changes in flow processes. The results show that the Mount Meager event could be reconstructed quite comparable to the actual event, apart from some minor differences. To accurately model smaller events like the Howson II and the Harold Price event with the extended version, some more information about the environmental topography like forested area, riverbeds etc. would be needed. Simulations with the extended version of all events showed strikingly faster maximum flow velocities compared to simulations with the other two versions. The faster flow speed can be explained by the larger volume of the entire mass flow or by the meltwater production or entrainment of saturated sediment which changes the flow property of the mass flow to a more fluid movement. Compared to the actual events, simulated maximum flow velocities of all events seem rather high. However, the flow speed estimated for the actual events are all estimations of mean velocities, or minimum velocities needed for tree uprooting or measured runup heights.

To model massive landslides with RAMMS, sufficient data about the actual event is crucial (Frank et al., 2017), and even more proper knowledge about the physics of landslide is needed to model events with the extended version. Thus, it is not advisable to start modelling landslides with this version without any help of experts. Although RAMMS is already a very usable and helpful numerical model to reconstruct complex mass movements, the developers are still gaining understanding about the flow mechanisms of landslides by analysing actual events. Especially the flow mechanisms of erosive debris flows is not yet fully understood and the analysis of further case studies is needed to improve the erosion algorithm implemented in the entrainment and the extended version (Frank et al., 2017).

### 5.2.3 Comparability to actual events

The comparability of the simulation results to the actual events differs for each of the simulated events.

The flow mechanics of the Mount Meager event could not be simulated adequately with the standard and the entrainment simulation to be compared to the actual event. The event extents of these two versions are much smaller than the extent of the actual events. Runup heights, as well as the entrained volume of the entrainment simulation, are too small to represent the actual event. The extended simulation, on the other hand, resulted in more realistic and more comparable results as the standard and the entrainment simulations. The event extent and the flow path could be modelled similarly to the actual event. The total mass of the extended version is around three million m<sup>3</sup> smaller than estimated by Roberti et al. (2018). This could explain the smaller runup height at the valley divergence. Compared to the straight flow path of the other two modelled events, the flow path of the Mount Meager rock slide-debris flow is more variable and winded. This different topography leads to more variable shear stresses and thus more variable erosion (Frank et al., 2017), which could be more accurately modelled by defining separate erosion areas with different erosion rates at the inner and the outer side of windings.

The extent of the Howson II event could be reconstructed quite accurately with the entrainment simulation, although the total volume was much smaller than the deposited volume of the actual event (~1.5 million m<sup>3</sup> vs 2.5 million m<sup>3</sup>). The extended version resulted in a more realistic entrainment ratio but led to a much larger event extent in forested areas. As well here, the standard simulation results cannot be compared to the actual event. The acquisition date of the DEM could play an essential role in the simulation result of this event. The DEM was taken nearly ten years after the event took place. In this time, the topography can change a lot, especially in such steep glaciated regions and thus lead to simulation results which cannot be compared to the actual event.

The results of the Harold Price simulation are difficult to compare to the actual event, because of the much larger event extent of the simulation results. Figure 31 shows the result of the extended simulation with stretched maximum flow height. This figure shows that the main flow path of the simulation is in the extent of the actual event and the mass outside of this area is maximum five meter high. For this event, the extent of the affected area was drawn visually and can thus differ from the extent of the actual event, especially in the deposition area where dense forest limited the view of the deposited material. Hence, the deposition area in the extended simulation outflowing the drawn event extent does not necessarily differ from the extent of the deposition area of the actual event, and comparison is therefore difficult.

As mentioned before, other studies modelled real landslide events with numerical models and elucidated the importance of adequate DEM resolution (Scheuner et al., 2009) or defined the importance of erosion and entrainment inclusion in the modelling (Frank et al., 2015). Other scientists like Sosio and colleagues, who modelled the Thurwieser rock avalanche with the numerical model DAN (2008), concluded that the sliding surface in the source area of the landslide is very important for accurate modelling of the initiation of the landslide and for the modelling of the subsequent flow path. They also saw that it is of utmost importance to change friction parameters for different surfaces like sediment or glacial ice to enhance the flow mobility and thus to increase realistic modelling of the landslide (Sosio et al., 2008). Applying these findings to this study, one can say that simulation results could be improved by defining lower friction parameters  $\mu$  for glacier surfaces. More realistic modelling of the initiation of the landslides without any outflow could be achieved with DEMs taken shortly before the event. Such DEMs would represent the exact topography before the event took place and probably lead to more realistic simulation results of the initiation as well as the subsequent flow path.

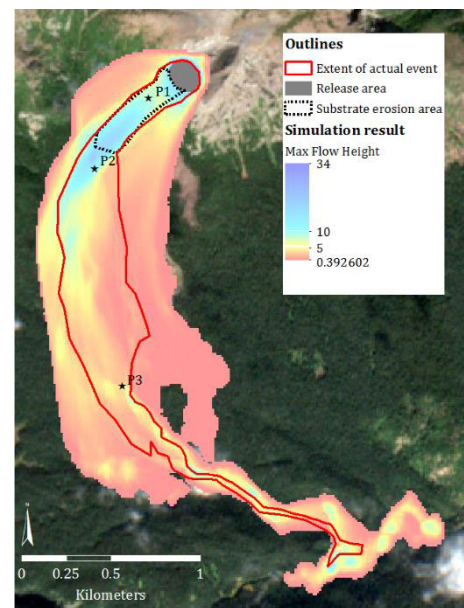


Figure 31 Extended simulation result of the Harold Price event  
Stretched colour of max flow height

### 5.3 Embedment in the context of Bondo

In the time of developing and writing this thesis, scientists gained more information about the process chain of the event in the Bondasca Valley. They found out that the primary source of water which allowed the subsequent debris flow to initiate was saturated sediment and not glacier ice, as assumed at the beginning of the event analysis (Amann et al., 2017). Nevertheless, the destroyed and incorporated glacier ice of the glacier Vadrec del Cengal played an important role in the movement of the initial rock avalanche.

The inventory analysis resulted differently as expected: The events cannot be compared intercontinentally, and thus similar events which happened in the (Swiss) Alps need to be compared to the event in Bondo to gain process understanding about this event. In the inventory, there are two events from the Alps, the Brenva Glacier rock slide and the Thurwieser rock avalanche. Since the Thurwieser rock avalanche did not incorporate much snow, ice or water and there was no flow transformation, this event is less suited to be compared to the one in Bondo. The Brenva Glacier rock slide, on the other hand, travelled 5.4 km over a glacier and incorporated a substantial amount of snow and ice. There was no flow transformation explicitly mentioned, but it is mentioned, that debris of a recent rock avalanche was mobilised, which could have been saturated with water (Bottino et al., 2002). The rock type is also the same as for the Bondo event, Granite. The angle of reach of the rock avalanche in Bondo is around 27°, the angle of reach of the debris flow is around 12°. The angle of reach of the Brenva Glacier rock slide is around 22° (Barla and Barla, 2001; Bottino et al., 2002). From literature it is not clear, where H was actually measured, because the event initiated after an increasing rockfall activity in the year before the event and the height could have been measured from the point of the rockfall and not from the initiating point of the rock slide. Furthermore, a part of the Brenva Glacier rock slide stopped on the glacier and a part of the material travelled over the glacier surface and incorporated ice and snow. Thus, the angle of reach of 22° goes only for that part of the rock slide mass which travelled over the glacier surface and not for the whole initially failed mass. However, the angle of reach of the rock avalanche in the Bondasca Valley and the angle of reach of the Brenva Glacier rock slide are very similar. As Bottino and colleagues modelled the Brenva Glacier rock avalanche with geomechanical input parameters of another, well-analysed landslide (2002), it would be interesting to model the rock avalanche-debris flow of Bondo with the same geomechanical parameters, to see if the simulation results are realistic and comparable to the actual event in Bondo.

Overall, this study shows that rock avalanches incorporating snow, ice or saturated sediment are complex and mostly not yet fully understood. Although interregional comparison of the events in the inventory is difficult, they all have one in common; interaction with and entrainment of snow, ice or saturated sediment is crucial for extraordinary long runout distances and flow transformation. For future scenarios in Bondo, this means that especially in winters with high snow cover, rock avalanches could incorporate considerable masses of snow and thus reach longer runout distances as expected. In summer however, heavy rain events will saturate the deposits of the rock avalanche from 2017 and could mobilize the material to start moving as a debris flow. Furthermore, it is possible that rock avalanches entrain the saturated sediment and reach long runout distances or even transform into a debris flow. Although such chain of events are worst case scenarios, they do happen, as seen in August 2017 and it is crucial to take such events into account when developing new hazard maps for the Bondasca Valley.

The event in Bondo on the other hand, demonstrated the power of nature and the incredible destruction potential of rock and water in mountainous regions. This event emphasized how little we know about the physical processes needed to transform an initially dry rock mass into a fast flowing, destructive debris flow. It is of utmost importance to gain knowledge about such complex chain of events to plan and construct protection measures in more and more populated and touristic mountain regions.



## 6 Conclusion

- I Create a worldwide inventory of large landslide events with long runout distances from the last 50 years, characterised by empirical parameters.
  - Where do such events happen usually?
  - How well are the events documented?

The inventory of the events showed that there are regions predefined for massive landslides to happen because of climatic conditions and topography like British Columbia and Alaska, and where events are documented well. However, this does not mean that these are the only regions predefined for large landslides. There are also other regions predestined for landslides, where the devices for the analysis of the events are not available or access to the area is impossible, and thus only a few information is available about those events. Furthermore, massive landslides in populated regions or touristic areas are mostly well analysed and discussed in literature because of the great popularity. Therefore, one can say that the documentation quality reflects the availability of devices for the analysis of an event and the interest of scientists and the population to gain information about it.

Since landslides initiating as rock avalanches and transforming into debris flows are rather exceptional, the lack of information about such events because of device-availability limitations is regrettable. Every unusual case of a landslide with flow transformation could help to understand such events better. Thus, it is crucial to develop the observation network of large landslides worldwide.

- II Gain process understanding through the analysis of the empirical parameters.
  - How does transition over glaciers influence the flow behaviour?
  - How do different water sources influence flow transformation mechanisms?

The path of a landslide over a glacier surface has different effects on the flow mechanism according to scientists (De Blasio, 2014; Evans and Clague, 1988; Persson, 2000; Tusima, 2010). However, the results of the analysis of the influence of the glacier path or glacier trajectory on the angle of reach, entrainment ratio or area of deposition do not support the findings of the scientists about the incorporation of glacier ice or melt-water from the glacier surface. Nor do they support the findings about the reduction of frictional resistance at the contact point of the landslide and the glacier. Laboratory experiments are usually under controlled conditions and in small-scale and can thus only partly be compared to events in nature. Furthermore, the analysis of the influence of glacier ice on a landslide travelling over it is merely possible right at that moment the event happens. It is very seldom that landslides as massive as those in the inventory are observed right in that moment they happen, because of the remoteness of the affected area or because it is too dangerous. Thus, it is difficult to comprehend the findings of laboratory experiments in natural events.

The influence of different sources of water on flow transformation mechanisms is usually tested in laboratory experiments. Schneider and colleagues made a huge step in understanding the influence of ice particles in gravel avalanches in their experiments with rotating drums (Schneider et al., 2011b). However, they did not include the factor size. Large rock avalanches incorporating glacier ice usually contain large boulders of rock and ice, and not only small gravel-sized particles as in their experiment. Thus, the influence of giant ice blocks entrained in the moving mass cannot be explained by their experiments, and this is still an unknown factor which is very difficult to measure. The effect of incorporated snow on the flow behaviour of landslides is still a poorly understood topic and needs some further investigation.

Another mechanism which is not yet fully understood is the influence of material erosion and entrainment on the velocity of a rock(-ice) avalanche or debris flow: Erosion and entrainment reduces the speed of the landslide through frictional resistance (Berger et al., 2011 in Frank et al., 2015), on the other hand, material entrainment increases the volume and thus increases the kinetic energy of the sliding mass. This is a crucial topic in understanding the flow mechanisms and flow velocity of landslides.

Overall, the analysis of the empirical parameters showed that the exact water source for flow transformation or for an elongation of the runout distance is mostly not defineable. Additionally, the effect of liquid water entrainment through saturated sediment is poorly understood and is probably the most important factor when analysing flow transformations of landslides.

- III Gain process understanding through numerical modelling of events of the inventory.
- Is it possible to reconstruct such complex events with state of the art two-dimensional numerical models?
  - Which model is best suited to reconstruct large landslides?
  - Which information is needed to model an event?

The simulation results showed that the standard version of RAMMS::DEBRISFLOW is not suitable to model landslide events including erosion of glacier ice or sediment material and flow transformation. But surely, this version can be used to model small debris flows in areas without erodible glaciers or loosely deposited sediment material. The simulation results of the entrainment version showed that it is possible to realistically reconstruct smaller events like the modelled Howson II and Harold Price event. Large events incorporating huge masses of ice or saturated sediment like the modelled Mount Meager event could not be adequately modelled with the entrainment version. On the other hand, the results of the extended version presented realistic modelling of the Mount Meager landslide. The extended version is therefore best suited to model complex and large landslide events like the Mount Meager event and the entrainment version can be used to model events with smaller areas of possible entrainment of saturated sediment or glacier ice. Nevertheless, with the complexity of a model, the complexity of the needed physical parameter and knowledge increases. Table 10 showed that most of the needed input parameters for the extended version must be estimated by the user based on knowledge about the flow mechanisms of other, similar events and cannot be measure after the event happened.

There is still potential to further refine the modelling of landslides with all tested RAMMS-versions by defining areas with different  $\mu$  and  $\xi$  friction values for glaciers or forested areas, or by defining several sediment erosion areas with different friction coefficients for the entrainment and the extended version to represent complex topography more precisely (Frank et al., 2015). Although this fine-tuning would probably lead to more realistic results, it is very time-consuming to define different  $\mu$ - and  $\xi$ -areas after investigating the affected area in nature. Furthermore, sediment input through rockfall activity and erosion would rapidly change friction parameters in the affected area, and a new analysis would be necessary. It would be worthwhile taking this time and defining several  $\mu$ - and  $\xi$ -areas to model landslides in regions where rock avalanches or debris flows threaten villages to improve hazard- and risk maps and to better plan protection measures.

- IV Synthesizing of the findings and embedment of a recent event in the Swiss Alps.
- How well can such complex events be compared?
  - Is it possible to gain process understanding of a recent event in the Swiss Alps with knowledge about other similar events?

The comparability of such complex events including change of flow processes and even flow transformation is quite difficult. There are a lot of environmental factors conditioning a rock slope before a collapse which varies all around the world but also on a very small scale. These conditioning factors make it challenging to compare complex events like the ones in the inventory.

The inventory analysis showed that it is imperative to understand and reconstruct the path and the process chain of an event. This analysis helps to define how and why the event initiated and helps to determine possible initial water sources like porewater, pore-ice, glacier ice or snow, and water sources incorporated into the moving mass during the event like glacier ice, snow or saturated sediment. A source of water is inevitable for a landslide to end in unexpectedly long runout distances or even for a flow transformation. Therefore, it is crucial to define the possible water source of an event which may even help to understand less-studied and less-understood events.

The highest challenge in defining the triggering factor or the water source of an event are combined climatic factors. Most seldom, there is only one triggering factor or one specific water source. Typically, there are interrelated climatic factors like high snow rate in winter followed by a fast temperature change in spring leading to high water availability to e.g. mobilise loosely deposited material of antecedent rockfalls or rock avalanches. Such interrelated factors are difficult de detect and make it even more challenging to define triggering factors and water sources of large landslides. Future climate change will lead to high changes in

## Conclusion

mountainous regions and cause more heavy rain events, glacier melting and thus debutting as well as permafrost melting and hence destabilising of rock walls. In most cases of the events in the inventory, the triggering factor was one or a combination of the mentioned consequences of climate change. Therefore, rock avalanche frequency will probably increase in mountainous regions in the near future and threaten villages and tourist areas all over the world. It is essential to understand the mechanism of massive landslides to improve risk maps and protection measures, to ensure the safety of mountaineers, winter tourists and people living in mountain villages.

The current stability situation of the Piz Cengalo in the Bondasca Valley induces assumptions of seasonally independent future rock avalanches of sizes up to 3 million m<sup>3</sup>. The impact of the 2017 rock avalanche has destroyed a significant part of the glacier Vadrec del Cengal. In future, a part of the glacier will regrow because of snow accumulation, but due to climate change, the whole glacier will probably be melted until 2060. Therefore, it is possible that a part of the glacier could be destroyed and incorporated again in a rock avalanche, depending on where the rock avalanche hits the glacier. The deposited material of the rock avalanche increases the disposition of debris flows and can be mobilised by high water input through precipitation or snowmelt. In a few years, this material will probably be stabilised, and thus the risk of mobilisation will decrease. Further rockfall- or rock avalanche deposits will also increase the disposition of debris flows in this region, and especially after heavy rain events, debris flows must be expected, in all seasons (Amann et al., 2017). The current situation in Bondo is thus still a delicate matter. However, the expert group evaluating the risk situation and managing the building of new protection measures is doing their best.

Overall, this thesis showed that a source of water in form of snow, ice or saturated sediment can lead to a catastrophic chain of events and elongate the runout distance of landslides immensely. Therefore, the risk of future landslides in the Bondasca Valley and in all glaciated high mountain regions with loosely deposited sediment is increased during winters with high snow load or in times of heavy rain events. Moreover, destabilisation and collapse of steep glaciers through climate change increases the input of loose ice which can be mobilized by and entrained into rock avalanches and there cause flow transformation.

## 7 Literature

- Abele, G., 1997. Rockslide movement supported by the mobilization of groundwater-saturated valley floor sediments. *Zeitschrift für Geomorphol.* 14, 1–20.
- Alean, J., 1984. Untersuchungen über Entstehungsbedingungen und Reichweiten von Eislawinen. doi:10.3929/ethz-a-010782581
- Allen, S., Huggel, C., 2013. Extremely warm temperatures as a potential cause of recent high mountain rockfall. *Glob. Planet. Change* 107, 59–69. doi:10.1016/j.gloplacha.2013.04.007
- Allstadt, K., 2013. Extracting source characteristics and dynamics of the August 2010 Mount Meager landslide from broadband seismograms. *J. Geophys. Res. Earth Surf.* 118, 1472–1490. doi:10.1002/jgrf.20110
- Amann, F., Bonanomi, Y., Funk, M., Hefti, R., Huss, M., Huwiler, A., Graf, C., Hählen, N., Keiser, M., Kos, A., Kühne, R., Lunz, E., Maissen, U., Phillips, M., Roth, M., Schweizer, J., Tognacca, C., Wilhelm, C., 2017. AWN Kurzbericht der Expertengruppe zu den Ereignissen Cengalo / Bondo für die Medienkonferenz.
- Anderson, J.D.J., 1996. *Computational Fluid Dynamics: The basics with applications.*
- Baer, P., Huggel, C., McArdell, B.W., Frank, F., 2017. Changing debris flow activity after sudden sediment input: a case study from the Swiss Alps. *Geol. Today* 33, 216–223. doi:10.1111/gto.12211
- Barla, G., Barla, M., 2001. Investigation and modelling of the Brenva Glacier rock avalanche on the Mount Blanc Range. *Rock Mech. - a Chall. Soc.* 35–40.
- Barla, G., Dutto, F., Mortara, G., 2000. Brenva glacier rock avalanche of 18 January 1997 on the Mount Blanc range, northwest Italy. *Landslide News* 13, 2–5.
- Bartelt, P., Bieler, C., Bühler, Y., Christen, M., Deubelbeiss, Y., Graf, C., McArdell, B.W., Salz, M., Schneider, M., 2013. RAMMS - rapid mass movements simulation, A numerical model for debris flows in research and practice, User Manual v1.7.0, Debris Flow, Manuscript update November 2017. WSL Institute for Snow and Avalanche Research SLF.
- Berger, C., McArdell, B.W., Schlunegger, F., 2011. Direct measurement of channel erosion by debris flows, Illgraben, Switzerland. *J. Geophys. Res.* 116. doi:10.1029/2010JF001722
- Bessette-Kirton, E.K., 2017. An analysis of landslide volume, structures, and kinematics from satellite imagery of the 2016 Lamplugh rock avalanche, Glacier Bay National Park and Preserve, Alaska. Colorado School of Mines.
- Bessette-Kirton, E.K., Coe, J.A., Zhou, W., 2018. Using Stereo Satellite Imagery to Account for Ablation, Entrainment, and Compaction in Volume Calculations for Rock Avalanches on Glaciers: Application to the 2016 Lamplugh Rock Avalanche in Glacier Bay National Park, Alaska. *J. Geophys. Res. Earth Surf.* 1–20. doi:10.1002/2017JF004512
- Bottino, G., Chiarle, M., Joly, A., Mortara, G., 2002. Modelling rock avalanches and their relation to permafrost degradation in glacial environments. *Permafr. Periglac. Process.* 13, 283–288. doi:10.1002/ppp.432
- Boulton, N., Stead, D., Schwab, J., Geertsema, M., 2006. The Zymoetz River rock avalanche, June 2002, British Columbia, Canada. *Eng. Geol.* 83, 76–93. doi:10.1016/j.enggeo.2005.06.038
- Bühler, Y.B., Christen, M., Kowalski, J., Bartelt, P., 2011. Sensitivity of snow avalanche simulations to digital elevation. *Ann. Glaciol.* 52, 72–80.
- Buser, O., Bartelt, P., 2009. Production and decay of random kinetic energy in granular snow avalanches. *J. Glaciol.* 55, 3–12.
- Buss, E., Heim, A., 1881. Der Bergsturz von Elm. *Zeitschrift der Dtsch. Geol. Gesellschaft* 33, 540–564.
- Calhoun, N.C., Clague, J.J., 2018. Distinguishing between debris flows and hyperconcentrated flows: An example from the eastern Swiss Alps. *Earth Surf. Process. Landforms* 1294, 1280–1294. doi:10.1002/esp.4313
- Caplan-Auerbach, Jacqueline, Huggel, C., 2007. Precursory seismicity associated with frequent, large ice avalanches on Iliamna volcano, Alaska, USA. *J. Glaciol.* 53, 128–140. doi:10.3189/172756507781833866
- Carey, J.M., Hancox, G.T., McSaveney, M.J., 2015. The January 2013 Wanganui River debris flood resulting from a large rock avalanche from Mt Evans, Westland, New Zealand. *Landslides* 12, 961–972. doi:10.1007/s10346-015-0607-0
- Carey, M., Huggel, C., Bury, J., Portocarrero, C., Haeberli, W., 2012. An integrated socio-environmental

- framework for climate change adaption and glacier hazard management: lessons from Lake 513, Cordillera Blanca, Peru. *Clim. Change* 112, 733–767.
- Christen, M., Gerber, W., Graf, C., Bühler, Y., Bartelt, P., Glover, J., Mcardell, B.W., Feistl, T., Steinkogler, W., 2012. Numerische Simulation von gravitativen Naturgefahren mit RAMMS (Rapid Mass Movements). *Zeitschrift für Wildbach-, Lawinen-, Erosions- und Steinschlagschutz* 169, 282–293.
- Christen, M., Kowalski, J., Bartelt, P., 2010. RAMMS: Numerical simulation of dense snow avalanches in three-dimensional terrain. *Cold Reg. Sci. Technol.* 63, 1–14. doi:10.1016/j.coldregions.2010.04.005
- Clague, J., Souther, J., 1982. The Dusty Creek landslide on Mount Cayley, British Columbia. *Can. J. Earth Sci.* 19, 524–539. doi:10.1139/e82-043
- Clague, J.J., Evans, S.G., 2000. A review of catastrophic drainage of moraine-dammed lakes in British Columbia. *Quat. Sci. Rev.* 19, 1763–1783.
- Coe, J.A., Baum, R.L., Allstadt, K.E., Kochevar, B.F., Schmitt, R.G., Morgan, M.L., White, J.L., Stratton, B.T., Hayashi, T.A., Kean, J.W., 2016. Rock-avalanche dynamics revealed by large-scale field mapping and seismic signals at a highly mobile avalanche in the West Salt Creek valley, western Colorado. *Geosphere* 12, 607–631. doi:10.1130/GES01265.1
- Cox, S.C., McSaveney, M.J., Spencer, J., Allen, S.K., Ashraf, S., Hancox, G.T., Sirguyev, P., Salichon, J., Ferris, B.G., 2015. Rock avalanche on 14 July 2014 from Hillary Ridge, Aoraki/Mount Cook, New Zealand. *Landslides* 12, 395–402. doi:10.1007/s10346-015-0556-7
- Crosta, G.B., Imposimato, S., Roddeman, D., 2009. Numerical modelling of entrainment/deposition in rock and debris-avalanches. *Eng. Geol.* 109, 135–145. doi:10.1016/j.enggeo.2008.10.004
- Cruden, D.M., Lu, Z.Y., 1992. The rockslide and debris flow from Mount Cayley, B.C. in June 1984. *Can. Geotech. Journal* 29, 614–626.
- Davidson, P.A., 2004. *Turbulence: An Introduction for Scientists and Engineers.*
- De Blasio, F.V., 2014. Friction and dynamics of rock avalanches travelling on glaciers. *Geomorphology* 213, 88–98. doi:10.1016/j.geomorph.2014.01.001
- De Graaf, K. De, Bowman, E., 2016. Influences of strain rate and shear rate on the propagation of large scale rock avalanches.
- Delaney, K.B., Evans, S.G., 2014. The 1997 Mount Munday landslide (British Columbia) and the behaviour of rock avalanches on glacier surfaces. *Landslides* 11, 1019–1036. doi:10.1007/s10346-013-0456-7
- Delaney, K.B., Evans, S.G., 2008. Application of digital cartographic techniques in the characterization and analysis of catastrophic landslides; the case of the 1997 Mount Munday rock avalanche, British Columbia. 4th Can. Conf. Geohazards From Cause to Manag. 141–146.
- Delcamp, A., Roberti, G., van Wyk de Vries, B., 2016. Water in volcanoes: evolution, storage and rapid release during landslides. *Bull. Volcanol.* 78. doi:10.1007/s00445-016-1082-8
- Deline, P., 2009. Interactions between rock avalanches and glaciers in the Mont Blanc massif during the late Holocene. *Quat. Sci. Rev.* 28, 1070–1083. doi:10.1016/j.quascirev.2008.09.025
- Deline, P., Hewitt, K., Reznichenko, N., Shugar, D., 2015. Rock Avalanches onto Glaciers, Landslide Hazards, Risks, and Disasters. doi:10.1016/B978-0-12-396452-6.00009-4
- Evans, S.G., Bishop, N.F., Fidel Smoll, L., Valderrama Murillo, P., Delaney, K.B., Oliver-Smith, A., 2009a. A re-examination of the mechanism and human impact of catastrophic mass flows originating on Nevado Huascarán, Cordillera Blanca, Peru in 1962 and 1970. *Eng. Geol.* 108, 96–118. doi:10.1016/j.enggeo.2009.06.020
- Evans, S.G., Clague, J.J., 1999. Rock avalanches on glaciers in the Coast and St. Elias Mountains, British Columbia, in: *Slope Stability and Landslides.* pp. 115–123.
- Evans, S.G., Clague, J.J., 1988. Catastrophic rock avalanches in glacial environments, in: Bonnard, C. (Ed.), *Landslides - Proceedings of the Fifth International Symposium on Landslides.* A.A. Balkema/Rotterdam/Brookfield, Lausanne, Switzerland, pp. 1152–1158.
- Evans, S.G., Delaney, K.B., 2014. Catastrophic Mass Flows in the Mountain Glacial Environment, Snow and Ice-Related Hazards, Risks, and Disasters. doi:10.1016/B978-0-12-394849-6.00016-0
- Evans, S.G., Tutubalina, O. V., Drobyshev, V.N., Chernomorets, S.S., McDougall, S., Petrakov, D.A., Hungr, O., 2009b. Catastrophic detachment and high-velocity long-runout flow of Kolka Glacier, Caucasus Mountains, Russia in 2002. *Geomorphology* 105, 314–321. doi:10.1016/j.geomorph.2008.10.008

- Feng, Z., 2011. The seismic signatures of the 2009 Shiaolin landslide in Taiwan. *Nat. Hazards Earth Syst. Sci.* 11, 1559–1569. doi:10.5194/nhess-11-1559-2011
- Frank, F., McArdell, B.W., Huggel, C., Vieli, A., 2015. The importance of entrainment and bulking on debris flow runout modeling: Examples from the Swiss Alps. *Nat. Hazards Earth Syst. Sci.* 15, 2569–2583. doi:10.5194/nhess-15-2569-2015
- Frank, F., Mcardell, B.W., Oggier, N., Baer, P., Christen, M., Vieli, A., 2017. Debris-flow modeling at Meretschibach and Bondasca catchments, Switzerland: sensitivity testing of field-data-based entrainment model. *Nat. Hazards Earth Syst. Sci.* 17, 801–815.
- Geertsema, M., 2012. Initial observations of the 11 June 2012 rock / ice avalanche, Lituya, in: *The First Meeting of Cold Region Landslides Network*, Harbin, China. pp. 1–5. doi:10.13140/2.1.2473.5682
- Geertsema, M., Clague, J.J., Schwab, J.W., Evans, S.G., 2006. An overview of recent large catastrophic landslides in northern British Columbia, Canada. *Eng. Geol.* 83, 120–143. doi:10.1016/j.enggeo.2005.06.028
- Gordon, J.E., Birnie, R. V., Timmist, R., 1978. A Major Rockfall and Debris Slide on the Lyell Glacier, South Georgia. *Arct. Alp. Res.* 10, 49–60.
- Gruber, S., Hoelzle, M., Haerberli, W., 2004. Permafrost thaw and destabilization of Alpine rock walls in the hot summer of 2003. *Geophys. Res. Lett.* 31, 1–4. doi:10.1029/2004GL020051
- Gruber, U., Bartelt, P., 2007. Snow avalanche hazard modelling of large areas using shallow water numerical methods and GIS. *Environ. Model. Softw.* 22, 1472–1481. doi:10.1016/j.envsoft.2007.01.001
- Guthrie, R.H., Friele, P., Allstadt, K., Roberts, N., Evans, S.G., Delaney, K.B., Roche, D., Clague, J.J., Jakob, M., 2012. The 6 August 2010 Mount Meager rock slide-debris flow, Coast Mountains, British Columbia: Characteristics, dynamics, and implications for hazard and risk assessment. *Nat. Hazards Earth Syst. Sci.* 12, 1277–1294. doi:10.5194/nhess-12-1277-2012
- Haerberli, W., Huggel, C., Kääb, A., Polkvoj, A., Zotikov, I., Osokin, N., 2003. Permafrost conditions in the starting zone of the Kolka-Karmadon rock/ice slide of 20 September 2002 in North Osetia (Russian Caucasus). *Eight Int. Conf. Permafr.* 49–50.
- Haerberli, W., Huggel, C., Kääb, A., Zraggen-Oswald, S., Polkvoj, A., Galushkin, I., Zotikov, I., Osokin, N., 2004. The Kolka-Karmadon rock/ice slide of 20 September 2002: An extraordinary event of historical dimensions in North Ossetia, Russian Caucasus. *J. Glaciol.* 50, 533–546. doi:10.3189/172756504781829710
- Hancox, G.T., McSaveney, M.J., Manville, V.R., Davies, T.R., 2005. The October 1999 Mt Adams rock avalanche and subsequent landslide dam-break flood and effects in Poerua river, Westland, New Zealand. *New Zeal. J. Geol. Geophys.* 48, 683–705. doi:10.1080/00288306.2005.9515141
- Hancox, G.T., Thomson, R., 2013. The January 2013 Mt Haast Rock Avalanche The January 2013 Mt Haast Rock Avalanche and Ball Ridge Rock Fall in Aoraki / Mt Cook National Park, New Zealand, GNS Science Report.
- Hanisch, J., Koirala, A., Bhandary, N.P., 2013. The Pokhara May 5th flood disaster: A last warning sign sent by nature? *46*, 1–10.
- Hatherton, T., Leopard, A.E., 1964. The densities of New Zealand rocks. *New Zeal. J. Geol. Geophys.* 7, 605–625. doi:10.1080/00288306.1964.10422108
- Hauser, A., 2002. Rock avalanche and resulting debris flow in Estero Parraguirre and Río Colorado, Región Metropolitana, Chile, *Catastrophic Landslides: Effects, Occurrence, and Mechanisms*. Geological Society of America Reviews in Engineering Geology: Boulder, CO.
- Heim, A., 1932. Bergsturz und Menschenleben. *Beiblatt zur Vierteljahrsschrift der Naturforschenden Gesellschaft Zürich* 1–218.
- Hewitt, K., 2009. Rock avalanches that travel onto glaciers and related developments, Karakoram Himalaya, Inner Asia. *Geomorphology* 103, 66–79. doi:10.1016/j.geomorph.2007.10.017
- Hewitt, K., 1988. Catastrophic Landslide Deposits in the Karakoram Himalaya. *Science (80- )*. 242, 64–67. doi:10.1126/science.242.4875.64
- Hibert, C., Ekström, G., Stark, C.P., 2014. Dynamics of the Bingham Canyon Mine landslides from seismic signal analysis. *Geophys. Res. Lett.* 41, 4535–4541. doi:10.1002/2014GL060592
- Huggel, C., 2009. Recent extreme slope failures in glacial environments: effects of thermal perturbation. *Quat. Sci. Rev.* 28, 1119–1130. doi:10.1016/j.quascirev.2008.06.007

- Huggel, C., Caplan-Auerbach, J., Waythomas, C.F., Wessels, R.L., 2007. Monitoring and modeling ice-rock avalanches from ice-capped volcanoes: A case study of frequent large avalanches on Iliamna Volcano, Alaska. *J. Volcanol. Geotherm. Res.* 168, 114–136. doi:10.1016/j.jvolgeores.2007.08.009
- Huggel, C., Caplan-Auerbach, J., Wessels, R., 2008a. Recent extreme avalanches: Triggered by climate change? *Eos (Washington, DC)*. 89, 469–470. doi:10.1029/2008EO470001
- Huggel, C., Gruber, S., Caplan-Auerbach, J., Wessels, R.L., Molnia, B.F., 2008b. The 2005 Mt. Steller, Alaska, rock-ice avalanche: What does it tell us about large slope failures in cold permafrost?, in: Ninth International Conference on Permafrost. pp. 747–752. doi:10.5167/uzh-3097
- Huggel, C., Salzmann, N., Allen, S., Caplan-Auerbach, J., Fischer, L., Haeberli, W., Larsen, C., Schneider, D., Wessels, R., 2010. Recent and future warm extreme events and high-mountain slope stability. *Philos. Trans. R. Soc. A Math. Phys. Eng. Sci.* 368, 2435–2459. doi:10.1098/rsta.2010.0078
- Huggel, C., Zraggen-Oswald, S., Haeberli, W., Kääh, A., Polkvoj, A., Galushkin, I., Evans, S.G., 2005. The 2002 rock/ice avalanche at Kolka/Karmadon, Russian Caucasus: assessment of extraordinary avalanche formation and mobility, and application of QuickBird satellite imagery. *Nat. Hazards Earth Syst. Sci.* 5, 173–187. doi:10.5194/nhess-5-173-2005
- Hungr, O., Evans, S.G., 2004. Entrainment of debris in rock avalanches: An analysis of a long run-out mechanism. *Bull. Geol. Soc. Am.* 116, 1240–1252. doi:10.1130/B25362.1
- Hungr, O., Leroueil, S., Picarelli, L., 2014. The Varnes classification of landslide types, an update. *Landslides* 11, 167–194. doi:10.1007/s10346-013-0436-y
- Hungr, O., McDougall, S., 2009. Two numerical models for landslide dynamic analysis. *Comput. Geosci.* 35, 978–992. doi:10.1016/j.cageo.2007.12.003
- Hussin, H.Y., Quan Luna, B., Van Westen, C.J., Christen, M., Malet, J.P., Van Asch, T.W.J., 2012. Parameterization of a numerical 2-D debris flow model with entrainment: A case study of the Faucon catchment, Southern French Alps. *Nat. Hazards Earth Syst. Sci.* 12, 3075–3090. doi:10.5194/nhess-12-3075-2012
- Iribarren Anaconda, P., Bodin, X., 2010. Geomorphic consequences of two large glacier and rock glacier destabilizations in the Central and Northern Chilean Andes. *Geophys. Res. Abstr.* 12, 7162.
- Jibson, R.W., Harp, E.L., Schulz, W., Keefer, D.K., 2006. Large rock avalanches triggered by the M 7.9 Denali Fault, Alaska, earthquake of 3 November 2002. *Eng. Geol.* 83, 144–160. doi:10.1016/j.enggeo.2005.06.029
- Jiskoot, H., 2011. Long-runout rockslide on glacier at Tsar Mountain, Canadian Rocky Mountains: Potential triggers, seismic and glaciological implications. *Earth Surf. Process. Landforms* 36, 203–216. doi:10.1002/esp.2037
- Korup, O., 2005. Large landslides and their effect on sediment flux in South Westland, New Zealand. *Earth Surf. Process. Landforms* 30, 305–323. doi:10.1002/esp.1143
- Kotlyakov, V.M., Rototaeva, O. V., Nosenko, G. a, 2004. The September 2002 Kolka glacier catastrophe in North Ossetia, Russian Federation: evidence and analysis. *Mt. Res. Dev.* 24, 78–83. doi:10.1659/0276-4741(2004)024[0078:tskgci]2.0.co;2
- Lipovsky, P.S., Evans, S.G., Clague, J.J., Hopkinson, C., Couture, R., Bobrowsky, P., Ekström, G., Demuth, M.N., Delaney, K.B., Roberts, N.J., Clarke, G., Schaeffer, A., 2008. The July 2007 rock and ice avalanches at Mount Steele, St. Elias Mountains, Yukon, Canada. *Landslides* 5, 445–455. doi:10.1007/s10346-008-0133-4
- McDougall, S., Boulton, N., Hungr, O., Stead, D., Schwab, J.W., 2006. The Zymoetz River landslide, British Columbia, Canada: Description and dynamic analysis of a rock slide-debris flow. *Landslides* 3, 195–204. doi:10.1007/s10346-006-0042-3
- Moore, J.R., Pankow, K.L., Ford, S.R., Koper, K.D., Hale, J.M., Aaron, J., Larsen, C.F., 2017. Dynamics of the Bingham Canyon rock avalanches (Utah, USA) resolved from topographic, seismic, and infrasound data. *J. Geophys. Res. Earth Surf.* 122, 615–640. doi:10.1002/2016JF004036
- Pankow, K.L., Moore, J.R., Mark Hale, J., Koper, K.D., Kubacki, T., Whidden, K.M., McCarter, M.K., 2014. Massive landslide at Utah copper mine generates wealth of geophysical data. *GSA Today* 24, 4–9. doi:10.1130/GSATG191A.1
- Persson, B.N.J., 2000. *Sliding Friction: Physical Principles and Applications*. Springer Verlag, Berlin.
- Petrakov, D. a., Chernomorets, S.S., Evans, S.G., Tutubalina, O. V., 2008. Catastrophic glacial multi-phase mass movements: a special type of glacial hazard. *Adv. Geosci.* 14, 211–218. doi:10.5194/adgeo-14-211-

2008

- Pirulli, M., 2009. The Thurwieser rock avalanche (Italian Alps): Description and dynamic analysis. *Eng. Geol.* 109, 80–92. doi:10.1016/j.enggeo.2008.10.007
- Preuth, T., Bartelt, P., Korup, O., Mcardell, B.W., 2010. A random kinetic energy model for rock avalanches : Eight case studies. *J. Geophys. Res.* 115, 1–22. doi:10.1029/2009JF001640
- Rickenmann, D., Laigle, D., Mcardell, B.W., Hübl, J., 2006. Comparison of 2D debris-flow simulation models with field events. *Comput. Geosci.* 10, 241–264. doi:10.1007/s10596-005-9021-3
- Roberti, G., Friele, P., van Wyk de Vries, B., Ward, B., Clague, J.J., Perotti, L., Giardino, M., 2017. Rheological evolution of the mount meager 2010 debris avalanche, southwestern british columbia. *Geosphere* 13, 1–22. doi:10.1130/GES01389.1
- Roberti, G., Ward, B., van Wyk de Vries, B., Friele, P., Perotti, L., Clague, J.J., Giardino, M., 2018. Precursory slope distress prior to the 2010 Mount Meager landslide, British Columbia. *Landslides* 15, 637–647. doi:10.1007/s10346-017-0901-0
- Salm, B., 1993. Flow, flow transition and run-out distances of flowing avalanches. *Ann. Glaciol.* 18, 221–226. doi:10.1017/S0260305500011551
- Salm, B.W., Burkard, A., Gubler, H., 1990. Berechnung von Fließlawinen: Eine Anleitung für Praktiker mit Beispielen.
- Sartoris, G., Bartelt, P., 2000. Upwinded finite difference schemes for dense snow avalanche modeling. *Int. J. Numer. Methods Fluids* 32, 799–821. doi:10.1002/(SICI)1097-0363(20000415)32:7<799::AID-FLD989>3.0.CO;2-2
- Sassa, K., 1985. The mechanism of debris flow, in: XI International Conference on Soil Mechanics and Foundation Engineering, San Francisco, California. pp. 1173–1176.
- Scheuner, T., Keusen, H.R., Mcardell, B.W., Huggel, C., 2009. Murgangmodellierung mit dynamisch-physikalischem und GIS-basiertem Fließmodell, Fallbeispiel Rotlauigraben, Guttannen, August 2005. *Wasser Energ. Luft* 15–21.
- Scheuner, T., Schwab, S., McArdell, B.W., 2011. Application of a two-dimensional numerical model in risk and hazard assessment in Switzerland, in: 5th DFHM, Padua, Italy.
- Schneider, D., Bartelt, P., Caplan-Auerbach, J., Christen, M., Huggel, C., McArdell, B.W., 2010. Insights into rock-ice avalanche dynamics by combined analysis of seismic recordings and a numerical avalanche model. *J. Geophys. Res. Earth Surf.* 115, 1–20. doi:10.1029/2010JF001734
- Schneider, D., Huggel, C., Haeblerli, W., Kaitna, R., 2011a. Unraveling driving factors for large rock-ice avalanche mobility. *Earth Surf. Process. Landforms* 36, 1948–1966. doi:10.1002/esp.2218
- Schneider, D., Kaitna, R., Dietrich, W.E., Hsu, L., Huggel, C., McArdell, B.W., 2011b. Frictional behavior of granular gravel-ice mixtures in vertically rotating drum experiments and implications for rock-ice avalanches. *Cold Reg. Sci. Technol.* 69, 70–90. doi:10.1016/j.coldregions.2011.07.001
- Schneider, J.F., 2006. Risk assessment of remote geohazards in Western Pamir, GBAE, Tajikistan, in: Haeblerli, W. (Ed.), *Proceedings of the International Conference on High Mountain Hazard Prevention*. Swiss Agency for Development and Cooperation, Vladikavkaz/Moscow, pp. 252–267.
- Schwab, J., Geertsema, M., Evans, S.G., 2003. Catastrophic rock avalanches, west-central British Columbia. *Proc. 3rd Can. Conf. Geotech. Nat. hazards* 291–298. doi:10.13140/2.1.3973.5361
- Shumskiy, P.A., 1960. Density of glacier ice. *J. Glaciol.* 3, 568–573.
- Sosio, R., Crosta, G.B., Hungr, O., 2008. Complete dynamic modeling calibration for the Thurwieser rock avalanche (Italian Central Alps). *Eng. Geol.* 100, 11–26. doi:10.1016/j.enggeo.2008.02.012
- Stoffel, M., Huggel, C., 2012. Effects of climate change on mass movements in mountain environments. *Prog. Phys. Geogr.* 36, 421–439. doi:10.1177/0309133312441010
- Stolz, A., Huggel, C., 2008. Debris flows in the Swiss National Park : the influence of different flow models and varying DEM grid size on modeling results. *Landslides* 5, 311–319. doi:10.1007/s10346-008-0125-4
- Tsou, C.Y., Feng, Z.Y., Chigira, M., 2011. Catastrophic landslide induced by Typhoon Morakot, Shiaolin, Taiwan. *Geomorphology* 127, 166–178. doi:10.1016/j.geomorph.2010.12.013
- Tusima, K., 2010. Estimation friction coefficient of stone and mechanism of curl, in: *Cold Regions Science and Technology Conference* 26. pp. 422–427.



- Varnes, D.J., 1978. Slope Movement Types and Processes. Spec. Rep. 176 Landslides Anal. Control. Transp. Res. Board, Washington, D.C. 11–33.
- Varnes, D.J., 1954. Landslide Types and Processes. Spec. Rep. 28 Highw. Res. Board. Natl. Acad. Sci. Washington, D.C. 20–47.
- Voight, B., Sousa, J., 1994. Lessons from Ontake-san: A comparative analysis of debris avalanche dynamics. Eng. Geol. 38, 261–297. doi:10.1016/0013-7952(94)90042-6
- Waythomas, C.F., Miller, T.P., Begét, J.E., 2000. Record of late holocene debris avalanches and lahars at Iliamna Volcano, Alaska. J. Volcanol. Geotherm. Res. 104, 97–130. doi:10.1016/S0377-0273(00)00202-X
- Yamasaki, S., Hidehisa, N., Kawaguchi, T., 2014. Long-traveling landslides in deep snow conditions induced by the 2011 Nagano Prefecture earthquake, Japan. Landslides 11, 605–613. doi:10.1007/s10346-013-0419-z

## 7.1 Online Sources

- <https://www.britannica.com/science/rock-geology#ref80185> (14.03.2018)
- <https://www.britannica.com/place/Coast-Mountains> (25.04.2018)
- <https://www.britannica.com/science/latent-heat> (13.08.2018)
- <http://ds.iris.edu/ds/> (19.04.2018)
- <http://ds.iris.edu/spud/esecc> (19.04.2018)
- <http://www.edumine.com/xtoolkit/tables/sgtables.htm> (14.03.2018)
- <https://geology.com/canada/british-columbia.shtml> (14.08.2018)
- <https://www.gr.ch/DE/Medien/Mitteilungen/MMStaka/2017/Seiten/2017121501.aspx> (22.05.2018)
- [https://lta.cr.usgs.gov/ALOS\\_Palsar](https://lta.cr.usgs.gov/ALOS_Palsar) (28.03.2018)
- <https://www.thoughtco.com/densities-of-common-rocks-and-minerals-1439119> (14.03.2018)

## 8 Appendix

### 8.1 Complete inventory of events

Table 11 Complete inventory of events

<i>Place Name of event</i>	<i>Year</i>	<i>Event</i>	<i>Triggering Factor</i>	<i>H<sub>f</sub> [m]</i>	<i>V<sub>i</sub> [m<sup>3</sup>]</i>	<i>p<sub>g</sub> [m]</i>	<i>t [s] / n</i>	<i>V<sub>f</sub> [m/s]</i>	<i>Water source</i>	<i>Water content</i>
<b>Alps, Italy</b>										
Brenva Glacier	1997	Rock slide/	Hydrostatic pressure		2.0E+06	5'400	xx/1		S, G	> 4.5E+06 m <sup>3</sup>
Thurwieser	2004	Rock avalanche	Not sure		2.0E+06	550	80-90/xx	30-40	No source	10 %
<b>Greenland</b>										
Nuugaatsiaq	2017	Landslide								
<b>Alaska, USA</b>										
Iliamna Red Glacier	1978	Ice-rock avalanche	Shear stress > shear strength		6.5E+06	7'000			G	60 %
Iliamna Red Glacier	1980	Ice-rock avalanche	Shear stress > shear strength		1.1E+07	7'300			S, G	60 %
Iliamna Red Glacier	1994	Ice-rock avalanche	Pore pressure, thermal effects, Shear stress > shear strength			9'500	500/xx	22-46	G	60 %
Iliamna Red Glacier	1997	Ice-rock avalanche	Pore pressure, thermal effects, Shear stress > shear strength			7'100	170/xx	22-51	G	~ 50-60 %
Iliamna Red Glacier	2000	Ice-rock avalanche	Pore pressure, thermal effects, Shear stress > shear strength			8'400		60-75	G	60 %
Iliamna Red Glacier	2003	Ice-rock avalanche	Pore pressure, thermal effects, Shear stress > shear strength		6.0E+06	8'000	180/xx	37-46	S, G	60-80 %
Iliamna Red Glacier	2008	Ice-rock avalanche	Pore pressure, thermal effects, Shear stress > shear strength						G	
Iliamna Red Glacier	2016	Rock and ice avalanche	Pore pressure, thermal effects, Shear stress > shear strength						G	

<i>Place Name of event</i>	<i>H [m]</i>	<i>L [m]</i>	<i>α [°]</i>	<i>A<sub>d</sub> [km<sup>2</sup>]</i>	<i>V<sub>d</sub> [m<sup>3</sup>]</i>	<i>ER</i>	<i>FT</i>	<i>Rock type</i>	<i>ρ [kg/m<sup>3</sup>]</i>	<i>E<sub>calc</sub> (E<sub>lit</sub>) [J]</i>	<i>MW prod. [m<sup>3</sup>]</i>	<i>Reference</i>
<b>Alps, Italy</b>												
Brenva Glacier	2'325	5'849	21.7	2.5	6.5E+06	3.3	X	Granite	2700	1.2E+14	4.0E+05	[1], [2], [3]
Thurwieser	1'296	2'697	25.7	0.4	2.9E+06	1.5	0	Dolomite	3000	7.6E+13	2.5E+05	[4], [5], [3]
<b>Greenland</b>												
Nuugaatsiaq		1'900	0.0		4.3E+07		X					[10]
<b>Alaska, USA</b>												
Iliamna Red Glacier	1'782	7'691	13.0		1.7E+07	2.6	0	Andesite	2700	3.1E+14	1.0E+06	[3], [6]
Iliamna Red Glacier	1'679	7'806	12.1		2.8E+07	2.6	0	Andesite	2700	4.8E+14	1.6E+06	[3], [6]
Iliamna Red Glacier	1'796	9'993	10.2	11.0	1.7E+07		0	Andesite	2700	7.8E+14	2.6E+06	[3], [6], [7], [8]
Iliamna Red Glacier	1'706	7'694	12.5	9.0	1.5E+07		0	Andesite	2700	6.6E+14	2.1E+06	[3], [6], [7], [8]
Iliamna Red Glacier	1'832	8'890	11.6		1.5E+07		0	Andesite	2700	7.0E+14	2.3E+06	[3], [6]
Iliamna Red Glacier	1'769	8'556	11.7	4.0	1.6E+07	2.7	0	Andesite	2700	2.8E+14	9.1E+06	[3], [6], [7]
Iliamna Red Glacier	1'708	7'447	12.9		1.1E+07		0	Andesite	2700	5.0E+14	1.6E+06	[6]
Iliamna Red Glacier	1'700	8'200	11.7	8.6	1.6E+07		0	Andesite	2700	7.2E+14	2.3E+06	[6], [10]

<i>Place Name of event</i>	<i>Year</i>	<i>Event</i>	<i>Triggering Factor</i>	$H_f$ [m]	$V_i$ [m <sup>3</sup> ]	$p_g$ [m]	$t$ [s] / $n$	$V_f$ [m/s]	<i>Water source</i>	<i>Water content</i>
Iliamna Lateral Glacier	2004	Rock-ice avalanche	Shear stress > shear strength		2.5E+06		110/xx	29-65	S, G, Ini	
Iliamna Umbrella Glacier	2004	Ice-rock avalanche	Pore pressure, thermal effects		1.0E+06	5'550	80/xx	35-70	G	50 %
Iliamna	2013	Ice avalanche	Pore pressure, thermal effects						G	
Hitchcock Hills, Marvine	1983	Ice avalanche	maybe earthquake from 14.7.83		1.0E+06	2'050			Firn	70 %
McGinnis Peak North	2002	Rock avalanche	Denali Fault earthquake		1.8E+07	10'500		40-54	S, G, Ini	2E+06 m <sup>3</sup>
McGinnis Peak South	2002	Rock avalanche	Denali Fault earthquake		1.1E+07	10'700			Possibly SD	
Black Rapids East	2002	Rock avalanche	Denali Fault earthquake		1.2E+07	3'600			G	
Black Rapids Middle	2002	Rock avalanche	Denali Fault earthquake		1.0E+07	3'200			G	
Black Rapids West	2002	Rock avalanche	Denali Fault earthquake		6.0E+06	2'200			G	
West Fork Glacier North	2002	Rock avalanche	Denali Fault earthquake					30-32	Possibly G	
West Fork Glacier South	2002	Rock avalanche	Denali Fault earthquake					30-32	G	
Mount Steller	2005	Rock-ice avalanche/ Slope failure and avalanche	Hanging glacier instability		1.5E+07	4'000	~2300/4	min. 100	S, G, Ini	3.6E+05 m <sup>3</sup>
Mount Steller North 1	2008	Landslide	rock slope instability, thermal effects		5.5E+05		xx/1		Ini	
Mount Steller North 2	2008	Landslide	Not sure				xx/2		G	
Mount Miller	2008	Rock-ice avalanche	Probably bedrock failure			3'650			Ini	
Lituya Mountain	2012	Rock-ice avalanche	Not sure, maybe debutting effect, snow load, permafrost thaw			6'500	290/1		G	
Redoubt Glacier	2015	Rock-ice avalanche								
Lamplugh Glacier	2016	Rock avalanche			5.2E+07	6'700			S, I	

<i>Place Name of event</i>	<i>H [m]</i>	<i>L [m]</i>	<i><math>\alpha</math> [°]</i>	<i><math>A_d</math> [km<sup>2</sup>]</i>	<i><math>V_d</math> [m<sup>3</sup>]</i>	<i>ER</i>	<i>FT</i>	<i>Rock type</i>	<i><math>\rho</math> [kg/m<sup>3</sup>]</i>	<i><math>E_{calc}</math> (<math>E_{lit}</math>) [J]</i>	<i>MW prod. [m<sup>3</sup>]</i>	<i>Reference</i>
Iliamna Lateral Glacier	1'740	5'160	18.6		5.0E+06	2.0	0			0.0E+00		[6], [7]
Iliamna Umbrella Glacier	1'765	6'036	16.3		4.0E+06	4.0	0	Andesite	2700	4.7E+13	1.5E+05	[3], [6], [7]
Iliamna	1'400	4'900	15.9	5.6	3.0E+06		0	Andesite	2700	1.1E+14	3.6E+05	[10]
Hitchcock Hills, Marvine	860	3'144	15.3	0.6	3.0E+06	3.0	0	Ice	920	7.8E+12	2.5E+04	[3], [9]
McGinnis Peak North	1'718	10'960	8.9	10.2	2.0E+07	1.1	0	Granite	2700	8.4E+14	2.7E+06	[3], [11]
McGinnis Peak South	1'904	11'463	9.4	5.7	1.1E+07	1.0	0	Granite	2700	5.7E+14	1.9E+06	[3], [11]
Black Rapids East	997	4'605	12.2	4.6	1.4E+07	1.2	X	Granite	2700	3.0E+14	9.9E+05	[3], [11]
Black Rapids Middle	827	4'478	10.5	4.6	1.4E+07	1.4	X	Granite	2700	2.2E+14	7.1E+05	[3], [11]
Black Rapids West	724	3'307	12.3	3.2	9.7E+06	1.6	X	Granite	2700	1.2E+14	3.7E+05	[3], [11]
West Fork Glacier North	737	3'296	12.6	1.4	4.1E+06		X	Granite	2700	8.0E+13	2.6E+05	[11]
West Fork Glacier South	1'005	4'249	13.3	1.5	4.4E+06		X	Granite	2700	1.2E+14	3.8E+05	[11]
Mount Steller	2'430	9'000	15.1	4.0	5.0E+07	3.3	X	Sedimentary Rock	2500	8.9E+14	2.9E+06	[3], [12]
Mount Steller north 1	822	1'767	24.9		1.5E+06	2.7	0	Sedimentary Rock	2500	1.1E+13	3.6E+04	[13]
Mount Steller north 2	476	2'200	12.2	0.5	1.5E+06		X	Sedimentary Rock	2500	1.8E+13	5.7E+04	[13]
Mount Miller	910	4'507	11.4	~5.5	2.2E+07		X	Basalt	3000	5.9E+14	1.9E+06	[3], [13]
Lituya Mountain	2'400	9'300	14.5	7.9	1.3E+07		X	Gabbro	3000	9.2E+14	3.0E+06	[3], [10], [14]
Redoubt Glacier	1'372	3'700	20.3	0.8	1.1E+06		X	Volcanic	2700	4.1E+13	1.3E+05	[10]
Lamplugh Glacier	1'500	10'500	8.1	22.2	7.0E+07	1.4	X	Greywacke	2700	2.1E+15	6.7E+06	[15], [16]

<i>Place Name of event</i>	<i>Year</i>	<i>Event</i>	<i>Triggering Factor</i>	<i>H<sub>f</sub> [m]</i>	<i>V<sub>i</sub> [m<sup>3</sup>]</i>	<i>p<sub>g</sub> [m]</i>	<i>t [s] / n</i>	<i>V<sub>f</sub> [m/s]</i>	<i>Water source</i>	<i>Water content</i>
Mount La Perouse	2014	Rock-ice avalanche								
<b>British Columbia, Canada</b>										
Devastation Glacier, Mount Meager	1975	Landslide	Glacial meltwater			2'500		30		
North Creek	1986	Landslide				1'000				
Kshwan Glacier	1992/93	Rockslide on glacier	Glacial debuttressing			1'400			G	
Mount Munday	1997	Rock avalanche	Possible freeze-thaw cycle	500	3.2E+06	> 4500	419/2	11	G	
Howson II	1999	Rockslide on glacier	Debuttressing and Destabilization		9.0E+05	150	xx/1	18-30	G	
Tsar Mountain	2000	Long-runout rockslide	Co-triggering of heavy rainfall, snowmelt, and overnight freezing	185	1.6E+06	1'700	56-108 / xx	22-45	S, G, SD	40 %
Zymoetz River	2002	Rock avalanche Rock slide-debris flow	Progressive, long-term degradation of tectonically deformed and altered rock mass; long-term degradation, possibly freeze-thaw cycles, pore water pressures		1.1E+06	Rock avalanche sliding over snow, not over glacier	xx/3	15-25	SD, Ini	
Mount Steele, Yukon	2007	Rock-ice avalanche	Possibly highly sheared igneous rocks		3.0E+06	4'050	100/1	35-65	S, G	95 %
Mount Steele, Yukon	2015	Rock avalanche					110/xx			
Mount Meager, Capricorn Glacier	2010	Rock slide-debris flow	Glacial retreat, hot summer temperatures	500	4.9E+07	< 500	~324/4	64	G, SD	< 1%
Harold Price	2002	Rock avalanche Rock slide-debris flow	Interstitial ice	300	7.0E+05		xx/1	28-35	Ini (rock glacier)	
<b>Colorado, USA</b>										
West Salt Creek main	2014	Rock slide and Rock avalanche	Not mentioned				207/2	20-26	SD	

<i>Place Name of event</i>	<i>H [m]</i>	<i>L [m]</i>	<i>α [°]</i>	<i>A<sub>d</sub> [km<sup>2</sup>]</i>	<i>V<sub>d</sub> [m<sup>3</sup>]</i>	<i>ER</i>	<i>FT</i>	<i>Rock type</i>	<i>ρ [kg/m<sup>3</sup>]</i>	<i>E<sub>calc</sub> (E<sub>lit</sub>) [J]</i>	<i>MW prod. [m<sup>3</sup>]</i>	<i>Reference</i>
Mount La Perouse	1'779	7'374	13.6	5.5	1.4E+07		X	Greywacke	2700	6.6E+14	2.6E+06	[10]
<b>British Columbia, Canada</b>												
Devastation Glacier, Mount Meager	1'170	6'568	10.1		1.2E+07		1	Volcanic (Andesite)	2700	3.7E+14	1.6E+06	[3], [17], [18]
North Creek	745	2'683	15.5		2.0E+06		X	Volcanic (Andesite)	2700	3.9E+13	1.3E+05	[3], [19]
Kshwan Glacier	675	2'205	17.0	0.68	3.1E+06		X	Volcanic (Andesite)	2700	5.5E+13	1.8E+05	[3], [20]
Mount Munday	850	4'650	10.4	2.6	5.0E+06	1.6	High fragment. subseq. debris flow	Volcanic (Andesite)	2700	4.2E+13 (4.33E13)	1.4E+05	[3], [20], [21], [22]
Howson II	1'296	2'700	25.6		2.5E+06	2.8		Granodiorite	2700	3.1E+13	1.0E+05	[19], [23]
Tsar Mountain	615	2'230	15.4		3.0E+06	1.9	X	Limestone Silt/Sand- stone	2500	7.3E+12 (7.3E12)	2.4E+04	[3], [24]
Zymoetz River	1'245	3'500	19.6		1.5E+06	1.4	1	Volcaniclas- tic	2700	3.6E+13	1.2E+05	[23], [25], [26]
Mount Steele, Yukon	2'160	5'800	20.4	5.3	4.0E+06	1.3	High fluidity	Granodiorite	2700	1.7E+14	5.6E+05	[3], [10], [27]
Mount Steele, Yukon	2'200	3'700	30.7		2.0E+07		X	Granodiorite	2700	1.2E+15	3.8E+06	[10]
Mount Meager, Cap- ricorn Glacier	2'183	12'700	9.8	9.7	4.9E+07	1.0	1	Volcanic (Andesite)	2700	6.4E+14	2.1E+06	[3], [10], [28], [29], [30], [31]
Harold Price	720	4'000	10.2		2.0E+06	2.9	1	Volcanic	2700	5.6E+12	1.8E+04	[19], [23]
<b>Colorado, USA</b>												
West Salt Creek main	636	4'590	7.9	2.3	5.4E+07		1	Sedimentary Rock	2500	8.5E+14	2.8E+06	[32]

<i>Place Name of event</i>	<i>Year</i>	<i>Event</i>	<i>Triggering Factor</i>	<i>H<sub>f</sub> [m]</i>	<i>V<sub>i</sub> [m<sup>3</sup>]</i>	<i>p<sub>g</sub> [m]</i>	<i>t [s] / n</i>	<i>V<sub>f</sub> [m/s]</i>	<i>Water source</i>	<i>Water content</i>
<b>Utah, USA</b>										
Bingham Canyon	2013	Massive land- slide Rock avalanche	Sliding-mode failures on a highly persistent basal fault		5.2E+07		180/2	36		
<b>Cascade Volcanoes, Washington, USA</b>										
Mount Adams	1997	Rock-ice avalanche								
Mount Adams	1997	Rock-ice avalanche								
Mount Adams	2008	Rock-ice avalanche								
<b>Cordillera Blanca, Peru</b>										
Nevados Huascarán	1970	mud-rich debris flow Ice-Rock ava- lanche	Earthquake		7.5E+06	2'400	180-270/xx	76	S, G	35 %
<b>Chile</b>										
Estero Parraguirre	1987	Rock avalanche - (hyperconcentrated) debris flow	High snowfall (winter) + high snowmelt (spring)		6.0E+06			19		
Tinguiririca	2007	Landslide	Exceptionally warm spring and summer tem- peratures → intense glac- ier downwasting and meltwater production						SD, S, Ini	
<b>South Georgia, Antarctica</b>										
Lyell Glacier	1975	Rockfall and de- bris slide	Not sure, possibly water lubrication			84km <sup>2</sup>	> 240/ several	60	SD, G	90 %



<i>Place Name of event</i>	<i>H [m]</i>	<i>L [m]</i>	<i>α [°]</i>	<i>A<sub>d</sub> [km<sup>2</sup>]</i>	<i>V<sub>d</sub> [m<sup>3</sup>]</i>	<i>ER</i>	<i>FT</i>	<i>Rock type</i>	<i>ρ [kg/m<sup>3</sup>]</i>	<i>E<sub>calc</sub> (E<sub>lit</sub>) [J]</i>	<i>MW prod. [m<sup>3</sup>]</i>	<i>Reference</i>
<b>Utah, USA</b>												
Bingham Canyon	850	2'950	16.1		5.3E+07	1.0	0	Porphyritic Copper	2000	8.7E+14	2.8E+06	[10], [33], [34], [35]
<b>Cascade Volcanoes, Washington, USA</b>												
Mount Adams	1'561	3'995	21.3		5.0E+06		X	Volcanic	2700	2.1E+14	6.7E+05	[36]
Mount Adams	1'683	4'472	20.6		4.0E+06		X	Volcanic	2700	1.8E+14	5.8E+05	[36]
Mount Adams	1'300	3'500	20.4	0.9	1.7E+06		X	Volcanic	2700	5.9E+13	1.9E+05	[10]
<b>Cordillera Blanca, Peru</b>												
Nevados Huascarán	3'966	16'880	13.2	22.0	5.8E+07	7.7	1	Granodiorite	2700	7.9E+14	2.6E+06	[3], [4], [18], [37]
<b>Chile</b>												
Estero Parraguirre	3'400	17'981	10.7		1.5E+07	2.5	1	Limestone	2500	5.0E+14	1.6E+06	[18], [38]
Tinguiririca	1'426	8'287	9.8		1.4E+07		X	Volcanic	2700	5.3E+14	1.7E+06	[39]
<b>South Georgia, Antarctica</b>												
Lyell Glacier	1'572	5'171	16.9		2.7E+06		Subseq. debris flow	Greywacke	2700	1.1E+14	3.7E+05	[40], [41]

<i>Place Name of event</i>	<i>Year</i>	<i>Event</i>	<i>Triggering Factor</i>	<i>H<sub>f</sub> [m]</i>	<i>V<sub>i</sub> [m<sup>3</sup>]</i>	<i>p<sub>g</sub> [m]</i>	<i>t [s] / n</i>	<i>V<sub>f</sub> [m/s]</i>	<i>Water source</i>	<i>Water content</i>
<b>Southern Alps, New Zealand</b>										
Beelzebub Glacier	1984	Rock slide/ avalanche								
Aoraki/Mount Cook	1991	Rock-ice avalanche	Large temperature changes the days before the event		1.2E+07	6'660	120/1	55-58	S, G	> 30E+06 m <sup>3</sup>
Mount Fletcher 1	1992	Rock avalanche			7.8E+06	2'290				
Mount Fletcher 2	1992	Rock avalanche			5.0E+06	2'360				
Mount Adams	1999	Large rock-ava- lanche	Earthquakes just before the event may have in- fluenced the timing of the collapse but not di- rectly triggered it		1.3E+07					
Hillary (South) Ridge/ Aoraki, Mount Cook	2014	Rock avalanche	Not sure		9.0E+05		189/2	51	S, G, SD	
Mount Haast/ Ao- raki, Mount Cook	2013	Rock avalanche	No direct trigger, heavy rainfall before the event may have influ- enced the timing		1.0E+06		65/1	44.44	S, G	
<b>Westland, New Zealand</b>										
Wanganui River Mt Evans	2013	Rock avalanche-de- bris flood	Heavy rain event		3.8E+06			>35	G	
<b>Pamir, Tajikistan</b>										
Vanch valley	2002	Landslide								
<b>Cashmir, Pakistan</b>										
Bualtar I	1986	Rock avalanche/ Landslide	Freeze-thaw cycle, pore pressure			3'000		62	G	

<i>Place Name of event</i>	<i>H [m]</i>	<i>L [m]</i>	<i>α [°]</i>	<i>A<sub>d</sub> [km<sup>2</sup>]</i>	<i>V<sub>d</sub> [m<sup>3</sup>]</i>	<i>ER</i>	<i>FT</i>	<i>Rock type</i>	<i>ρ [kg/m<sup>3</sup>]</i>	<i>E<sub>calc</sub> (E<sub>lit</sub>) [J]</i>	<i>MW prod. [m<sup>3</sup>]</i>	<i>Reference</i>
<b>Southern Alps, New Zealand</b>												
Beelzebub Glacier	402	1'012	21.7	0.2	2.0E+06		X	Volcanic	2700	2.1E+13	6.9E+04	[42]
Aoraki/Mount Cook	2'720	7'008	21.2	7.0	6.0E+07	5.0	X	Greywacke	2700	8.6E+14	2.8E+06	[3], [13], [43]
Mount Fletcher 1	1'364	3'806	19.7	1.8	1.0E+07	1.3	X	Volcanic	2700	2.8E+14	9.2E+05	[3]
Mount Fletcher 2	1'440	3'800		1.8		0.0	X	Volcanic	2700	1.9E+14	6.2E+05	[3]
Mount Adams	1'850	2'800	33.5	1.6	1.5E+07	1.2	X	Schist	2700	6.1E+14	2.0E+06	[42], [44]
Hillary (South) Ridge/ Aoraki, Mount Cook	1'600	3'900	22.3	1.4	3.0E+06	3.3	fluid-like flow of debris	Greywacke	2700	3.8E+13	1.2E+05	[45]
Mount Haast/ Aoraki, Mount Cook	290			0.8	2.0E+06	2.0	0	Greywacke	2700	7.7E+12	2.5E+04	[46]
<b>Westland, New Zealand</b>												
Wanganui River Mt Evans		5'000	0.0		4.5E+06	1.2	X	Volcanic	2700	0.0E+00		[47]
<b>Pamir, Tajikistan</b>												
Vanch valley	1'549	9'138	9.6		8.0E+06		X			0.0E+00		[48]
<b>Cashmir, Pakistan</b>												
Bualtar I	1'490	4'808	17.2	4.5	2.0E+07		X	Marble and Schist	2500	7.3E+14	2.4E+06	[49], [50]

Place Name of event	Year	Event	Triggering Factor	$H_f$ [m]	$V_i$ [m <sup>3</sup> ]	$p_g$ [m]	$t$ [s] / $n$	$v_f$ [m/s]	Water source	Water content
<b>Taiwan</b>										
Shiaolin	2009	Landslide	Large amount of precipitation in short time (1676mm in 3 days)	830				20.4-33.7	W	
<b>Japan</b>										
Tatsunokuchi	2011	Long-travelling landslide	Earthquake		5.0E+04			14	S	
<b>Nepal</b>										
Pokhara valley	2012	Rock avalanche-debris flow		1200	1.3E+07		1766/8-27	13.3	G	
<b>Caucasus, Russia</b>										
Kolka/Karmadon	2002	Rock/ice avalanche; Glacier surge & ice-water-stone mud-flow; Debris flow	Accumulation of sub-glacial meltwater possibly through volcanic activity	950	2.3E+07	3'100	390/2	70-90	S, G, W, SD, Firn	90E+06 m <sup>3</sup>

$H_f$ , fall height,  $V_i$ , initial volume;  $p_g$ , path onto glacier surface;  $t$ , duration;  $n$ , number of surges;  $v_f$ , flow speed; water source (W, Water; S, Snow; G, Glacier ice; SD, Saturated debris; Ini, Ice and snow in initial failure mass);  $H$ , vertical distance;  $L$ , horizontal distance;  $\alpha$ , angle of reach;  $A_d$ , area of deposition;  $V_d$ , deposited volume; ER, entrainment ratio (Initial vs deposited volume); FT, flow transformation (0, NO; 1, YES; X, no information);  $\rho$ , rock density;  $E_{cal}$ , calculated energy;  $E_{lit}$ , energy in literature; MW prod., Meltwater production

<i>Place Name of event</i>	<i>H [m]</i>	<i>L [m]</i>	<i>α [°]</i>	<i>A<sub>d</sub> [km<sup>2</sup>]</i>	<i>V<sub>d</sub> [m<sup>3</sup>]</i>	<i>ER</i>	<i>FT</i>	<i>Rock type</i>	<i>ρ [kg/m<sup>3</sup>]</i>	<i>E<sub>calc</sub> (E<sub>lit</sub>) [J]</i>	<i>MW prod. [m<sup>3</sup>]</i>	<i>Reference</i>
<b>Taiwan</b>												
Shiaolin	830	2'830	16.3		2.5E+07		X	Marble and Schist	2500	5.1E+14	1.7E+06	[51], [52]
<b>Japan</b>												
Tatsunokuchi						0.0	X	Volcanic	2700	0.0E+00		[53]
<b>Nepal</b>												
Pokhara valley		23'500	0.0		2.2E+07	1.8	1			0.0E+00		[54]
<b>Caucasus, Russia</b>												
Kolka/Karmadon	2'047	19'379	6.0		1.3E+08	5.7	1	Ice	920	2.0E+14	6.4E+05	[3], [4], [18], [55], [56], [57], [58], [59], [60]

[1] (Bottino et al., 2002), [2] (Barla et al., 2000), [3] (Deline et al., 2015), [4] (Sosio et al., 2008), [5] (Pirulli, 2009), [6] (Huggel et al., 2007), [7] (Caplan-Auerbach et al., 2007), [8] (Waythomas et al., 2000), [9] (Alean, 1984), [10] IRIS, [11] (Jibson et al., 2006), [12] (Huggel et al., 2008b), [13] (Huggel et al., 2010), [14] (Geertsema, 2012), [15] (Bessette-Kirton, 2017), [16] (Bessette-Kirton et al., 2018), [17] (Clague and Souther, 1982), [18] (Petrakov et al., 2008), [19] (Geertsema et al., 2006), [20] (Evans and Clague, 1999), [21] (Delaney and Evans, 2008), [22] (Delaney and Evans, 2014), [23] (Schwab et al., 2003), [24] (Jiskoot, 2011), [25] (McDougall et al., 2006), [26] (Boulton et al., 2006), [27] (Lipovsky et al., 2008), [28] (Allstadt, 2013), [29] (Guthrie et al., 2012), [30] (Roberti et al., 2017), [31] (Roberti et al., 2018), [32] (Coe et al., 2016), [33] (Pankow et al., 2014), [34] (Moore et al., 2017), [35] (Hibert et al., 2014), [36] (Schneider et al., 2011a), [37] (Evans et al., 2009a), [38] (Hauser, 2002), [39] (Iribarren Anaconda and Bodin, 2010), [40] (Deline, 2009), [41] (Gordon et al., 1978), [42] (Korup, 2005), [43] (Schneider et al., 2010), [44] (Hancox et al., 2005), [45] (Cox et al., 2015), [46] (Hancox and Thomson, 2013), [47] (Carey et al., 2015), [48] (Schneider, 2006), [49] (Hewitt, 1988), [50] (Hewitt, 2009), [51] (Feng, 2011), [52] (Tsou et al., 2011), [53] (Yamasaki et al., 2014), [54] (Hanisch et al., 2013), [55] (Haeberli et al., 2003), [56] (Haeberli et al., 2004), [57] (Kotlyakov et al., 2004), [58] (Huggel et al., 2005), [59] (Evans et al., 2009b), [60] (Huggel, 2009)

## 8.2 RAMMS logfiles

### 8.2.1 Mount Meager

#### Standard

RAMMS::DEBRIS FLOW RAMMS OUTPUT LOGFILE

Output filename: C:\Users\Miriam\Documents\Uni\Masterarbeit\RAMMS\_Simulations\Standard\_AP\_Meager\Standard\_AP\_Meager\_500\_01.out.gz

Simulation stopped due to LOW FLUX!

Simulation stopped after 280.000s

Calculation time (min.): 15.30

Simulation resolution (m): 12.50

SIMULATION RESULTS

Number of cells: 341294

Number of nodes: 343154

Calculated Release Volume (m3): 4.65808e+007

Overall MAX velocity (m/s): 71.1779

Overall MAX flowheight (m): 147.730

Overall MAX pressure (kPa): 13679.0

\*\*\*\*\*

RAMMS::DEBRIS FLOW 1.7.15 INPUT LOGFILE

Date: Thu May 03 14:31:44 2018

Input filename: C:\Users\Miriam\Documents\Uni\Masterarbeit\RAMMS\_Simulations\Standard\_AP\_Meager\Standard\_AP\_Meager\_500\_01.db2

Project: Standard\_AP\_Meager

Details:

DEM / REGION INFORMATION:

DEM file: C:\Users\Miriam\Documents\Uni\Masterarbeit\RAMMS\_Simulations\Standard\_AP\_Meager\Standard\_AP\_Meager.xyz

DEM resolution (m): 12.50

(imported from: C:\Users\Miriam\Documents\Uni\Masterarbeit\RAMMS\_Simulations\dem\ap\_meager\_large\_ascii.txt)

Nr of nodes: 1386705

Nr of cells: 1384304

Project region extent:

E - W: 477685.28 / 459735.28

S - N: 5600075.3 / 5612125.3

CALCULATION DOMAIN:

C:\Users\Miriam\Documents\Uni\Masterarbeit\RAMMS\_Simulations\Standard\_AP\_Meager\calcDom\_Meager\_large.dom

GENERAL SIMULATION PARAMETERS:

Simulation time (s): 2000.00

Dump interval (s): 10.00

Stopping criteria (momentum threshold) (%): 5

Constant density (kg/m3): 2700

Lambda (): 1.0

NUMERICS:

Numerical scheme: SecondOrder

H cutoff (m): 0.000001

Curvature effects are ON!

RELEASE:

Depth: 60.00 m Vol: 46575100.0 m3 Delay: 0.00 s Name: release\_meager\_new.shp

Estimated release volume: 46575072.00 m3

FRICITION MUXI:

Mu (): 0.100

Xi (m/s2): 500

COHESION:

No COHESION specified.

MAP / ORTHOPHOTO INFO:

OrthoPhoto file: C:\Users\Miriam\Documents\Uni\Masterarbeit\RAMMS\_Simulations\orthophoto\Meager\_rgb\_large.tif

*Entrainment*

## RAMMS::DEBRIS FLOW RAMMS OUTPUT LOGFILE

Output filename: C:\Users\Miriam\Documents\Uni\Masterarbeit\RAMMS\_Simulations\Erosion\_AP\_Meager\Erosion\_AP\_Meager\_2\_0025\_01\_1\_2.out.gz

Simulation stopped due to LOW FLUX!

Simulation stopped after 280.000s

Calculation time (min.): 17.95

Simulation resolution (m): 12.50

## SIMULATION RESULTS

Number of cells: 341294

Number of nodes: 343154

Calculated Release Volume (m3): 4.65808e+007

Overall MAX velocity (m/s): 71.1712

Overall MAX flowheight (m): 147.730

Overall MAX pressure (kPa): 13676.4

\*\*\*\*\*

## RAMMS::DEBRIS FLOW 1.7.15 INPUT LOGFILE

Date: Tue May 08 21:17:12 2018

Input filename: C:\Users\Miriam\Documents\Uni\Masterarbeit\RAMMS\_Simulations\Erosion\_AP\_Meager\Erosion\_AP\_Meager\_2\_0025\_01\_1\_2.db2

Project: Erosion\_AP\_Meager

Details:

## DEM / REGION INFORMATION:

DEM file: C:\Users\Miriam\Documents\Uni\Masterarbeit\RAMMS\_Simulations\Erosion\_AP\_Meager\Erosion\_AP\_Meager.xyz

DEM resolution (m): 12.50

(imported from: C:\Users\Miriam\Documents\Uni\Masterarbeit\RAMMS\_Simulations\dem\ap\_meager\_large\_ascii.txt)

Nr of nodes: 1386705

Nr of cells: 1384304

Project region extent:

E - W: 477685.28 / 459735.28

S - N: 5600075.3 / 5612125.3

## CALCULATION DOMAIN:

C:\Users\Miriam\Documents\Uni\Masterarbeit\RAMMS\_Simulations\Erosion\_AP\_Meager\calcDom\_Meager\_large.dom

## GENERAL SIMULATION PARAMETERS:

Simulation time (s): 2000.00

Dump interval (s): 10.00

Stopping criteria (momentum threshold) (%): 5

Constant density (kg/m3): 2700

Lambda (): 1.0

## NUMERICS:

Numerical scheme: SecondOrder

H cutoff (m): 0.000001

Curvature effects are ON!

## RELEASE:

Depth: 60.00 m Vol: 46575100.0 m3 Delay: 0.00 s Name: release\_meager\_new.shp

Estimated release volume: 46575072.00 m3

## FRICTION MUXI:

Mu (): 0.100

Xi (m/s2): 500

## COHESION:

No COHESION specified.

## EROSION polygon shapefiles:

(Density - MaxErodRate - ShearFactor - CriticalShear - LimitErod - Name)

2000.0 0.025 0.100 1.00 2.00 Substrate\_Meager.shp (C:\Users\Miriam\Documents\Uni\Masterarbeit\RAMMS\_Simulations\Meager\_Erosion\_Shapefiles)

## MAP / ORTHOPHOTO INFO:

OrthoPhoto file: C:\Users\Miriam\Documents\Uni\Masterarbeit\RAMMS\_Simulations\orthophoto\Meager\_rgb\_large.tif

*Extended*

## RAMMS::AVALANCHE RAMMS OUTPUT LOGFILE

Output filename: C:\Users\Miriam\Documents\Uni\Masterarbeit\RAMMS\_Simulations\Extended\_AP\_Meager\Extended\_AP\_Meager\_60mRel.out.gz

Simulation stopped due to LOW FLUX!

Simulation stopped after 540.000s

Real calculation time (min.): 59.48

Simulation resolution (m): 12.50

## SIMULATION RESULTS

Number of cells: 341279

Number of nodes: 343Z38

Calculated Release Volume (m3): 46532463.55

Overall MAX velocity (m/s): 100.89

Overall MAX flowheight (m): 170.69

Overall MAX core height (m): 170.74

Overall MAX pressure (kPa): 27482.93

Overall MAX core pressure (kPa): 27481.02

\*\*\*\*\*

## RAMMS::AVALANCHE 2.7.11 INPUT LOGFILE

Date: Tue Jun 05 09:01:10 2018

Input filename: C:\Users\Miriam\Documents\Uni\Masterarbeit\RAMMS\_Simulations\Extended\_AP\_Meager\Extended\_AP\_Meager\_60mRel.av2

Project: Extended\_AP\_Meager

Info: .

## DEM / REGION INFORMATION:

DEM file: C:\Users\Miriam\Documents\Uni\Masterarbeit\RAMMS\_Simulations\Extended\_AP\_Meager\Extended\_AP\_Meager.xyz

DEM resolution (m): 12.50

(imported from: C:\Users\Miriam\Documents\Uni\Masterarbeit\RAMMS\_Simulations\dem\ap\_meager\_large\_ascii.txt)

Nr of nodes: 1386705

Nr of cells: 1384304

Project region extent:

E - W: 477691.53 / 459741.53

S - N: 5600081.5 / 5612131.5

## CALCULATION DOMAIN:

C:\Users\Miriam\Documents\Uni\Masterarbeit\RAMMS\_Simulations\Extended\_AP\_Meager\calcDom\_Meager\_large.dom

## GENERAL SIMULATION PARAMETERS:

Simulation time (s): 1000.00

Dump interval (s): 10.00

Stopping criteria (momentum threshold) (%): 5

Constant density (kg/m3): 2700

Lambda ( ): 1.0

Linear Velocity Profile Factor: 2.00

Parabolic Density Profile Factor: 2.00

## NUMERICS:

Numerical scheme: SecondOrder

H cutoff: 0.000001

Curvature effects are ON!

## RELEASE:

C:\Users\Miriam\Documents\Uni\Masterarbeit\RAMMS\_Simulations\Extended\_AP\_Meager\release\_Meager\_new.rel

Release height (m): 60.0000

Estimated release volume: 49316 m3

## FRICTION MUXI:

Mu ( ): 0.100

Xi (m/s2): 500

## COHESION:

Cohesion value: 300.000 Pa

## RKE Energy Parameters:

Generate: 5.00000 (%)

Decay: 1.00000 (1/s)

R0: 12.0000 (kJ/m3)

## EROSION:

Additional EROSION polygon files:



## Appendix

1st additional EROSION file: C:\Users\Miriam\Documents\Uni\Masterarbeit\RAMMS\_Simulations\Extended\_AP\_Meager\Glacier\_Meager.shp H: 10.00m Rho: 2700kg/m<sup>3</sup> K: 1.00 T: -2.00° Vol: 0.00  
2nd additional EROSION file: C:\Users\Miriam\Documents\Uni\Masterarbeit\RAMMS\_Simulations\Extended\_AP\_Meager\Substrate\_Meager.shp H: 2.00m Rho: 1800kg/m<sup>3</sup> K: 1.00 T: 2.00° Vol: 10.00  
Erosion law: 0  
(0: Velocity - 1: Momentum - 2: Velocity square)  
MAP / ORTHOPHOTO INFO:  
OrthoPhoto file: C:\Users\Miriam\Documents\Uni\Masterarbeit\RAMMS\_Simulations\orthophoto\Meager\_rgb\_large.tif

### 8.2.2 Howson II

#### *Standard*

RAMMS::DEBRIS FLOW RAMMS OUTPUT LOGFILE

Output filename: C:\Users\Miriam\Documents\Uni\Masterarbeit\RAMMS\_Simulations\Standard\_AP\_Howson\Standard\_AP\_Howson\_1000\_015.out.gz  
Simulation stopped due to LOW FLUX!  
Simulation stopped after 150.000s  
Calculation time (min.): 0.55  
Simulation resolution (m): 12.50  
SIMULATION RESULTS  
Number of cells: 32516  
Number of nodes: 33016  
Calculated Release Volume (m<sup>3</sup>): 904725.  
Overall MAX velocity (m/s): 62.7584  
Overall MAX flowheight (m): 40.6096  
Overall MAX pressure (kPa): 10634.3

\*\*\*\*\*

RAMMS::DEBRIS FLOW 1.7.15 INPUT LOGFILE

Date: Thu Apr 12 09:00:43 2018  
Input filename: C:\Users\Miriam\Documents\Uni\Masterarbeit\RAMMS\_Simulations\Standard\_AP\_Howson\Standard\_AP\_Howson\_1000\_015.db2  
Project: Standard\_AP\_Howson  
Details: 24m release depth, Xi 1000, Mu 0.15  
DEM / REGION INFORMATION:  
DEM file: C:\Users\Miriam\Documents\Uni\Masterarbeit\RAMMS\_Simulations\Standard\_AP\_Howson\Standard\_AP\_Howson.xyz  
DEM resolution (m): 12.50  
(imported from: C:\Users\Miriam\Documents\Uni\Masterarbeit\RAMMS\_Simulations\dem\ap\_howson\_clip\_ascii.txt)  
Nr of nodes: 137256  
Nr of cells: 136514  
Project region extent:  
E - W: 580615.06 / 576327.56  
S - N: 6040144.3 / 6045119.3  
CALCULATION DOMAIN:  
C:\Users\Miriam\Documents\Uni\Masterarbeit\RAMMS\_Simulations\Standard\_AP\_Howson\calcDom\_Howson\_large.dom  
GENERAL SIMULATION PARAMETERS:  
Simulation time (s): 2000.00  
Dump interval (s): 5.00  
Stopping criteria (momentum threshold) (%): 5  
Constant density (kg/m<sup>3</sup>): 2700  
Lambda (): 1.0  
NUMERICS:  
Numerical scheme: SecondOrder  
H cutoff (m): 0.000001  
Curvature effects are ON!  
RELEASE:  
Depth: 24.00 m Vol: 904589.0 m<sup>3</sup> Delay: 0.00 s Name: release\_Howson.shp  
Estimated release volume: 904588.94 m<sup>3</sup>  
FRICTION MUXI:  
Mu (): 0.150  
Xi (m/s<sup>2</sup>): 1000  
COHESION:  
No COHESION specified.

## Appendix

### MAP / ORTHOPHOTO INFO:

OrthoPhoto file: C:\Users\Miriam\Documents\Uni\Masterarbeit\RAMMS\_Simulations\orthophoto\Howson\_rgb\_clip\_utm9n.tif

### Entrainment

#### RAMMS::DEBRIS FLOW RAMMS OUTPUT LOGFILE

Output filename: C:\Users\Miriam\Documents\Uni\Masterarbeit\RAMMS\_Simulations\Erosion\_AP\_HP\Erosion\_AP\_HP\_0025\_01\_1\_2.out.gz

Simulation stopped due to LOW FLUX!

Simulation stopped after 290.000s

Calculation time (min.): 0.63

Simulation resolution (m): 12.50

#### SIMULATION RESULTS

Number of cells: 30071

Number of nodes: 30541

Calculated Release Volume (m3): 731623.

Overall MAX velocity (m/s): 43.6253

Overall MAX flowheight (m): 31.8848

Overall MAX pressure (kPa): 5138.56

\*\*\*\*\*

#### RAMMS::DEBRIS FLOW 1.7.15 INPUT LOGFILE

Date: Wed May 30 10:53:06 2018

Input filename: C:\Users\Miriam\Documents\Uni\Masterarbeit\RAMMS\_Simulations\Erosion\_AP\_HP\Erosion\_AP\_HP\_0025\_01\_1\_2.db2

Project: Erosion\_AP\_HP

Details:

#### DEM / REGION INFORMATION:

DEM file: C:\Users\Miriam\Documents\Uni\Masterarbeit\RAMMS\_Simulations\Erosion\_AP\_HP\Erosion\_AP\_HP.xyz

DEM resolution (m): 12.50

(imported from: C:\Users\Miriam\Documents\Uni\Masterarbeit\RAMMS\_Simulations\dem\ap\_hp\_ascii.txt)

Nr of nodes: 84665

Nr of cells: 84048

Project region extent:

E - W: 631875.13 / 629325.13

S - N: 6102362.8 / 6107512.8

#### CALCULATION DOMAIN:

C:\Users\Miriam\Documents\Uni\Masterarbeit\RAMMS\_Simulations\Erosion\_AP\_HP\calcDom\_HP.dom

#### GENERAL SIMULATION PARAMETERS:

Simulation time (s): 2000.00

Dump interval (s): 5.00

Stopping criteria (momentum threshold) (%): 5

Constant density (kg/m3): 2700

Lambda (): 1.0

#### NUMERICS:

Numerical scheme: SecondOrder

H cutoff (m): 0.000001

Curvature effects are ON!

#### RELEASE:

Depth: 30.00 m Vol: 730414.0 m3 Delay: 0.00 s Name: release\_HP.shp

Estimated release volume: 730413.88 m3

#### FRICITION MUXI:

Mu (): 0.100

Xi (m/s2): 1000

#### COHESION:

No COHESION specified.

#### EROSION polygon shapefiles:

(Density - MaxErodRate - ShearFactor - CriticalShear - LimitErod - Name)

2000.0 0.025 0.100 1.00 2.00 Substrate\_HP.shp

### MAP / ORTHOPHOTO INFO:

OrthoPhoto file: C:\Users\Miriam\Documents\Uni\Masterarbeit\RAMMS\_Simulations\orthophoto\HaroldPrice\_rgb\_clip\_utm9n.tif

*Extended*

## RAMMS::AVALANCHE RAMMS OUTPUT LOGFILE

Output filename: C:\Users\Miriam\Documents\Uni\Masterarbeit\RAMMS\_Simulations\Extended\_AP\_Howson\Extended\_AP\_Howson\_24m\_rel.out.gz

Simulation stopped due to LOW FLUX!

Simulation stopped after 175.000s

Real calculation time (min.): 1.85

Simulation resolution (m): 12.50

## SIMULATION RESULTS

Number of cells: 32522

Number of nodes: 33021

Calculated Release Volume (m3): 911858.79

Overall MAX velocity (m/s): 97.38

Overall MAX flowheight (m): 41.35

Overall MAX core height (m): 63.97

Overall MAX pressure (kPa): 25604.90

Overall MAX core pressure (kPa): 25203.29

\*\*\*\*\*

## RAMMS::AVALANCHE 2.7.11 INPUT LOGFILE

Date: Wed Jun 06 09:09:36 2018

Input filename: C:\Users\Miriam\Documents\Uni\Masterarbeit\RAMMS\_Simulations\Extended\_AP\_Howson\Extended\_AP\_Howson\_24m\_rel.av2

Project: Extended\_AP\_Howson

Info: .

## DEM / REGION INFORMATION:

DEM file: C:\Users\Miriam\Documents\Uni\Masterarbeit\RAMMS\_Simulations\Extended\_AP\_Howson\Extended\_AP\_Howson.xyz

DEM resolution (m): 12.50

(imported from: C:\Users\Miriam\Documents\Uni\Masterarbeit\RAMMS\_Simulations\dem\ap\_howson\_clip\_ascii.txt)

Nr of nodes: 137256

Nr of cells: 136514

Project region extent:

E - W: 580621.31 / 576333.81

S - N: 6040150.5 / 6045125.5

## CALCULATION DOMAIN:

C:\Users\Miriam\Documents\Uni\Masterarbeit\RAMMS\_Simulations\Extended\_AP\_Howson\calcDom\_Howson\_large.dom

## GENERAL SIMULATION PARAMETERS:

Simulation time (s): 2000.00

Dump interval (s): 5.00

Stopping criteria (momentum threshold) (%): 5

Constant density (kg/m3): 2700

Lambda ( ): 1.0

Linear Velocity Profile Factor: 2.00

Parabolic Density Profile Factor: 2.00

## NUMERICS:

Numerical scheme: SecondOrder

H cutoff: 0.000001

Curvature effects are ON!

## RELEASE:

C:\Users\Miriam\Documents\Uni\Masterarbeit\RAMMS\_Simulations\Extended\_AP\_Howson\release\_Howson.rel

Release height (m): 24.0000

Estimated release volume: 0 m3

## FRICTION MUXI:

Mu ( ): 0.150

Xi (m/s2): 1000

## COHESION:

Cohesion value: 300.000 Pa

## RKE Energy Parameters:

Generate: 5.00000 (%)

Decay: 1.00000 (1/s)

R0: 12.0000 (kJ/m3)

## EROSION:

Additional EROSION polygon files:

## Appendix

1st additional EROSION file: C:\Users\Miriam\Documents\Uni\Masterarbeit\RAMMS\_Simulations\Extended\_AP\_Howson\Glacier\_Howson.shp H: 10.00m Rho: 2700kg/m3 K: 1.00 T: -2.00° Vol: 0.00  
2nd additional EROSION file: C:\Users\Miriam\Documents\Uni\Masterarbeit\RAMMS\_Simulations\Extended\_AP\_Howson\Substrate\_Howson.shp H: 2.00m Rho: 1800kg/m3 K: 1.00 T: 2.00° Vol: 10.00  
Erosion law: 0  
(0: Velocity - 1: Momentum - 2: Velocity square)  
MAP / ORTHOPHOTO INFO:  
OrthoPhoto file: C:\Users\Miriam\Documents\Uni\Masterarbeit\RAMMS\_Simulations\orthophoto\Howson\_rgb\_clip\_utm9n.tif

### 8.2.3 Harold Price

#### Standard

RAMMS::DEBRIS FLOW RAMMS OUTPUT LOGFILE  
Output filename: C:\Users\Miriam\Documents\Uni\Masterarbeit\RAMMS\_Simulations\Standard\_AP\_HP\Standard\_AP\_HP\_1000\_01.out.gz  
Simulation stopped due to LOW FLUX!  
Simulation stopped after 240.000s  
Calculation time (min.): 1.15  
Simulation resolution (m): 12.50  
SIMULATION RESULTS  
Number of cells: 81600  
Number of nodes: 82209  
Calculated Release Volume (m3): 731623.  
Overall MAX velocity (m/s): 43.9404  
Overall MAX flowheight (m): 31.8850  
Overall MAX pressure (kPa): 5213.06

\*\*\*\*\*

RAMMS::DEBRIS FLOW 1.7.15 INPUT LOGFILE  
Date: Wed May 30 10:15:41 2018  
Input filename: C:\Users\Miriam\Documents\Uni\Masterarbeit\RAMMS\_Simulations\Standard\_AP\_HP\Standard\_AP\_HP\_1000\_01.db2  
Project: Standard\_AP\_HP  
Details:  
DEM / REGION INFORMATION:  
DEM file: C:\Users\Miriam\Documents\Uni\Masterarbeit\RAMMS\_Simulations\Standard\_AP\_HP\Standard\_AP\_HP.xyz  
DEM resolution (m): 12.50  
(imported from: C:\Users\Miriam\Documents\Uni\Masterarbeit\RAMMS\_Simulations\dem\ap\_hp\_ascii.txt)  
Nr of nodes: 84665  
Nr of cells: 84048  
Project region extent:  
E - W: 631875.13 / 629325.13  
S - N: 6102362.8 / 6107512.8  
CALCULATION DOMAIN:  
C:\Users\Miriam\Documents\Uni\Masterarbeit\RAMMS\_Simulations\Standard\_AP\_HP\Standard\_AP\_HP.dom  
GENERAL SIMULATION PARAMETERS:  
Simulation time (s): 2000.00  
Dump interval (s): 5.00  
Stopping criteria (momentum threshold) (%): 5  
Constant density (kg/m3): 2700  
Lambda (): 1.0  
NUMERICS:  
Numerical scheme: SecondOrder  
H cutoff (m): 0.000001  
Curvature effects are ON!  
RELEASE:  
Depth: 30.00 m Vol: 730414.0 m3 Delay: 0.00 s Name: release\_HP.shp  
Estimated release volume: 730413.88 m3  
FRICTION MUXI:  
Mu (): 0.100  
Xi (m/s2): 1000  
COHESION:  
No COHESION specified.  
MAP / ORTHOPHOTO INFO:

## Appendix

OrthoPhoto file: C:\Users\Miriam\Documents\Uni\Masterarbeit\RAMMS\_Simulations\orthophoto\Har-oldPrice\_rgb\_clip\_utm9n.tif

### *Entrainment*

RAMMS::DEBRIS FLOW RAMMS OUTPUT LOGFILE

Output filename: C:\Users\Miriam\Documents\Uni\Masterarbeit\RAMMS\_Simulations\Erosion\_AP\_HP\Erosion\_AP\_HP\_0025\_01\_1\_2.out.gz

Simulation stopped due to LOW FLUX!

Simulation stopped after 290.000s

Calculation time (min.): 0.63

Simulation resolution (m): 12.50

SIMULATION RESULTS

Number of cells: 30071

Number of nodes: 30541

Calculated Release Volume (m3): 731623.

Overall MAX velocity (m/s): 43.6253

Overall MAX flowheight (m): 31.8848

Overall MAX pressure (kPa): 5138.56

\*\*\*\*\*

RAMMS::DEBRIS FLOW 1.7.15 INPUT LOGFILE

Date: Wed May 30 10:53:06 2018

Input filename: C:\Users\Miriam\Documents\Uni\Masterarbeit\RAMMS\_Simulations\Erosion\_AP\_HP\Erosion\_AP\_HP\_0025\_01\_1\_2.db2

Project: Erosion\_AP\_HP

Details:

DEM / REGION INFORMATION:

DEM file: C:\Users\Miriam\Documents\Uni\Masterarbeit\RAMMS\_Simulations\Erosion\_AP\_HP\Erosion\_AP\_HP.xyz

DEM resolution (m): 12.50

(imported from: C:\Users\Miriam\Documents\Uni\Masterarbeit\RAMMS\_Simulations\dem\ap\_hp\_ascii.txt)

Nr of nodes: 84665

Nr of cells: 84048

Project region extent:

E - W: 631875.13 / 629325.13

S - N: 6102362.8 / 6107512.8

CALCULATION DOMAIN:

C:\Users\Miriam\Documents\Uni\Masterarbeit\RAMMS\_Simulations\Erosion\_AP\_HP\calcDom\_HP.dom

GENERAL SIMULATION PARAMETERS:

Simulation time (s): 2000.00

Dump interval (s): 5.00

Stopping criteria (momentum threshold) (%): 5

Constant density (kg/m3): 2700

Lambda (): 1.0

NUMERICS:

Numerical scheme: SecondOrder

H cutoff (m): 0.000001

Curvature effects are ON!

RELEASE:

Depth: 30.00 m Vol: 730414.0 m3 Delay: 0.00 s Name: release\_HP.shp

Estimated release volume: 730413.88 m3

FRICITION MUXI:

Mu (): 0.100

Xi (m/s2): 1000

COHESION:

No COHESION specified.

EROSION polygon shapefiles:

(Density - MaxErodRate - ShearFactor - CriticalShear - LimitErod - Name)

2000.0 0.025 0.100 1.00 2.00 Substrate\_HP.shp

MAP / ORTHOPHOTO INFO:

OrthoPhoto file: C:\Users\Miriam\Documents\Uni\Masterarbeit\RAMMS\_Simulations\orthophoto\Har-oldPrice\_rgb\_clip\_utm9n.tif

### *Extended*

RAMMS::AVALANCHE RAMMS OUTPUT LOGFILE

Output filename: C:\Users\Miriam\Documents\Uni\Masterarbeit\RAMMS\_Simulations\Extended\_AP\_HP\Extended\_AP\_HP\_2mEr\_2000relWater.out.gz

## Appendix

Simulation stopped due to LOW FLUX!

Simulation stopped after 330.000s

Real calculation time (min.): 2.32

Simulation resolution (m): 12.50

SIMULATION RESULTS

Number of cells: 30100

Number of nodes: 30572

Calculated Release Volume (m3): 781736.89

Overall MAX velocity (m/s): 57.39

Overall MAX flowheight (m): 33.50

Overall MAX core height (m): 33.50

Overall MAX pressure (kPa): 8891.67

Overall MAX core pressure (kPa): 8588.78

\*\*\*\*\*

RAMMS::AVALANCHE 2.7.11 INPUT LOGFILE

Date: Wed Jun 06 09:34:48 2018

Input filename: C:\Users\Miriam\Documents\Uni\Masterarbeit\RAMMS\_Simulations\Extended\_AP\_HP\Extended\_AP\_HP\_2mEr\_2000relWater.av2

Project: Extended\_AP\_HP

Info: .

DEM / REGION INFORMATION:

DEM file: C:\Users\Miriam\Documents\Uni\Masterarbeit\RAMMS\_Simulations\Extended\_AP\_HP\Extended\_AP\_HP.xyz

DEM resolution (m): 12.50

(imported from: C:\Users\Miriam\Documents\Uni\Masterarbeit\RAMMS\_Simulations\dem\ap\_hp\_ascii.txt)

Nr of nodes: 84665

Nr of cells: 84048

Project region extent:

E - W: 631881.38 / 629331.38

S - N: 6102369.0 / 6107519.0

CALCULATION DOMAIN:

C:\Users\Miriam\Documents\Uni\Masterarbeit\RAMMS\_Simulations\Extended\_AP\_HP\calcDom\_HP.dom

GENERAL SIMULATION PARAMETERS:

Simulation time (s): 2000.00

Dump interval (s): 5.00

Stopping criteria (momentum threshold) (%): 5

Constant density (kg/m3): 2700

Lambda ( ): 1.0

Linear Velocity Profile Factor: 2.00

Parabolic Density Profile Factor: 2.00

NUMERICS:

Numerical scheme: SecondOrder

H cutoff: 0.000001

Curvature effects are ON!

RELEASE:

C:\Users\Miriam\Documents\Uni\Masterarbeit\RAMMS\_Simulations\Extended\_AP\_HP\release\_HP.rel

Release height (m): 30.0000

Estimated release volume: 0 m3

FRICITION MUXI:

Mu ( ): 0.100

Xi (m/s2): 1000

COHESION:

Cohesion value: 300.000 Pa

RKE Energy Parameters:

Generate: 5.00000 (%)

Decay: 1.00000 (1/s)

R0: 12.0000 (kJ/m3)

EROSION:

Additional EROSION polygon files:

1st additional EROSION file: C:\Users\Miriam\Documents\Uni\Masterarbeit\RAMMS\_Simulations\Extended\_AP\_HP\Substrate\_HP.shp H: 2.00m Rho: 1800kg/m3 K: 1.00 T: 2.00° Vol: 10.00

Erosion law: 0

(0: Velocity - 1: Momentum - 2: Velocity square)

MAP / ORTHOPHOTO INFO:

OrthoPhoto file: C:\Users\Miriam\Documents\Uni\Masterarbeit\RAMMS\_Simulations\orthophoto\Har-oldPrice\_rgb\_clip\_utm9n.tif

## **Acknowledgements**

Great thanks go to my supervisor Christian Huggel and to my co-supervisors Brian McArdell and Florian Amann. Thank you all for the interesting discussions, the helpful inputs and suggestions on my thesis and for making time to explain the complexity and physical basics of landslides.

Thanks to Anja Dufresne who is analysing rock avalanche depositions for information about events mentioned in my inventory and for inputs about other, firstly unknown events.

Thanks to Perry Bartelt from the slf for introducing me into the extended version of RAMMS and making time to have a look at the simulation results and giving me feedback. Also, great thanks go to Marc Christen from the slf for all the help with RAMMS issues. I am very grateful for the good collaboration with the RAMMS team as well as with the whole slf.

Great thanks go to my co-students in the G10-Master-Thesis-room for their support, their help with Microsoft- and ArcGIS-issues and their time for pauses.

Many thanks go to my partner and my family for their mental support, their interest in my thesis and their very important inputs from different perspectives, making my thesis more understandable for people common and uncommon with this topic.





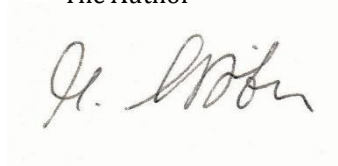
## Personal Declaration

I hereby declare that the submitted thesis is the result of my own, independent work. All external sources are explicitly acknowledged in the thesis.

Place, Date

The Author

Zurich, 22.08.2018

A handwritten signature in black ink on a light-colored background. The signature is cursive and appears to read 'J. M. ...'.